# Electron and nuclear spin dynamics in GaAs microcavities

Rakshyakar Giri

Université Montpellier 2
Sciences et Techniques du Languedoc

# Electron and nuclear spin dynamics in GaAs microcavities

**Thèse**

pour obtenir le grade de
**Docteur de l'Université Montpellier 2**
Spécialité : Physique
École Doctorale : I2S - Information, Structures et Systèmes
Laboratoire : L2C - Laboratoire Charles Coulomb

par

**Rakshyakar Giri**

Soutenue le 18 juin 2013 devant le jury composé de :

| | | |
|---|---|---|
| Denis SCALBERT | Directeur de recherche | Directeur de thèse |
| Thierry AMAND | Directeur de recherche | Rapporteur |
| Daniel PAGET | Directeur de recherche | Rapporteur |
| Guillaume CASSABOIS | Professeur des Universités | Examinateur |
| Maria VLADIMIROVA | Chargé de recherche | Invité |
| Michel DYAKONOV | Professeur émérite | Invité |

# Abstract

The rotation of the plane of polarization of light upon transmission through a magnetized medium is known as Faraday rotation (FR). In non-magnetic semiconductors FR can be produced by optically orienting the spin of electrons. The main objectives of this thesis is (i) to demonstrate large FR due to optically oriented electrons using an n-doped bulk GaAs microcavity, and (ii) to show that the FR can also be used to measure the nuclear spin dynamics without disturbing it.

By using optical orientation of electron gas in n-doped bulk GaAs confined in a microcavity (MC), FR up to 19° in the absence of magnetic field is obtained. This strong rotation is achieved because the light makes multiple round trips inside the MC. Fast optical switching of FR in sub-microsecond time scale is demonstrated by sampling the FR in a one shot experiment under pulsed excitation. A concept of FR cross-section as a proportionality coefficient between FR angle, electron spin density and optical path is introduced. This FR cross-section which defines the efficiency of spin polarized electrons in producing FR is estimated quantitatively and compared with the experimental results.

Non-destructive measurement of nuclear magnetization in n-GaAs via cavity enhanced FR of an off-resonant light beam is also demonstrated. In contrast with the existing optical methods, this detection scheme does not require the presence of non-equilibrium electrons. Applying this detection scheme to the metallic n-GaAs sample, nuclear FR is found to vary non-monotonously after pump beam is switched off. It consists of two components: one with short decay time ($\sim$10 s) and another with longer decay time and opposite sign ($\sim$200 s). These two contributions to nuclear FR are attributed to two groups of nuclei: (i) nuclear spins situated within the localization radius of donor-bound electrons, which are characterized by fast dynamics, and (ii) all other nuclear spins in the sample characterized by much slower relaxation rate. The results suggest that, even in degenerate semiconductors nuclear spin relaxation is limited by the presence of localized electron states and spin diffusion, rather than by Korringa mechanism. Nuclear FR in the insulating sample, in contrast with the metallic sample, is found to vary monotonously, but again consists of two components. The fast component is even faster than that of the metallic sample ($\sim$1

s), and the slow component decays in the same time scale as that of the metallic sample. Main microscopic mechanisms responsible for nuclear FR is found to be conduction band spin splitting induced by Overhauser field. It dominates nuclear FR in both metallic (conduction band states partly occupied) and insulating (Fermi level below the bottom of the conduction band) samples. FR resulting from the spin unbalanced occupation of donor bound electron states is only observed in metallic sample.

*I dedicate this thesis to the memory of my beloved brother, Babu, for his love, care and support throughout my life. What I am today and whatever little I have achieved in life, I owe everything to him.*

# Acknowledgements

First of all, I would like to thank my supervisor Dr. Denis Scalbert, for giving me the opportunity to work in his group. He personally helped me in the lab and also helped me understand the experimental results. Moreover, I would like to thank him for his patience and detailed explanations of any kind of question I had during the last three years. I would also like to thank my co-supervisor Dr. Maria Vladimirova for her help in understanding the experimental results. She helped me improve my presentation skills and also helped me while I was writing my thesis. I would also like to thank Dr. Steeve Cronenberger for his help in the lab. He patiently explained to me the pump-probe experiments. He also participated in the experiments. He was always there to help me, whenever I needed him, be it in the lab or any personal problem I face. It is only because of the support, kindness and friendly behavior of Denis, Masha and Steeve, I could survive three years in Montpellier. I would also like to thank Dr. Thierry Guillet, who was responsible for Clermont 4 project in Montpellier, for his honest opinion of my presentation skills. His constructive criticisms certainly helped.

I would like to thank our collaborators Dr. Kirill Kavokin and Dr. Mikhail Glazov. Kirill participated in some of the experiments. Mikhail provided theoretical explanations for some of the experimental results. Whenever I had any questions, he promptly provided me with the explanations. I would like to thank Dr. Jacqueline Bloch and Dr. Aristide Lemaître, for providing the samples for this work. I am thankful to Mr. Pierre Solignac for constructing the electrically controlled shutter, which made it possible to fully automatize the experimental setups, Mr. Jean Lyonnet for preparing the samples for measurements using the cryostats, and Mr. Christian L'henoret for his help whenever we needed to do something in the workshop.

I acknowledge the financial support provided by the Marie Curie initial training network (MC-ITN), CLERMONT 4 for this work. It also provided me with the opportunity to participate and present my work in many international schools and conferences.

Finally, I would like to thank my parents, my wife, my brother, Biswal sir, and my friends, for their support and encouragement.

# Contents

# Symbols and abbreviations

## Abbreviations

AOM Acousto-optic modulator

BS Babinet-Soleil compensator

DNP Dynamic nuclear polarization

FR Faraday rotation

NMR Nuclear magnetic resonance

PEM Photoelastic modulator

rf Radio frequency

## Physical constants

$\mu_B$ Bohr magneton

$\mu_N$ Nuclear magneton

$a_B$ Bohr radius

$k_B$ Boltzmann constant

## Symbols

$\alpha$ Absorption coefficient

$\alpha_+/\alpha_-$ Absorption coefficient for $\sigma^+/\sigma^-$ polarized light

$\beta_e$ Inverse electron temperature

$\beta_N$ Reciprocal nuclear spin temperature

| | |
|---|---|
| $\Delta$ | Detuning between the cavity mode and energy gap |
| $\Delta_N$ | Splitting of electron spin state in the nuclear field |
| $\Delta_{HF}$ | Hartree-Fock field |
| $\Delta_{SO}$ | Energy Spin-orbit splitting |
| $\lambda_{res}$ | Resonance wavelength in vacuum |
| $\langle S_z \rangle$ | Electron spin density |
| $\mathcal{D}(E_F)$ | Density of states at the Fermi energy |
| $\mathcal{D}_L$ | Degeneracy of each Landau level |
| $\mu$ | Proportionality constant between $\Theta_F$ and $\rho_e$ |
| $\mu_\pm$ | Chemical potential for spin up and spin down electrons |
| $\Omega$ | Electron Larmor frequency |
| $\omega$ | Frequency of light |
| $\omega_c$ | Cyclotron frequency |
| $\omega_N$ | Precession frequency of nuclear spin in the Knight field |
| $\rho_c$ | Degree of circular polarization of PL |
| $\rho_e$ | Degree of spin polarization of electrons |
| $\rho_i$ | Initial degree of spin polarization of electrons |
| $\tau$ | Lifetime of an equilibrium hole |
| $\tau_J$ | Lifetime of an electron in the conduction band |
| $\tau_s$ | Electron spin relaxation time |
| $\tau_c$ | Correlation time |
| $\Theta_F$ | Faraday rotation angle |
| $\Theta_N$ | Nuclear spin temperature |
| $\varepsilon'/\varepsilon''$ | Dielectric susceptibilities |

| | |
|---|---|
| $A$ | Hyperfine coupling constant |
| $a$ | Localization radius of electrons |
| $B$ | Magnetic field |
| $B_T$ | Total transverse field (external+nuclear) |
| $B_x$ | Transverse magnetic field |
| $B_z$ | Longitudinal magnetic field |
| $B_e$ | Knight field |
| $b_e$ | Knight field at saturation |
| $B_L$ | Fluctuating local field created by nuclei due to dipole-dipole interaction |
| $B_N$ | Nuclear field |
| $b_N$ | Nuclear field at saturation |
| $B_{rf}$ | Radio frequency field |
| $D$ | Nuclear spin diffusion coefficient |
| $d_{eff}$ | Effective length light travels inside the cavity |
| $f$ | Modulation frequency of PEM |
| $f_c$ | Chopper frequency |
| $f_{\pm 1/2}$ | Distribution function of conduction electrons |
| $G$ | Generation rate of electron-hole pairs |
| $g_e$ | Electron spin g-factor |
| $I$ | Nuclear spin polarization |
| $I_+/I_-$ | PL intensity for $\sigma^+/\sigma^-$ polarized light |
| $L$ | Sample thickness/Cavity length |
| $l_B$ | Magnetic length |
| $n$ | Refractive index |

$n_+/n-$ Refractive index for $\sigma^+/\sigma^-$ polarized light

$n_e$ Electron density

$n_L$ Landau level number

$n_{\pm 1/2}$ Density of spin up and down electrons

$Q$ Quality factor of the cavity

$R$ Reflection coefficient

$S$ Electron spin polarization in the steady state

$S_z$ Electron spin polarization (z-component)

$S_0$ Initial electron spin polarization

$T$ Temperature

$T_b$ Nuclear spin relaxation time due to localized electrons

$T_D$ Nuclear spin relaxation time due to spin diffusion

$T_e$ Electron temperature

$T_K$ Nuclear spin relaxation time due to Korringa mechanism

$T_s$ Spin lifetime of electrons

$T_{1e}$ Nuclear spin relaxation time due to interaction with electrons

$T_1$ Nuclear spin-lattice relaxation time

$T_2$ Transverse nuclear spin relaxation time

$V$ Verdet constant

$V_N$ Nuclear Verdet constant

# Chapter 1

# Introduction

## 1.1 State of the art and motivation

The first experiments on optical orientation of free carriers in semiconductors were done in 1960's and 1970's by Lampel (Si) [Lam68], Parsons (p-GaSb) [Par69], Ekimov and Safarov (n- and p-AlGaAs) [ES70], Garbuzov *et al.* (p-AlGaAs) [GES71], and Zakharchenya *et al.* (p-GaAs) [ZFD$^+$71]. Most of these experiments were done on p-type materials. In this case, only the spins of the non-equilibrium electrons created by circularly polarized light excitation are oriented. These oriented electrons recombine with the holes already present in the sample and the polarization of the luminescence is due to spin polarization of the electrons. The optical orientation of equilibrium electrons in n-type semiconductors was predicted theoretically by Dyakonov and Perel [DP71a], and was observed experimentally for the first time by Ekimov and Safarov [ES71] in n-AlGaAs ($n_e \sim 10^{16}$ cm$^{-3}$). In these experiments (except for the first experiment by Lampel on Si), the spin polarization of the electrons was deduced from the degree of circular polarization of photoluminescence. The spin relaxation time was measured from the depolarization of photoluminescence in a transverse magnetic field (Hanle effect). The photoluminescence polarization was strong for p-type materials, and the spin polarization degree and spin lifetime was measured from the luminescence polarization. However, it was observed, that for n-type materials, the photoluminescence polarization was weak and it was difficult to measure the spin lifetime correctly [ES70].

In 1990's Dzhioev *et al.* observed large spin diffusion length in weakly doped n-GaAs ($n_e \sim 1 \times 10^{11}$ cm$^{-3}$) using Hanle effect on photoluminescence [DZKS97]. Kikkawa and Awschalom studied spin dynamics n-type bulk GaAs using time resolved Faraday rotation (FR). They reported spin lifetime of electrons up to 100 ns for doping densities $n_e \sim 1 \times 10^{16}$ cm$^{-3}$ to $8 \times 10^{18}$ cm$^{-3}$, and explored the spin relaxation mechanisms and spin transport in this doping regime [KA98, KA99]. This strong dependence of spin lifetime on doping density implies different spin relaxation mechanisms in different doping regimes. This behaviour was studied in a systematic manner by Dzhioev *et al.* in n-type GaAs with doping density from $n_e \sim 1 \times 10^{14}$ cm$^{-3}$ to $5 \times 10^{17}$ cm$^{-3}$ [DKK$^+$02]. They observed two maxima in the spin lifetime dependence of doping density, one in either side of the metal to insulator transition point ($n_e \sim 2 \times 10^{16}$ cm$^{-3}$). In the insulating regime, maximum spin lifetime of about 180 ns was observed at $n_e \sim 3 \times 10^{15}$ cm$^{-3}$, and the main spin relaxation mechanisms are anisotropic exchange interaction and hyperfine interaction. In the metallic regime, maximum spin lifetime of about 200 ns was observed close to the transition point, and the spin relaxation is governed by the Dyakonov-Perel mechanism. Dzhioev *et al.* used Hanle depolarization of photoluminescence to measure spin relaxation of non-equilibrium electrons, and observed a strong dependence of the spin relaxation time on excitation power. Spin relaxation of electrons in n-GaAs at various doping concentrations is reviewed by K. Kavokin [Kav08].

Recently Crooker *et al.* used spin noise spectroscopy to study equilibrium electrons in n-type GaAs, and reported a spin relaxation time of about 160 ns [CCS09]. Römer *et al.* measured the spin relaxation time of equilibrium electrons for different doping concentrations over a wide temperature range [RBM$^+$10].

Because of the long spin relaxation time of electrons in GaAs, it is possible to create large spin polarization by optical pumping. These spin polarized electrons can produce FR dependent on the thickness of the spin polarized area [AI73]. Because the spin polarized volume is limited by absorption and usually very small, the experimentally observed values of Faraday rotation in GaAs is of the order of milliradian [CCS09]. It has been suggested, that a microcavity can be used to enhance Faraday rotation in semiconductors and semiconductor nanostructures [KVK97, GLJ$^+$02, SM05]. It was shown, that the amplification factor was proportional to the number of round trips made by the light at the cavity resonance frequency. One of the the objective

of this thesis is to (1) demonstrate large Faraday rotation due to optically oriented electrons using an n-doped bulk GaAs microcavity, and (2) measure the efficiency of Faraday rotation by spin polarized electrons.

Not only the optically oriented electrons, but the spin polarized nuclei can also produce FR. Under optical pumping conditions, the optically oriented electrons interact with the lattice nuclei and polarize them, a process known as dynamic nuclear polarization (DNP). This was first observed by Lampel in n-Si [Lam68], and revealed by an increase of nuclear magnetic resonance signal upon excitation with circularly polarized light. Ekimov and Safarov [ES72a, ES72b] showed, that the dynamic nuclear polarization can be studied by optical methods. They were able to optically detect nuclear magnetic resonance (NMR) in AlGaAs by observing that the degree of circular polarization of luminescence changes at nuclear spin resonances. The dynamically polarized nuclei create an effective magnetic field, which act on the electrons due to hyperfine interaction, and thereby on the circular polarization of the luminescence. Dyakonov and Perel [DP75] proposed, that dynamic nuclear polarization under optical orientation was a result of cooling of the nuclear spin system, and this hypothesis was proved experimentally by Fleisher *et al.* [FDZ76]. Subsequently, dynamic nuclear polarization in p-GaAs, and the effect of small external magnetic field on the electron-nuclear spin system was studied in detail by Paget *et al.*, using luminescence depolarization due to Hanle effect [PLSS77]. Later Paget studied the nuclear spin relaxation process in GaAs using optically detected NMR [Pag82]. The results of the theoretical and experimental work carried out during 1960's-1980's on bulk GaAs and AlGaAs are summarized in the book *Optical Orientation* edited by F. Meier and B. P. Zakkharchenya [MZ84].

During 1990's and 2000's, the study of dynamic nuclear polarization has been extended to semiconductor nanostructures e.g. quantum dots [UMA+13]. The NMR was detected form the shift of the PL spectrum induced by the effective nuclear field (Overhauser field) [GBS+97, MKI09]. In the quantum dots, the nuclear spins are considered as the main source of relaxation for electron spins. Alongside the work on quantum dots, there has been a renewed interest for spin relaxation in bulk GaAs. Bulk n-GaAs is particularly interesting, because the system is similar to QDs in the low doping regime, and also the nuclear spin lattice relaxation time is long. Kikkawa and Awschalom observed magnetic resonance behaviour in n-type GaAs, induced

as well as detected optically. They suggested, that the delocalized electrons can polarize the nuclei, and used the Knight field from optically generated spin polarized electrons to manipulate the nuclear spin polarization. The NMR was detected from the measurement of electron Larmor precession frequency, which was probed by time resolved Kerr/Faraday rotation [KA00]. Recently Chen *et al.* used on-chip microcoils to manipulate spin polarization, and the variation in spin polarization induced by rf field was probed by time resolved Kerr rotation. They did NMR measurements on each species of GaAs in a bulk n-GaAs sample [CHL+11, CHR+11, CRWB11]. The dynamic nuclear polarization in n-GaAs, and the effect of doping concentration on the nuclear spin-lattice relaxation was studied by Lu *et al.* and Huang *et al.* employing optical detection of NMR [LHK+06, HCL+12]. In a very recent work by Kölbl *et al.*, nuclear spin relaxation in n-GaAs was studied using transport measurements, where they have reported the breakdown of Korringa law of nuclear spin relaxation (nuclear spin relaxation rate proportional to electronic temperature) [KZF+12].

The experimental methods employed to study DNP and nuclear spin relaxation in the earlier works are: (1) Optical techniques (e.g. luminescence depolarization or time resolved Faraday/Kerr rotation), (2) NMR, and (3) transport measurements. Out of these three methods, the optical techniques are most sensitive to study DNP and nuclear spin relaxation. However, the presence of spin polarized carriers in the sample is necessary in order to observe either circular polarization of luminescence, or the Larmor resonance frequency shift (Overhauser shift) due to nuclear magnetization. The spin polarized electrons used for the measurement, can also provide a strong feedback, which may greatly complicate and modify the behavior of nuclear spin system [MZ84]. In addition, because the time needed for nuclear polarization build up or relaxation is much longer than recombination and even spin relaxation time in semiconductors, no single-shot measurements is possible by these techniques. This means that measured nuclear field is averaged over many realizations.

It was suggested in early eighties, that all these problems can be avoided, if the experiment could be carried out in two stages [AM85]. First, the nuclear spins are polarized by conventional optical pumping by circularly polarized light in the presence of a longitudinal magnetic field. Then, the pump beam is switched off, and the time evolution of the nuclear field is detected via Faraday rotation of the weak linearly polarized probe beam. Because electron spin relaxation is about $10^9$ times

faster than the nuclear spin relaxation, this technique should allow for detection of nuclear spin dynamics in the absence of non-equilibrium electron spin created by the pump. In this thesis, we report on the experimental realization of this technique. Non-destructive detection is an important advantage of this technique with respect to other methods. The related research objectives of this thesis are: (1) study nuclear spin dynamics in n-GaAs in the absence of non-equilibrium electrons, (2) measure the efficiency of Faraday rotation due to nuclei spins and identify underlying microscopic mechanisms, and (3) explore the effect of doping density on the nuclear spin dynamics in n-GaAs.

## 1.2 Organization of the thesis

The thesis is organized as follows:

Chapter 2 gives a summary of the important physical concepts relevant for this thesis, such as: optical orientation of electrons in GaAs, nuclear spin system in GaAs, hyperfine interaction between electrons and nuclei, relaxation of nuclear spin by interaction with electrons in the insulating as well as in the metallic regime, dynamic polarization of nuclei by optically oriented electrons, concept of nuclear spin temperature, Faraday effect in semiconductors, and semiconductor microcavities.

Chapter 3 presents the GaAs microcavity samples, and the experimental techniques employed in the study of electron and nuclear spin dynamics.

In Chapter 4, experimental results on the Faraday rotation (FR) induced by spin polarized electrons created either by optical pumping, or by magnetic field are presented. Optically oriented electrons produce FR of a linearly polarized probe beam. The effects of pump power, pump polarization, and the wavelength of the probe on FR are discussed. Spin lifetime of the electrons is measured using Hanle effect on FR. The degree of spin polarization of optically oriented electron is measured using different methods. A concept of FR cross-section is introduced, which provides a measure of the efficiency of a spin density in producing FR. The photoinduced FR cross-section is calculated theoretically and compared with the one obtained from experimental results. A theory of photoinduced FR is formulated. The FR induced by external magnetic field is studied as a function of detuning and at different temperatures. The temperature dependent FR is explained by a simple theoretical

model. The field induced FR cross-section is calculated theoretically and compared with the values obtained from the experimental results. Fast optical switching of photo induced FR in a nanosecond time scale is demonstrated.

In Chapter 5, experimental results on the nuclear FR on the metallic sample are presented. Various techniques to study nuclear spin dynamics in semiconductors, and in particular the advantages of optical techniques are discussed. The dynamics of nuclear FR is studied in the dark, that is in the absence of optically created carriers. Contrary to expectations, the decay of the nuclear FR was non-monotonous, and consists of two components: one which decays very fast and another which decays slowly. In order to verify their nuclear origin, a detailed investigation of the effect of pump helicity and pumping duration, effect of static field during measurement, as well as the effect of rf magnetic field on the fast and slow components is done. From these measurements nuclear origin of both components is confirmed. The nuclear field created by the nuclei cooled in a longitudinal field by circular polarized pumping is measured. A parameter called nuclear Verdet constant, which describes the efficiency of nuclear FR is introduced, and this constant is determined experimentally for the slow component. A theory on the origin of the two components of nuclear FR is proposed.

In Chapter 6, experimental results on the nuclear FR on the insulating sample is presented. The mechanisms of nuclear polarization in the insulating regime in n-GaAs is discussed. FR in the presence of optical pumping is studied as a function of pumping time. Strong enhancement of FR is observed when nuclear field builds up. It could be explained in terms of field dependent electron spin relaxation. In order to verify this, the effect of strong longitudinal field during pumping on the FR is studied. The FR induced by the spin polarized nuclei is studied as a function of time. The results are compared with the results obtained on the metallic sample. In contrast to the metallic sample, the decay of the nuclear FR is monotonous, but still consists of two components. In order to verify, that they originate from the nuclei, a detailed investigation of the effect of pump helicity and pumping duration on the fast and slow components is done .

Finally, Chapter 7 summarizes the important results obtained in each of the chapters, discusses the implications of the results and concludes with a discussion of the future experiments.

# Chapter 2

# Fundamental concepts

This Chapter provides a brief overview of the fundamental physical concepts relevant for this thesis. Band structure of GaAs, and the optical orientation of electrons in GaAs are described in Section 2.1. The nuclear spin system in GaAs is described in Section 2.2. Hyperfine interaction between electrons and nuclei, and the resulting nuclear and electrons fields acting on electrons and nuclei respectively are described in Section 2.3. Relaxation of nuclear spin by interaction with electrons in the insulating as well as in the metallic regime is described in Section 2.4. The theory of dynamic nuclear polarization is presented in Section 2.5. A brief introduction to the concept of nuclear spin temperature is provided in Section 2.6. Faraday rotation in general, and the convention to define the sign of Faraday rotation are discussed in Section 2.7. Faraday rotation in semiconductors is discussed in Section 2.8. The Hanle effect and how it is used to determine spin lifetime of electrons is discussed in Section 2.9, and finally Section 2.10 introduces semiconductor microcavities. For more details on Sections 2.1-2.6 one can refer to Chapter 2 of the book *Optical Orientation* [MZ84].

## 2.1 Optical orientation of electrons in GaAs

The spin-orbit interaction plays an important role in determination of band structure in GaAs . The spin-orbit coupling gives rise to a splitting $\Delta_{SO}$ between the heavy-hole and light-hole on one hand and split-off valence band on the other hand

($\Delta_{SO}$=0.34 eV for GaAs). The large splitting between the heavy/light-hole band and the split-off band enables optical generation of spin polarizations in GaAs.

The band structure of GaAs is shown schematically in Fig. 2.1 near the Γ - point point (k = 0). The conduction band is s-like with orbital angular momentum $L = 0$ and two-fold degenerate with two spin states ($S = 1/2, S_z = \pm 1/2$). The valence bands are p-like with orbital angular momentum $L = 1$ in addition with spin angular momentum. The uppermost valence bands consists of three doubly degenerate sub bands: The heavy hole band ($J = 3/2, J_z = \pm 3/2$), the light hole band ($J = 1/2, J_z = \pm 1/2$) and the split-off band ($J = 3/2, J_z = \pm 1/2$).

The large spin-orbit splitting in GaAs enables circular polarized light to selectively couple to a particular spin state. Fig. 2.1 shows the various optical transitions in bulk GaAs and their relative amplitudes for circular polarized light excitation.

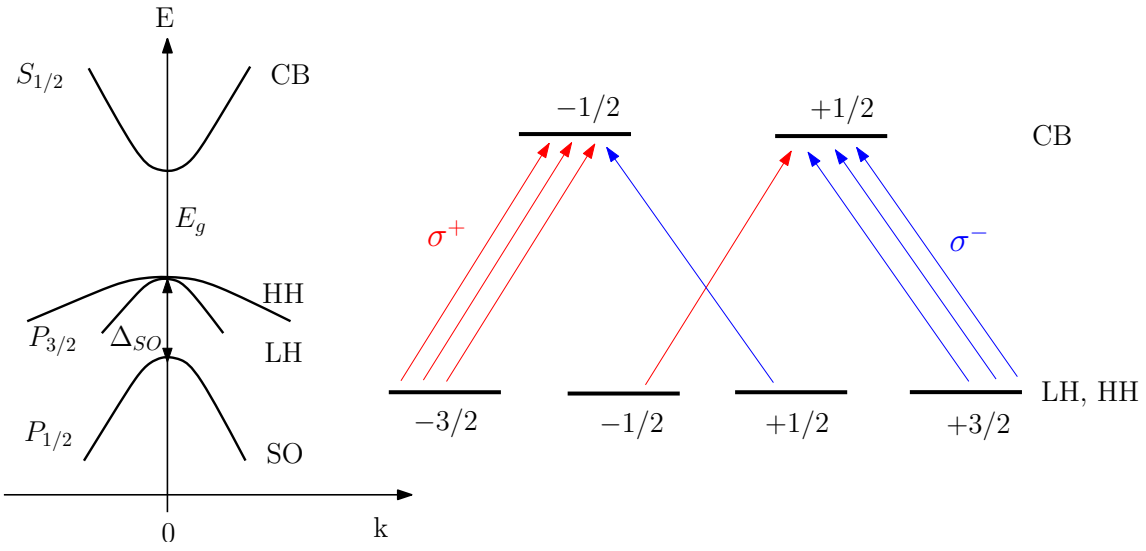


Figure 2.1: The figure shows the band structure of GaAs considering the effect of spin-orbit interaction (left side), and the optical selection rules for $\sigma^+$ and $\sigma^-$ polarized excitation light in bulk GaAs (right side).

If $\sigma^+$ polarized light, with energy greater than the band gap energy $E_g$ but less than $E_g + \Delta_{SO}$, is incident on the sample, electrons can only be excited from the $J = -3/2$ valence band state to the $J = -1/2$ conduction band state and from the $J = -1/2$ valence band state to the $J = 1/2$ conduction band state as shown in Fig. 2.1. The strengths of these two transitions are not equal (3 : 1) and an

initial electron spin of $S_0 = 0.25$ (corresponding to 50% polarization) will result. The average electron spin polarization for n-doped GaAs under steady state condition can be written as [ES70]

$$S = \frac{S_0}{1 + \tau_J/\tau_s}, \tag{2.1}$$

where $\tau_J$ is the lifetime of an electron in the conduction band and $\tau_s$ is the electron spin lifetime. In the steady state, the recombination rate is proportional to the generation rate of carriers by photo excitation, $\tau_J = n_e/G$. Here $n_e$ is the electron density and $G$ is generation rate of electron-hole pairs by light. Then the average spin polarization is given as,

$$S = \frac{S_0}{1 + n_e/G\tau_s} = \frac{S_0 G\tau_s}{G\tau_s + n_e}. \tag{2.2}$$

Eq. 2.2 shows that for small intensities of light ($G\tau_s \ll n_e$), the average spin polarization is proportional to intensity and saturates at $S_0$ for higher intensity of light ($G\tau_s > n_e$). The excess electron concentration is $\Delta n = G\tau$, where $\tau$ is the lifetime of a non-equilibrium hole. If $\tau \ll \tau_s$, orientation will saturate for values of $G$ when $\Delta n \ll n_e$. Thus orientation occurs by replacing the non oriented equilibrium electrons by oriented photoexcited electrons. The optical orientation technique is used to create spin polarized electron gas in GaAs.

## 2.2 Nuclear spin system in GaAs

All the isotopes present in GaAs have spin I=3/2. The nuclear spin system is isolated from the lattice owing to long spin-lattice relaxation time $T_1$ ($\sim$ seconds to hours). But the interactions inside the nuclear spin system (dipole-dipole interaction of the nuclear magnetic moments) are characterized by much shorter times.

Each of the nuclei experiences a fluctuating local field $B_L$ created by its neighbours. This field is typically a few Gauss. The period of the nuclear spin precession in $B_L$, which is of the order of $10^{-4}$ s defines the characteristic time of interaction $T_2$ in the nuclear spin system. Because of the internal interactions, the spin system reaches internal thermodynamic equilibrium during a time $\sim T_2$ . This equilibrium state is defined by a parameter called spin temperature $\Theta_N$ [AP58], which may differ strongly

from lattice temperature. The rate at which equilibrium is reached between nuclear spins and the lattice is defined by the long spin-lattice relaxation time $T_1$.

The dipole-dipole interaction does not conserve the total nuclear spin. Thus in the absence of an external magnetic field, the average nuclear spin is zero. In the presence of an external magnetic field $\boldsymbol{B}$, the average nuclear spin $\langle \boldsymbol{I} \rangle$ is given by

$$\langle \boldsymbol{I} \rangle = \frac{1}{3} I(I+1) \frac{\mu_N \boldsymbol{B}}{k_B \Theta_N}, \tag{2.3}$$

where $\mu_N$ is the nuclear magnetic moment.

In an external magnetic field, the energy of the nuclear spin system contains two parts: (1) the Zeeman energy of all the nuclei in the system and (2) the spin-spin nuclear interaction energy. When $B \leq B_L$, there is an exchange of energy between the two parts in time $T_2$, which leads to common spin temperature. But if $B \gg B_L$, the exchange time may exceeds $T_1$ and the Zeeman and spin-spin reservoir are described by different temperatures [AP58].

Once the nuclei are cooled down to $\Theta_N$, the nuclear spin polarization $\langle \boldsymbol{I} \rangle$ and its relaxation at different magnetic field $\boldsymbol{B}$ can be studied.

## 2.3 Hyperfine interaction between electrons and nuclei

The interaction between electron and nuclear spins in semiconductors is dominated by the Fermi contact interaction:

$$\hat{H}_{hf} = \frac{16\pi}{3I} \mu_B \mu_N |\psi(\boldsymbol{R})|^2 \boldsymbol{I}.\boldsymbol{S}, \tag{2.4}$$

where $\psi(\boldsymbol{R})$ is the wave function of the electron at the nucleus, $\boldsymbol{I}$ is the nuclear spin polarization, $\boldsymbol{S}$ is the electron spin polarization, $\mu_B$ is the Bohr magneton and $\mu_N$ is the nuclear magnetic moment.

Eq. 2.4 can be written as

$$\hat{H}_{hf} = A\boldsymbol{I}.\boldsymbol{S} |\Psi(\boldsymbol{R})|^2 \nu_0, \tag{2.5}$$

where $\nu_0$ is the volume of the unit cell, $A = \frac{16\pi}{3I}\frac{\mu_B\mu_N}{\nu_0}\eta$ is the hyperfine coupling constant; $\eta = |u(0)|^2$ and $u(0)$ is the Bloch amplitude at the site of the nucleus; and $\Psi(\boldsymbol{R})$ is the envelope function of the electrons. For homogeneous distribution of electrons in the unit cell $\eta = 1$. However the electron wave function is strongly peaked at the nucleus and for GaAs, $\eta_{Ga} = 2.7 \times 10^3$, $\eta_{As} = 4.5 \times 10^3$ and $A \simeq 100$ $\mu$eV [PLSS77].

The hyperfine interaction can be described in terms of effective fields acting on both electrons and nuclei. The effective field due to electrons acting on the nuclei is known as Knight field and the effective field due to nuclei acting on the electrons is known as Overhauser field. These field are discussed in the following sections.

### 2.3.1 Overhauser field

If the lattice nuclei are polarized, then an electron experiences a field called Overhauser field due to Fermi contact hyperfine interaction. This field is due to the effect of all nuclear species in the sample and is given by:

$$\boldsymbol{B}_N = \frac{\nu_0 \sum_\alpha A_\alpha \langle \boldsymbol{I}_\alpha \rangle}{\mu_B g_e} = \sum_\alpha b_{N\alpha} \langle \boldsymbol{I}_\alpha \rangle / \langle I \rangle, \tag{2.6}$$

where $\langle \boldsymbol{I}_\alpha \rangle$ is the mean spin of the nuclei and the summation is over all the nuclei of a particular species. This field depends on electron localization volume for non-homogeneous nuclear polarization and is independent of the electrons localization volume for homogeneous nuclear polarization. Here $b_{N\alpha} = \frac{16\pi}{3g_e\nu_0}\mu_{N\alpha}\eta\xi$ is the nuclear field at saturation, and $\xi$ is the number of nuclei of the species considered in the unit cell. The sign of $b_{N\alpha}$ is defined by the sign of $g_e$, which is negative for GaAs.

$b_{N\alpha}$ is the nuclear field of a particular species of nuclei, which would appear for the case of complete nuclear polarization. For GaAs, $b_N(Ga^{69})$= -13.7 kG, $b_N(Ga^{71})$= -11.7 kG, $b_N(As^{75})$= -27.6 kG and the total nuclear field due to all the species of nuclei in GaAs is $\approx$ 5.3 T [PLSS77]. Thus in GaAs, even if the nuclear polarization is relatively small, the electron spin are subjected to a large nuclear field.

### 2.3.2 Knight field

Due to Fermi contact interaction, the nuclei also experience an effective field due to the polarized electrons known as Knight field $\boldsymbol{B}_e$.

For delocalized electrons,

$$\boldsymbol{B}_e^{del.} = \frac{8\pi}{3I} n_e \mu_B \eta 2\boldsymbol{S} = 2b_e \boldsymbol{S}, \tag{2.7}$$

where $\boldsymbol{S}$ is the average electron spin polarization and $b_e$ is the Knight field at saturation of electron spin polarization given by,

$$b_e = \frac{8\pi}{3I} n_e \mu_B \eta. \tag{2.8}$$

From Section 2.3, $\eta_{Ga} = 2.7 \times 10^3$, $\eta_{As} = 4.5 \times 10^3$. Therefore using Eq. 2.8, $b_e^{Ga}/n_e = 1.4 \times 10^{-16}$ G.cm$^{-3}$ and $b_e^{As}/n_e = 2.3 \times 10^{-16}$ G.cm$^{-3}$.

For n$_e$=2$\times$ 10$^{16}$ cm$^{-3}$, the average Knight field at saturation is $b_e = (b_e^{Ga} + b_e^{As})/2$= 3.7 G.

For localized electrons, the Knight field is proportional to its localization volume,

$$\boldsymbol{B}_e^{loc.} = -\frac{\nu_0 A}{\mu_N} |\Psi(\boldsymbol{R})|^2 \boldsymbol{S}. \tag{2.9}$$

For a localized state, the Knight field is determined by the occupation of the state and by electron spin direction. It may vary significantly as a result of capture/release of electrons by the localization center, via the exchange interaction with other electrons and precession of the electron spin in the Overhauser field. The Knight field is spatially inhomogeneous and it considerably changes from one nuclear species to another within one crystal cell.

The average Knight field at the center of the donor site at saturation due to the localized electrons at the center of the donor site is $b_e = (b_e^{Ga} + b_e^{As})/2 \simeq 100$ G [PLSS77]. Thus the Knight field due to localized as well as delocalized electrons is very weak compared to the Overhauser field.

## 2.4 Nuclear spin relaxation due to electrons

The fluctuation of the Knight field leads to spin relaxation of nuclei. The spin relaxation time of nuclei $T_{1e}$ due to interaction with electrons is given as,

$$\frac{1}{T_{1e}} = \omega_N^2 \tau_c, \tag{2.10}$$

where $\omega_N$ is the precession frequency of nuclear spin in the fluctuating effective field created by the electrons and $\tau_c$ is the correlation time of these fluctuations. In the presence of an external magnetic field $\boldsymbol{B}$,

$$\frac{1}{T_{1e}} = \frac{\omega_N^2 \tau_c}{1 + \Omega^2 \tau_c^2}, \tag{2.11}$$

where $\Omega = g_e \mu_B B/\hbar$ is the electron Larmor frequency. This shows that the relaxation rate is lowered in an external magnetic field, because the Knight field averages to zero by rapid electron spin precession.

For an electron localized in a region of radius $r_0$,

$$\omega_N^2 \sim \left(\frac{A}{\hbar N}\right)^2 F, \tag{2.12}$$

where $N \sim r_0^3/v_0$ is the number of nuclei in the localization region, $F$ is the probability for an electron to be in the localization region and $(A/\hbar N)$ is the precession frequency of a nuclear spin in the magnetic field created by a single electron.

For the case of free non-degenerate electrons, $r_0$ stands for thermal de Broglie wavelength $\lambda \sim \hbar(mT)^{-1/2}$, which implies $F \sim n_e \lambda^2$. The correlation time in this case is just the time needed for an electron to travel the distance of the order of $\lambda$. This implies $\tau_c \sim \hbar/T$. Thus for interaction of nuclei with free electrons ,

$$\frac{1}{T_{1e}} \sim A^2 v_0^2 n_e m^{3/2} T^{1/2} \hbar^{-4} \tag{2.13}$$

For the case of degenerate free electrons in the presence of an external field $\boldsymbol{B}$, the nuclear spin-lattice relaxation is governed by the well known Korringa mechanism [Abr61]. The nuclear spin relaxation is induced by flip-flops with the

thermally broadened Fermi edge electrons. The Korringa relation in the single electron approximation is given by [LHK+06],

$$\frac{1}{T_{1e}} = \frac{64}{9}\pi^3\gamma_e^2\gamma_n^2\hbar^3\eta^2 k_B T\rho^2(E_F), \tag{2.14}$$

where $\gamma_e$ and $\gamma_e$ are gyromagnetic ratios of electrons and nuclei and $\rho(E_F)$ the density of states at the Fermi level $E_F$.

For GaAs with $n_e = 2 \times 10^{16}\text{cm}^{-3}$, $T$ =2 K, $T_{1e} \sim 10^4$ s.

For the case of electrons localized in the donor, $r_0 \sim a_B$ ($a_B$ is the Bohr radius), the filling factor is $F = n_e/N_D$ ($n_e$ is the donor concentration), $\tau_e(=\tau_c)$ is the lifetime of an electron in the bound state. Then for a nucleus located at a distance $r$ from the donor site [KKF82],

$$\frac{1}{T_{1e}} \sim F\left(\frac{A^2 v_0^2 \tau_e}{a_B^6\hbar^2}\right) e^{(-4r/a_B)} \tag{2.15}$$

For a shallow donor in GaAs with $n_e = 2\times10^{15}$ cm$^{-3}$, for $r \ll a_B$, F=1, $\tau_e \sim 10^{-10}$ s, $T_{1e} \sim 0.01$ s.

This shows that localized electrons are much more effective in nuclear spin relaxation than free electrons.

## 2.5 Dynamic polarization of nuclear spins

Pumping with circularly polarized light creates non-equilibrium spin polarization in the conduction band of zincblende semiconductors e.g. GaAs. Through contact hyperfine interaction, non equilibrium spin polarization of electrons is transferred to the nuclear spins in the lattice.

$$\hat{H}_{hf} = A(\boldsymbol{I}.\boldsymbol{S}) = A(S_z.I_z + \frac{S_+I_- + S_-I_+}{2}), \tag{2.16}$$

where $\boldsymbol{I}$ is the nuclear spin operator and $\boldsymbol{S}$ is the electron spin operator. The raising and lowering operators are given by $I_\pm = I_x \pm iI_y$. The second term is responsible for spin flip-flop. This equation implies that the contact hyperfine interaction conserves the total spin of the electronic-nuclear spin system and that through mutual spin flips, or flip-flop interactions, angular momentum can be transferred from the electronic to

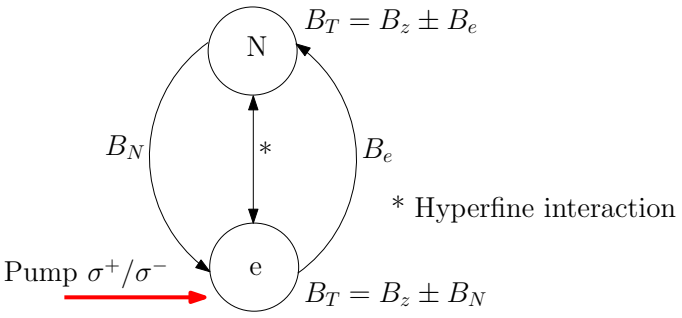


Figure 2.2: The figure shows the process of optical orientation, transfer of spin polarization to nuclei from oriented electrons and the effective fields experienced by electrons and nuclei.

the nuclear spins and vice-versa. So the total angular momentum of the electronic-nuclear spin system is conserved. The nuclear polarization along the applied magnetic field arises as a result of the establishment of thermal equilibrium between these two reservoirs. Since the longitudinal relaxation time of the nuclear spin $T_1$ is very long, the nuclear spins are isolated from the lattice in an applied magnetic field. If the external magnetic field is strong, so that $B \gg B_L$(where $B_L$ is the local field due to dipole coupling between nuclei), then spin-spin interactions between neighbour nuclei can be neglected and interactions of each nuclear spin with electrons can be considered separately. The total spin of the electron-nuclear spin system is conserved, so the balance equation for steady-state populations $N_\mu$ of nuclear spin levels can be written as,

$$W_{\mu,\mu-1} N_\mu n_{-1/2} = W_{\mu-1,\mu} N_{\mu-1} n_{+1/2}, \tag{2.17}$$

where $\mu$ is the projection of the nuclear spin in the direction of $\boldsymbol{B}$, $n_{\pm 1/2} = 1/2 \pm \langle S \rangle$ are the populations of the spin up and spin down electrons and $W_{\mu,\mu-1}, W_{\mu-1,\mu}$ are the transition probabilities from and to the level with spin population $N_\mu$.

The transition probabilities are connected by thermodynamic relations:

$$W_{\mu,\mu-1} = e^{(g\mu_B B/k_B T)} W_{\mu-1,\mu}. \tag{2.18}$$

The exponent contains the energy difference between states of the electron and nuclear spins, in which Zeeman energy of the nucleus is neglected. The energy required for each transitions is taken from the lattice, which is represented as a reservoir of

temperature $T$ .

From Eqs. (2.17) and (2.18)

$$\frac{N_\mu}{N_{\mu-1}} = \frac{(1+2\langle S\rangle)(1-2S_T)}{(1-2\langle S\rangle)(1+2S_T)}, \tag{2.19}$$

where $\langle S\rangle$ is the average electron spin and $S_T = -\frac{1}{2}\tanh(\frac{g\mu_B B}{2k_B T})$ is the equilibrium value of average electron spin. The average nuclear spin $\langle I\rangle = \sum_\mu \mu N_\mu$ can be expressed in terms of the Brillouin function,

$$\langle I\rangle = IB_I\left(\ln\left(\frac{(1+2\langle S\rangle)(1-2S_T)}{(1-2\langle S\rangle)(1+2S_T)}\right)\right). \tag{2.20}$$

Under the conditions of optical pumping $\langle S\rangle \gg S_T$, so $S_T$ can be neglected. Then retaining the first term in the expansion of the Brillouin function in terms of $\langle S\rangle$, we have

$$\langle I\rangle = \frac{4}{3}I(I+1)\langle S\rangle. \tag{2.21}$$

Generalizing Eq. (2.21) into vector form,

$$\langle \boldsymbol{I}\rangle = \frac{4}{3}I(I+1)\frac{(\langle \boldsymbol{S}\rangle.\boldsymbol{B})\boldsymbol{B}}{B^2}. \tag{2.22}$$

The dynamic nuclear polarization is caused by the component of electron spin along the applied field and the nuclear polarization is parallel to $\boldsymbol{B}$ and the average electron spin polarization.

Under the condition of optical orientation, the stationary value of dynamic polarization of nuclei is reached during time $T_{1e}$. Nuclear polarization is usually achieved due to electrons bound to donors. One can see from Eq. 2.15 that the characteristic time $T_{1e}$ increases with the increasing distance from the nucleus and the donor site. This effect was observed by Kalevich *et al.* [KKF82].

The direct polarization of nuclei located far enough from the donor center becomes ineffective. The peripheral nucleus are polarized due to nuclear spin diffusion described by diffusion coefficient $D \sim 10^{-13}$ cm$^2$/s [Pag82]. The propagation of nuclear polarization over a distance $\delta$, due to diffusion , occurs during a time of the order of $\delta^2/D$. If the time of diffusion over the distance $\delta$ is greater than $T_{1e}(\delta)$, the diffusion

ratios may be reduced as a solution of the equation $T_{1e}(\delta) = \delta^2/D$.

Nuclei for which $r < \delta$ (near nuclei) are polarized directly, while nuclei in the peripheral region $r > \delta$ are polarized by spin diffusion. Usually the optical manifestation of nuclear polarization are due to nuclei close to the donors.

## 2.6 Nuclear spin temperature

The nuclei gets polarized due to optically oriented electrons in a characteristic time $T_{1e}$. This spin transfer results in a change in Zeeman energy ($\mu_N B$) of the nuclear spin system. If this energy is of the same order as the dipole-dipole interaction between nuclei, this leads to a relaxation of nuclear nuclear spins with characteristic time $T_2$. The dipole-dipole interaction is characterized by a local field $B_L$ ($\sim$ 1-3 G for GaAs). For GaAs at B=0, $T_{1e} \gg T_2$, which implies that probability to create nuclear polarization is negligible. However it was shown that it is possible to create substantial non-equilibrium nuclear spin polarization in a weak magnetic field [DP75, FDZ76]. This is conveniently described on the basis of spin temperature concept, although a thermodynamic equilibrium is difficult to reach at field $B \gg B_L$ [AP58]. Since $T_1 \gg T_{1e}$, where $T_1$ is the spin-lattice relaxation time, the nuclear spin system is isolated from the crystal lattice. Therefore the nuclear spin relaxes to thermodynamic equilibrium in characteristic time $T_2$ of the dipole-dipole interaction and the equilibrium state is characterized by a certain nuclear spin temperature $\Theta_N$. During optical orientation, the entropy of the nuclear spin state is reduced. Then reducing $B \to 0$ allows for the nuclear spin to reach thermal equilibrium by exchanging energy between Zeeman and spin-spin reservoirs. This state is characterized by a spin temperature $\Theta_N$. When the nuclear spin temperature is very low, the external magnetic field induces an equilibrium nuclear polarization which becomes independent of the external field for $B \gg B_L$ and decays with characteristic time $T_1$.

The reciprocal nuclear spin temperature under steady state optical pumping conditions in an external field $\boldsymbol{B}$ can be expressed as [DP75, FDZ76]:

$$\beta_N = (k_B \Theta_N)^{-1} = \frac{4I}{\mu_N} \frac{(\boldsymbol{B} + \boldsymbol{B}_e).\boldsymbol{S}}{(\boldsymbol{B} + \boldsymbol{B}_e)^2 + \xi \boldsymbol{B}_L^2}, \tag{2.23}$$

where $\xi$ is a numerical factor depends on spin-spin interaction $\sim 1-3$, $B_e$ is the Knight

field defined in Eq. 2.7. The spin temperature is minimum for $|\boldsymbol{B} + \boldsymbol{B}_e| = \sqrt{\xi}|\boldsymbol{B}_L|$ and can be as low as $\approx 10^{-7}$ K for S=0.25 [DP75]. The experimentally reached spin temperature for n-GaAs is $\approx 10^{-6}$ K [KKF82].

The sign of $\beta_N$ depends on the mutual orientation of $\boldsymbol{B}$ and $\boldsymbol{S}$. More discussion about positive and negative spin temperature is provided in Appendix C.

## 2.7 Faraday rotation

In 1845, Michael Faraday discovered that the plane of polarization of a linearly polarized light is rotated upon transmission through a transparent medium in the presence of a magnetic field along the light. This is known as Faraday effect/rotation (FR). This rotation is due to magnetic field dependent circular birefringence (a difference in refractive indices for the left and right circular polarization). The refractive index difference leads to an accumulated phase shift between the two circular polarization components that comprises linearly polarized light, which is manifested as a rotation in the linear polarization axis.

The FR angle for a sample of thickness $L$, subjected to a magnetic field $\mathbf{B}$ is given as [BHL62, Bos64]:

$$\Theta_F = \frac{1}{2}\frac{\omega}{c}(n_- - n_+)L, \tag{2.24}$$

where $n_-$ and $n_+$ are the refractive indices for $\sigma^-$ and $\sigma^+$ polarized light respectively. In general, $(n_- - n_+)$ is proportional to the applied magnetic field. Therefore, Eq. 2.24 can be written as:

$$\Theta_F = VBL, \tag{2.25}$$

where $V$ is called the Verdet constant which characterizes the efficiency of the material in producing FR.

The FR is non reciprocal, i.e, the rotation is independent of the propagation direction of the light. The sign of the FR is defined to be positive (negative), if the rotation is clockwise (anti-clockwise) for an observer looking along the direction of the field $\mathbf{B}$ [BHL62]. In semiconductors, the sign of FR is important and different contributions to FR can have different signs [Car61].

Note, that in Eq. 2.24, the FR angle is proportional to $(n_- - n_+)$. In most of the optics books, it is shown to be proportional to $(n_+ - n_-)$. This difference is because

of the different convention used to define the helicity of light.

## 2.8 Faraday rotation in semiconductors

### 2.8.1 Microscopic mechanisms underlying FR

The FR in semiconductors in the presence of an external magnetic field has two main contributions. These are related to different kinds of polarization sensitive optical transitions [Car61, BHL62, BL63, Pil63, PP63, Pil64, Rot64, Bos64, AB68, JGAF94]: Free carriers contribution and interband contribution.

– Free carriers contribution (FC) (far in the transparency region)

The free carrier contribution results from virtual intra conduction band transitions between the Zeeman split Landau levels. This contribution gives a positive FR, depends on doping concentration and is dominant at higher wavelength away from the band edge (varies as $\lambda^2$) [AB68, JGAF94].

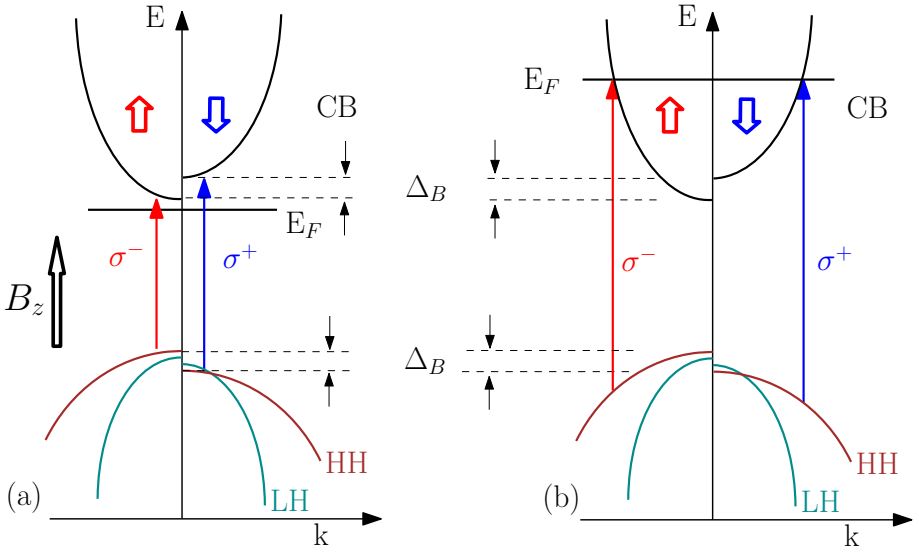


Figure 2.3: Schematic diagram of the band structure of GaAs in the presence of an external field $B_z$. This field splits the conduction and valence bands ($\Delta_B$) and creates a net spin polarization. The interband transitions for $\sigma^+$ and $\sigma^-$ component of a linearly polarized probe, for the case when the conduction band is empty (a), and when the conduction band states are occupied (b). Note that the real valence band structure is much more complicated in reality [Lut56].

- Interband contribution (close to the fundamental absorption edge)
  - Zeeman splitting (ZS)
  - Phase space filling effect (PSF)

The interband contribution results from virtual interband transitions of valence electrons from Zeeman split Landau levels of the valence band to the conduction band. This is dominant for wavelengths close to the absorption edge and decreases as the wavelength increases. The interband contribution has two sub contributions depending on whether the conduction band is empty (pure interband contribution) or the conduction band is occupied with carriers (spin contribution).

Fig. 2.3 shows the band structure of GaAs in the presence of an external field. Only the lowest Landau level is shown. The interband transitions for $\sigma^+$ and $\sigma^-$ component of a linearly polarized probe is different, because of the splitting of the valence and conduction bands in an external magnetic field. The conduction band is assumed to be empty. This results in the interband contribution to FR [AB68, JGAF94].

There is an additional contribution to FR in doped semiconductors. When the conduction band is occupied by carriers, the interband transition probability for $\sigma^+$ is different form the transition probability for $\sigma^-$ due to Pauli spin blocking (Phase space filling effect), which results in the spin contribution to the FR (see Fig. 2.3). The spin contribution depends on doping concentration and varies with wavelength as $1/\lambda$ [AB68, JGAF94].

Therefore the magnetic field induced Faraday effect has three distinct contributions:

$\Theta_F = \Theta^{FC} + \Theta^{ZS} + \Theta^{PSF}$.

### 2.8.2 Optically induced Faraday rotation

Magnetization in semiconductors can also be created optically by optical orientation mechanism [MZ84, AI73, CCS09]. Under circular polarized pumping, the chemical potential for spin up and spin down electrons changes which results in spin polarization. Also there is a splitting of the conduction band due to exchange interaction between the spin polarized electrons. This can result in the difference in refractive index $n_+$ and $n_-$. Therefore the two contributions to optically induced FR

are:

- Phase space filling effect (PSF)
- Exchange splitting of the conduction band (e-e)

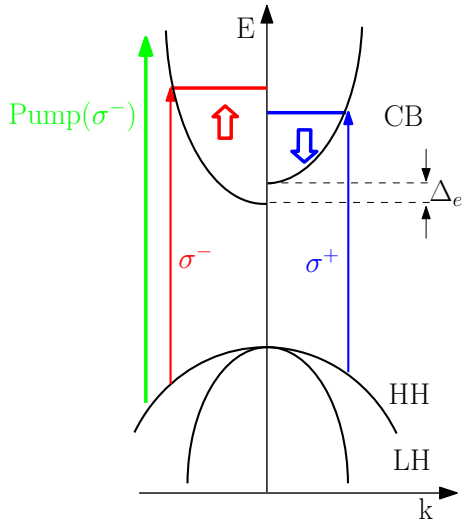


Figure 2.4: Creation of non-equilibrium spin polarization by optically pumping with circularly polarized light and the splitting of conduction band due exchange interaction of the electrons. The interband absorption for $\sigma^+$ and $\sigma^-$ components of a linearly polarized light is different because of phase space filling effect as well as splitting of the conduction band.

The phase space filling effect can be explained on the basis of optical selection rules described in section 2.1. Because of the selection rules, there are two absorption spectra, one for $\sigma^+$ and another for $\sigma^-$. A net spin polarization due to optical pumping causes blocking of absorption to these filled states (Pauli blocking) and the absorption edge is shifted. According to the Kramers-Kronig relation a difference in absorption leads to a difference in refractive indices for $\sigma^+$ and $\sigma^-$ polarizations. Since the FR arises from the difference in refractive indices, its rotation angle is proportional to the spin polarization along the direction of the light.

The exchange term of the e-e Coulomb interaction leads to a spin splitting of the conduction band, when the electrons are spin polarized. Since this interaction is ferromagnetic, it lowers the energy of the most populated spin subband. This results in a difference in absorption for $\sigma^+$ and $\sigma^-$ components of a linearly polarized probe, which causes FR.

Therefore, there are two contributions to optically induced FR:
$\Theta_F = \Theta^{e-e} + \Theta^{PSF}$.

## 2.9 Hanle effect

The depolarization of electron spins in a transverse magnetic field is known as Hanle effect. The Hanle effect is generally detected via photoluminescence. This effect was discovered by Hanle in 1924, in the fluorescence of gases [Han24], and was later applied in optical orientation experiments in semiconductors by Parsons in 1969 [Par69].

The Hanle effect can be understood in terms of a competition between spin precession and relaxation. Consider that the spins are initialized along the z-direction and the magnetic field is applied along the x-direction. Then the photoexcited spins will precess in the transverse magnetic field $B_x$ with Larmor frequency $\Omega = g_e \mu_B B_x/\hbar$. Since $B_x$ is perpendicular to the direction of light, the component of the spin along z-direction changes periodically with frequency $\Omega$.

The spin lifetime of the electrons is given as,

$$\frac{1}{T_s} = \frac{1}{\tau_J} + \frac{1}{\tau_s}, \tag{2.26}$$

where $\tau_J$ is the lifetime of an electron in the conduction band, and $\tau_s$ is the spin relaxation time. This implies, the electron spins vanishes as a result of recombination as well as relaxation. In the steady state, the recombination rate is proportional to the generation rate of carriers by photo excitation, $\tau_J = n_e/G$. Here $n_e$ is the concentration of equilibrium electrons and $G$ is the carrier generation rate [DKK+02]. Then, the spin lifetime of the electrons is given by,

$$\frac{1}{T_s} = \frac{G}{n_e} + \frac{1}{\tau_s}. \tag{2.27}$$

If during the lifetime $T_s$, the electron spin makes many revolutions around $B_x$, then the component of average spin along the initial direction will be small.

After a time t, the z-component of the spin precesses according to

$$S_z(B,t) = S_0 \cos(\Omega t) \exp(-t/\tau_s), \tag{2.28}$$

For a simple exponential decay process, the normalized number of emitted photons at a given time is

$$W(t) = \frac{1}{\tau_J} \exp(-t/\tau_J), \tag{2.29}$$

The average measured value of $S_z$ is then given by,

$$S_z(B) = \int_0^\infty W(t) S_z(t) dt = S_0 \int_0^\infty \frac{1}{\tau_J} \exp(-t/\tau_J) \cos(\Omega t) \exp(-t/\tau_s) dt, \tag{2.30}$$

which gives the well known expression for Hanle curves,

$$S_z(B) = \frac{S_z(0)}{1 + (\Omega T_s)^2} = \frac{S_z(0)}{1 + (g_e \mu_B B_x T_s/\hbar)^2}, \quad S_z(0) = \frac{S_0}{1 + \tau_J/\tau_s} \tag{2.31}$$

In this thesis, we will detect the Hanle effect via Faraday rotation. By applying a variable magnetic field transverse to the direction of initialized electron spins, we will be able to determine the spin lifetime of the electrons. The reduction of electron spin polarization and thus $\Theta_F$, in a transverse magnetic field is described by the Lorentz curve [DKK+02],

$$\Theta_F(B) = \frac{\Theta_F(0)}{1 + (g_e \mu_B B_x T_s/\hbar)^2}. \tag{2.32}$$

where $\mu_B$ is the Bohr magneton, $T_s$ is the electron spin lifetime and $g_e$ is the electron g-factor.

The full width at half maximum (FWHM) of the Lorentz curve is inversely proportional to the spin lifetime:

$$B_{FWHM} = (2\hbar/g_e \mu_B T_s). \tag{2.33}$$

This allows for the measurement of the spin lifetime and and by extrapolation to G=0, the spin relaxation time.

## 2.10 Planar semiconductor microcavities

Semiconductor planar microcavity structures are fabricated using either metallic or dielectric distributed Bragg reflectors (DBRs). The highest quality DBRs such as $Al_xGa_{1-x}As$/AlAs are fabricated using molecular beam epitaxy (MBE), which allows the growth of layers with atomic-scale thickness control. The light is localized strongly in the cavity allowing for strong light-matter interaction and the strength of the localization is defined by the quality factor of the cavity, $Q$. The cross-section of a typical Fabry-Perot cavity is shown in Fig. 2.5, with the cavity material placed in between the two DBRs. For a Fabry-Perot cavity cavity with ideal mirrors, the resonance conditions are given by $L = m\lambda/2$, where $m$ is an integer and $L$ is the cavity length and $\lambda$ is the wavelength of the light within the cavity.

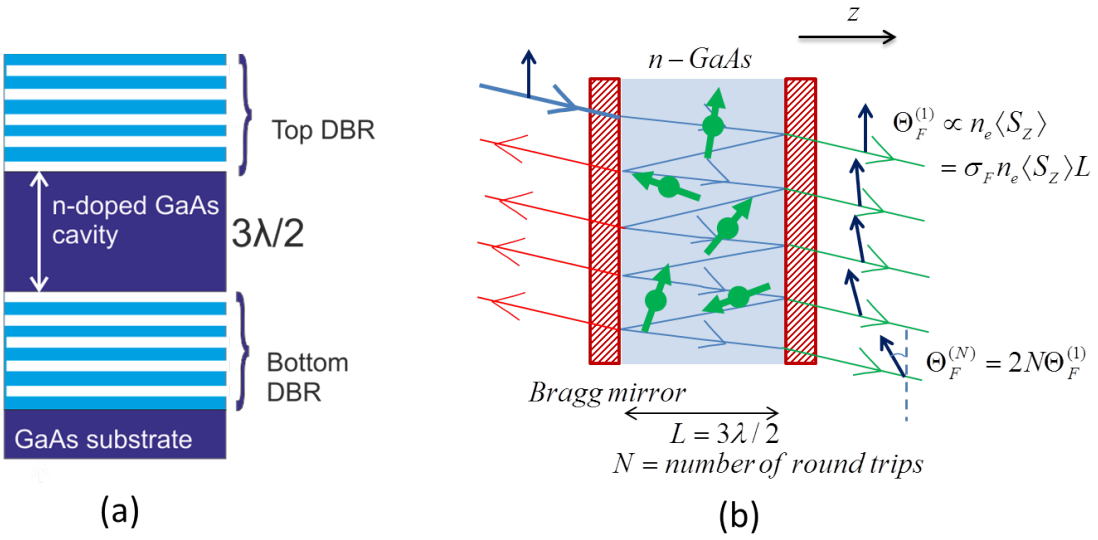


Figure 2.5: (a) Cross-section of a typical Fabry-Perot cavity where two DBR mirrors are separated by the cavity material (n-doped GaAs), (b) the incident light travels multiple round trips inside the cavity, and the plane of polarization is rotated which depends on the number of round trips and thickness of the cavity material.

The calculated reflectivity spectra of a GaAs microcavity with $Al_xGa_{1-x}As$/AlAs DBRs is shown in Fig. 2.6. One can see the Bragg plateau characterized with almost 100 % reflectivity and the cavity mode at the energy defined by resonance condition.

The optical absorption in GaAs is possible only at small thickness, because above

$E_g$ the penetration depth is about 1 $\mu$m ( absorption coefficient $10^4$ cm$^{-1}$). Therefore, spin polarization is created in thickness $\sim$ 1 $\mu$m. Since FR is proportional to the thickness of the spin polarized area, the rotation angle is expected to be small. We will use a microcavity to amplify the FR induced by the optically oriented electrons. This enhancement is due to multiple round trips of light between the Bragg mirrors. This idea has already been employed to study the FR in quantum wells embedded in a microcavity where polarization was induced either by optical orientation [KVK97], or magnetic field [SM05].

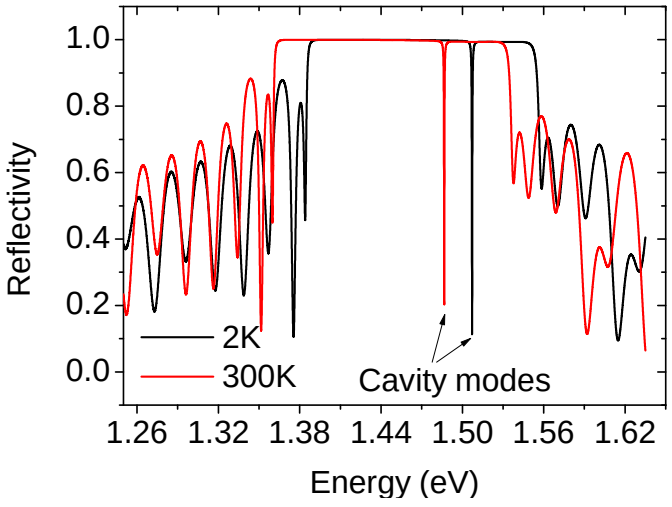


Figure 2.6: The calculated reflectivity spectra of a GaAs microcavity with light incident at 0° at temperatures 2 K and 300 K showing the temperature dependent cavity modes.

One can roughly estimate the amplification factor of FR by the microcavity, as being two times the number of round trips of light in the microcavity.

$$\Theta_F^{cav} = 2N\Theta_F, \tag{2.34}$$

where $N$ is the number of round trips inside the cavity.

For a $m\lambda/2$ cavity of thickness $L$, $N$ can be calculated as follows:
Thickness of the cavity is,

$$L = \frac{m}{2}\frac{\lambda_{res}}{n}, \tag{2.35}$$

where $\lambda_{res}$ is the vacuum resonance wavelength and $n$ is the refractive index of the cavity medium. Therefore,

$$\lambda_{res} = \frac{2}{m} nL. \tag{2.36}$$

$$\nu_{res} = \frac{c}{\lambda_{res}} = m\frac{c}{2nd} = m\nu_{FSR}, \tag{2.37}$$

where $\nu_{FSR}$ is the free spectral range.

Effective length the light travels inside the cavity,

$$d_{eff} = N.2L, \tag{2.38}$$

where $N$ is the number of round trips inside the cavity.

The number of round trips inside the cavity is,

$$\begin{aligned} N &= \frac{\tau}{\tau_{1trip}} = \nu_{FSR}.\tau = \nu_{FSR}\frac{1}{2\pi\Delta\nu} \\ &= \frac{\nu_{res}}{m}\frac{1}{2\pi\Delta\nu} = \frac{1}{2\pi m}\frac{\nu_{res}}{\Delta\nu} = \frac{Q}{2\pi m}, \end{aligned} \tag{2.39}$$

where $\Delta\nu$ is the full width at half maximum of the cavity modes, $Q$ is the quality factor of the cavity, $\tau$ is the lifetime of the photons in the cavity and $\tau_{1trip}$ is the time for one round trip of light inside the cavity.

$$\begin{aligned} d_{eff} = N.2L &= \frac{Q}{2\pi m}2L = \frac{QL}{m\pi} \\ &= \frac{Q}{m\pi}(m\frac{\lambda_{res}}{2n}) = \frac{Q\lambda_{res}}{2\pi n}. \end{aligned} \tag{2.40}$$

Using equation 2.38 and 2.40,

$$N = \frac{Q\lambda_{res}}{4\pi nL}. \tag{2.41}$$

The Quality factor of the microcavity is related with the width of the cavity mode and we can calculate N, if we know the cavity mode and its width. The Faraday rotation amplified by the microcavity is,

$$\Theta_F^{cav} = 2N\Theta_F = \frac{Q}{m\pi}\Theta_F. \tag{2.42}$$

# Chapter 3

# Samples and experimental techniques

In this Chapter, the samples and the experimental techniques employed in the study of spin dynamics of electrons and nuclei are discussed. In Section 3.1, a detailed description of the microcavity samples is provided. The quality factor of the microcavity is measured using interferometric method and its detuning dependence is studied (see Section 3.1.1). The schemes used to detect Faraday rotation (FR) and the conventions used to determine the sign of FR are described in Section 3.2. Finally the laser systems, cryostats and various optical setups used to perform Faraday rotation and polarized photoluminescence experiments are introduced in Section 3.3.

## 3.1 GaAs microcavity samples

In this thesis we studied two different n-GaAs layers, sandwiched between Bragg mirrors to form a semiconductor microcavity. The samples are grown by molecular beam epitaxy (MBE) at LPN, Marcoussis, France. Each sample consists of about 3581 Å thick Si-doped GaAs cavity sandwiched between two Bragg mirrors, consisting of 25(30) AlAs/$Al_{0.1}Ga_{0.9}As$ pairs for the upper (bottom) mirrors. The doping density of the cavity layers are $n_e = 2 \times 10^{16}$ cm$^{-3}$ (sample 98P180) and $n_e = 2 \times 10^{15}$ cm$^{-3}$ (sample C7T76). The samples are grown on a 400 $\mu$m thick undoped GaAs substrate. The optical cavity length is $3\lambda/2$ and is wedge-shaped in order to have the possibility

to tune the cavity mode energy by varying the spot position on the samples. The samples are designed to have a cavity mode $\sim$ 20 meV below the band gap of GaAs and the stop band limit about $\sim$ 30 meV above the band gap, to allow for optical orientation via pumping above the stop band . The schematic cross-section of the structure and the calculated transmitted spectrum of the cavity is shown in Fig. 3.1.

(a)

| | | |
|---|---|---|
| | Air | Epaisseur (A) |
| | GaAs | 597 |
| | AlAs | 714 |
| X 25 | $Al_{0.1}Ga_{0.9}As$ | 607 |
| | AlAs | 714 |
| 3λ/2 Cavity | GaAs dopé n = $2x10^{16}$/ $2x10^{15}$ | 3581 |
| X 30 | AlAs | 714 |
| | $Al_{0.1}Ga_{0.9}As$ | 607 |
| | AlAs | 714 |
| | Substrat non dopé | |

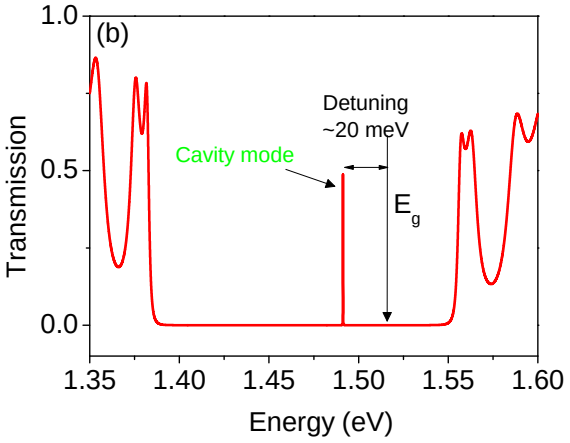


Figure 3.1: (a) The $n$-doped GaAs microcavity sample, and (b) the calculated transmission spectrum of the cavity showing the stop band and the cavity mode.

### 3.1.1 Measurement of the quality factor of the microcavity

The quality factor of the sample was measured using a homemade Michelson interferometer. From the width of the interferogram, $\Delta t$ (Fig. 3.2(a)), we can deduce $\Delta\nu$ by using $\Delta\nu = 0.612/\Delta t$, which is valid for Gaussian pulses. The quality factor is obtained using the formula: Q=E/h$\Delta\nu$.

We measured the quality factor of the sample 98P180 at different position in the sample to find out the detuning dependence. One can see from Fig. 3.2(b) that variation of quality factor with detuning is not significant and $Q \approx 19280 \pm 480$. Since the structure of the sample C7T76 is same except for the doping density, the quality factor would be of the same order.

Then the effective length the light travels inside the cavity, using equation 2.40, is $d_{eff} = \frac{QL}{3\pi} \approx 0.7$ mm.

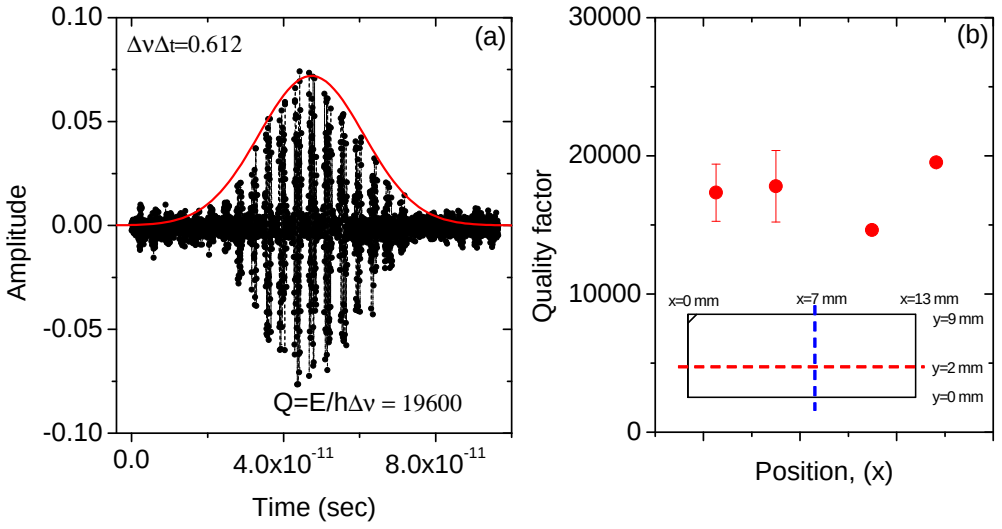


Figure 3.2: (a) A typical interferogram, used for the measurement of the quality factor, obtained at a certain position in the sample. The red curve is a Gaussian fit of the envelope of the interferogram $\Delta t$. (b) The quality factor measured at different positions (detuning) in the sample. It indicates that variation of quality factor with detuning is not significant.

## 3.2 Detection of Faraday rotation

The Faraday rotation (FR) experimental setup is shown in Fig. 3.3. The detection scheme is analyzed within the Jones formalism [Fow89, BW02], deriving a relation between the detector signal and the change in polarization state of the transmitted light.

Suppose the laser beam is polarized along the x-axis and is propagating along the z-axis. The electric field in terms of Jones formalism is:

$$E(t) = \begin{pmatrix} 1 \\ 0 \end{pmatrix} E_0 e^{i(kz-\omega t)}, \tag{3.1}$$

where $E_0$ is the amplitude of the electric field of the laser beam.

After passing through the sample, the polarization of the laser is rotated by a

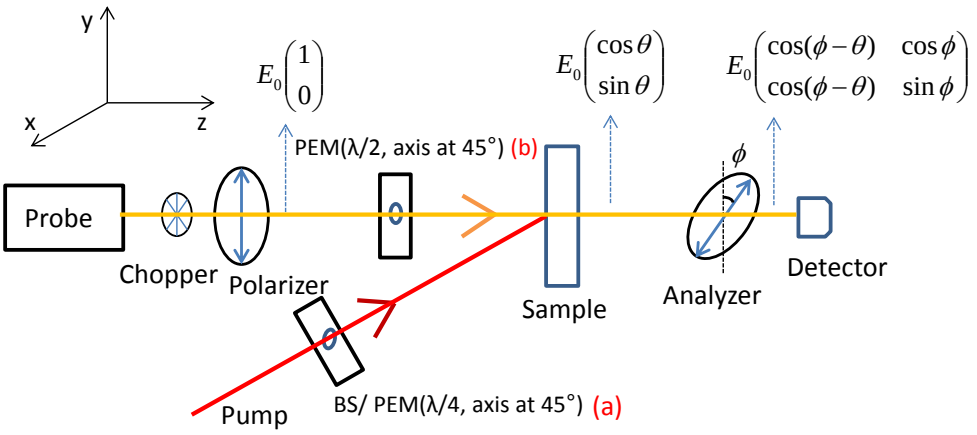


Figure 3.3: Detection scheme of Faraday rotation. The photoelastic modulator (PEM) is used to either modulate the pump polarization between $\sigma^+$ and $\sigma^-$ (a), or to modulate the probe between two linear polarizations (b).

small angle $\theta$ and is represented as:

$$E(t) = \begin{pmatrix}\cos\theta\\\sin\theta\end{pmatrix} E_0 e^{i(kz-\omega t)}. \tag{3.2}$$

The electric field of the laser after passing through the analyzer, which is set at an angle $\phi$ with respect to the polarizer is given as:

$$E(t) = \begin{pmatrix}\cos(\phi-\theta) & \cos\phi\\\cos(\phi-\theta) & \sin\phi\end{pmatrix} E_0 e^{i(kz-\omega t)}. \tag{3.3}$$

The light intensity measured by the detector is

$$I(t) = E(t)E(t)^* = E_0^2\cos^2(\phi-\theta). \tag{3.4}$$

Equation (3.4) implies that the FR ($\theta$) manifests itself as a change in intensity at the detector. To get maximum change in intensity, the analyzer angle needs to be optimized.

Differentiating the intensity with respect to $\theta$, we get

$$\begin{aligned}\frac{dI(t)}{d\theta} &= 2E_0^2\cos(\phi-\theta)\sin(\phi-\theta)\\ &= E_0^2\sin 2(\phi-\theta).\end{aligned} \tag{3.5}$$

If Faraday rotation $\theta << \phi$, maximum modulation of the probe is obtained when the polarizer and analyzer are set at $\phi = 45°$ with each other.

Simplifying Eq. (3.4), total intensity measured by the detector is

$$\begin{aligned}I(t) &= \frac{E_0^2}{2}[1+\cos 2(\phi-\theta)]\\ &= \frac{E_0^2}{2}[1+\cos(2\phi)\cos(2\theta)+\sin(2\phi)\sin(2\theta)].\end{aligned} \tag{3.6}$$

For $\phi = 45°$, we have

$$I(t) = \frac{I_0}{2}[1+\sin 2\theta]. \tag{3.7}$$

Two modulation schemes are used depending on whether nuclear polarization is desired or not. These two conditions are described as follows:

**Scheme (a):** In this case, the intensity of the probe is modulated by the chopper and the rotation angle is modulated by modulating the pump polarization. Then,

$$I(t) = \frac{I_0(t)}{2}[1+\sin 2\theta(t)]. \tag{3.8}$$

Modulation of the circular polarization of the pump beam with a photoelastic modulator (PEM) (with modulation frequency $f$) results in modulation of the spin polarization of the electrons and therefore in modulation of FR.

$$\theta(t) = \theta_0\sin(2\pi ft). \tag{3.9}$$

Therefore

$$I(t) = \frac{I_0(t)}{2}[1+\sin(2\theta_0\sin(2\pi ft))]. \tag{3.10}$$

Expanding $\sin(2\theta_0 \sin(2\pi ft))$ in a Fourier series by using Bessel functions, we get

$$I(t) = \frac{I_0(t)}{2}[1 + 2J_1(2\theta_0)\sin(2\pi ft) + 2J_3(2\theta_0)\sin(6\pi ft) + \text{higher odd harmonics of f}]. \tag{3.11}$$

The transmitted probe intensity is modulated by the chopper at frequency $f_c$. Keeping only the first harmonic we get

$$I_0(t) = I_0[\frac{1}{2} + \frac{2}{\pi}\sin(2\pi f_c t)] + ..... \tag{3.12}$$

For small rotation angle, $J_1(2\theta_0)$ can be approximated to be $\theta_0$. Then Eq. 3.11 can be written as:

$$I(t) = I_0[\frac{1}{2} + \frac{2}{\pi}\sin(2\pi f_c t)][\frac{1}{2} + \theta_0 \sin(2\pi ft) + ...] \tag{3.13}$$

$$= I_0[\frac{1}{4} + \frac{1}{\pi}\sin(2\pi f_c t) + \frac{\theta_0}{2}\sin(2\pi ft) + ...]. \tag{3.14}$$

Assuming that the gain of the detector does not depend on frequency, demodulation of the signal at frequencies $f$ ($I_f$) and $f_c$ ($I_c$) gives the amplitude of the FR as,

$$\theta_0 = \frac{2}{\pi}\frac{I_f}{I_c}. \tag{3.15}$$

In practice, we use $\theta_0 = C\frac{I_f}{I_c}$, where C is the calibration factor determined by rotating the analyzer by a known angle.

**Scheme (b):** In this case, the intensity of the probe is modulated by the chopper and polarization of the probe beam is modulated by the PEM. FR angle can be calculated similar to the previous case.

### 3.2.1 Definition of the sign of Faraday rotation

Fig. 3.4 shows the experimental setup for a typical FR measurement. The analyzer is rotated by 90° with respect to the linear polarizer and no light is detected. By application of an external field, the polarization plane of the light is rotated proportional to the electron spin polarization, and we detect some signal at the detector. The angle by which the analyzer has to be rotated again in order to obtain

zero signal at the detector is the FR angle. If this rotation is clockwise looking in the direction of the field **B**, then the angle is defined as positive.

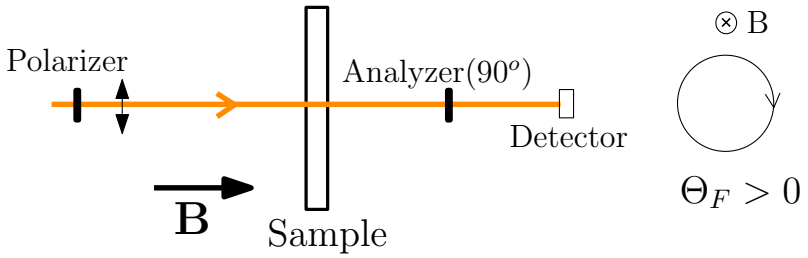


Figure 3.4: Convention used to determine the sign of Faraday rotation.

For the case of optically induced FR there is no magnetic field, and we adopt the convention that if the rotation is clockwise looking along the direction of spin polarization, then the angle is positive.

## 3.3 Overview of experimental setups

### 3.3.1 Laser system

The pump laser source used for all the experiments is a diode laser emitting at 780 nm which gives up to 40 mW of continuous wave power. The circular polarizations of the pump was set using either a Babinet-Soleil compensator (BS) or a Fresnel Rhomb retarder (to have fixed pump polarization) or with a photoelastic modulator (PEM) set at retardance of $\lambda/4$ (to have modulated circular polarization).

The probe laser used is either a continuous wave $Al_2O_3$:Ti laser (Spectra physics 3900) or a pulsed $Al_2O_3$:Ti laser (Spectra-Physics Tsunami) delivering 80 fs pulses at repetition rate of 82 MHz which can give power up to 800 mW. For the cw laser, the birefringent filter within the cavity is used to tune the output laser light in the region 700-1000 nm. But most of the experiments were done with the pulsed laser. At the beginning pulses were not filtered, but for later experiments, particularly with the sample C7T76, the pulses were filtered with dispersion line. The wavelength of the probe used is centered around 828 nm which is resonant with the cavity mode. The output from Ti:Sapphire laser was linearly polarized and during some experiments a

photoelastic modulator set at retardance of $\lambda/2$ was used to obtain modulated linear polarization.

### 3.3.2 Liquid Helium Cryostat

The spin lifetime of electrons in GaAs depends strongly on temperature. Therefore all the experiments were done at cryogenic temperatures using either Helium bath cryostat (Homemade) or a cold finger cryostat (Oxford instruments) or a magneto optical cryostat (Cryogenics Ltd.).

The Helium bath cryostat operates at temperature of 2 K only. The sample is mounted at the end of a sample rod and is placed in the inner region of the cryostat which is thermally isolated by a high vacuum outer chamber.

The He-flow cryostat has a cold finger that is cooled by liquid Helium. The temperature of the sample is controlled by Helium flow and the operates at temperature from 4 K- 300 K. The cryostats are placed on a x, y, z stage to control position of the sample. The cryostats are placed in between a large Helmholtz coil which can provide field up to 200 G. Also a three axis Helmholtz coil is used to compensate the laboratory field in three directions which can provide field up to 10 G in any direction. These two cryostats are used for most of the experiments.

The magneto optical cryostat from Cryogenics Ltd. was used for field induced Faraday rotation measurements. It operates at temperature from 2 K to 300 K and can provide field up to 10 T. The cryostat has four windows that allow optical access to the sample both in Voigt and Faraday geometry.

### 3.3.3 Photoinduced Faraday rotation and Hanle effect

The experimental setup used to measure the cw-FR and the Hanle effect is shown in Fig. 3.5. A photoelastic modulator (PEM), set to $\lambda/4$ retardance, was used to modulate the pump polarization between $\sigma^+$ and $\sigma^-$ polarization at $f$=50 kHz, and thus the electron spin polarization (see Scheme (a) in Section 3.2). As the modulation frequency is larger than the nuclear spin relaxation rate, the dynamic nuclear polarization of the nuclei is strongly suppressed. Helmholtz coils are used to apply field either in the longitudinal or transverse direction. The spin polarization of

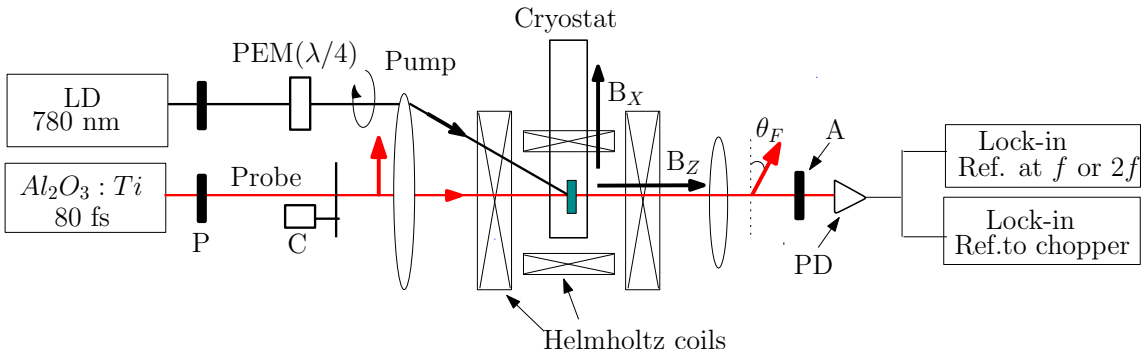


Figure 3.5: The setup for cw-Faraday rotation and Hanle effect experiments. Helmholtz coils used to apply longitudinal and/or transverse magnetic field (LD: laser diode, P: polarizer, C: chopper, PEM: photoelastic modulator, A: analyzer, PD: photodiode).

photoexcited electrons is partly transferred to the electron gas, which gets polarized and induces a modulated FR of the probe beam.

The FR is detected with a linear polarization analyzer and a photodiode. The total signal ($I_c$) was recorded with chopper frequency ($f_c$) and the differential signal ($I_f$) was recorded with PEM $f$ reference and the FR angle is obtained using Eq. 3.15. A transverse magnetic field causes depolarization of the electron spin (Hanle effect), which reduces $\theta_F$. The spin relaxation time of the electrons is extracted from the Hanle curves, as discussed in section 4.1.3.

### 3.3.4 Time resolved Faraday rotation

The setup used for time resolved measurement of the FR induced by a pump pulse is shown in Fig. 3.6. The aim of such experiment is to measure directly the build up and relaxation time of electron spin polarization. Microsecond long pulses with rise time and decay time of about 10 ns are shaped from the cw-laser diode by an acousto-optic modulator (AOM). A Babinet-Soleil compensator (BS) is used to set the polarization either as $\sigma^+$ or $\sigma^-$. The build up of electron spin polarization during pumping and its decay after the pump is switched off are monitored via FR ($\theta_F(t)$) of the probe beam delivered by cw-$Al_2O_3$:Ti laser.

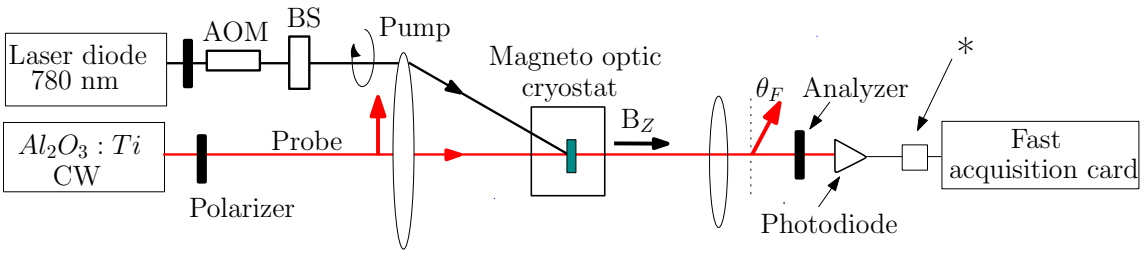


Figure 3.6: Set up for measuring time resolved Faraday rotation induced by micro-second lung pulses. The symbol (∗) represents the low noise and large bandwidth transimpedance pre-amplifier.

The intensity incident on the detector, using Eq. 3.14 is,

$$I(t) = I_0(t)[\frac{1}{2} + \theta_F(t)]. \tag{3.16}$$

This signal was sampled with a fast acquisition card with sampling rate of 200 MHz.

### 3.3.5 Polarized Photoluminescence

The setup used for the polarized photoluminescence (PL) measurements is shown in Fig. 3.7. This is used to measure spin polarization of electrons and compare with the determination from Knight field. The excitation intensity was modulated at about 300 Hz and the PEM was used to modulate the polarization between $\sigma^+$ and $\sigma^-$ at 50 kHz. The photoluminescence was collected, passed through a circular polarization analyzer (BS) and then a grating spectrometer (IHR 550). A photomultiplier tube connected with two lock-in amplifiers was used to extract the signal. One lock-in amplifier operated synchronously with the PEM to detect the differential signal $(I_+ - I_-)$ and the other lock-in operated synchronously with the optical chopper to provide the total signal $(I_+ + I_-)$, where $I_+$ and $I_-$ are the intensity of the $\sigma^+$ and $\sigma^-$ polarized PL respectively.

The degree of circular polarization of the luminescence is obtained using the equation,

$$\rho_c = C(I_+ - I_-)/(I_+ + I_-), \tag{3.17}$$

where the calibration factor $C$ is determined by placing a circular polarizer before the BS.

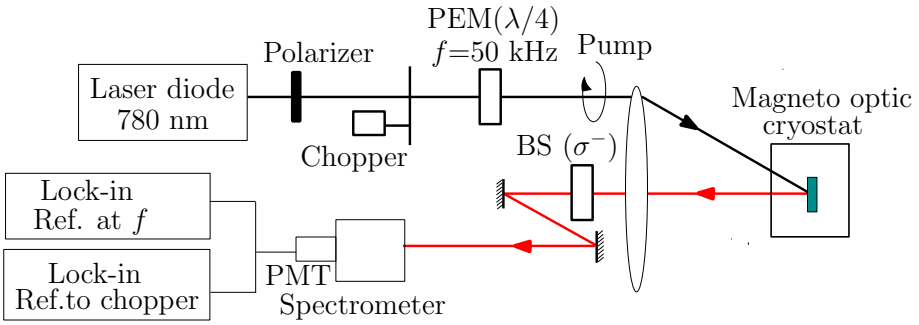


Figure 3.7: Setup for measurement of polarized photoluminescence.

### 3.3.6 Nuclear spin cooling and nuclear magnetic resonance

The experimental setup used to dynamically polarize the nuclei, measure the Knight and Overhauser fields, measure nuclear FR and detect the nuclear magnetic resonance using FR, is shown in Fig. 3.8. The Helmholtz coils placed outside the cryostat are used to apply field either in the longitudinal or transverse direction. A small Helmholtz coil surrounding the sample is placed inside the cryostat in order to have the possibility to apply rf-field. A Babinet-Soleil compensator is used to set a fixed pump polarization (either $\sigma^+$ or $\sigma^-$). The linear polarization of the probe is modulated with a PEM set at retardance of $\lambda/2$ (see Scheme (b) in Section 3.2). The total signal ($I_c$) was recorded with chopper frequency ($f_c$) and the differential signal ($I_{2f}$) was recorded with PEM $2f$ reference and the nuclear FR is obtained using Eq. 3.15.

For the measurement of nuclear FR in the sample C7T76 (see Chap. 6), we have used a liquid crystal (LC) variable phase retarder (ARCoptix) to obtain fixed or modulated circular polarizations of the pump. The optical phase retardance is electrically tunable and we controlled it using the LC driver from ARCoptix. We have also used a homemade electrically controlled shutter, to be able to switch on/off the pump beam automatically. Using the LC phase retarder and the shutter, we can do a sequence of nuclear FR measurements, where the change of pump polarization or switching on/off the pump are fully automated.

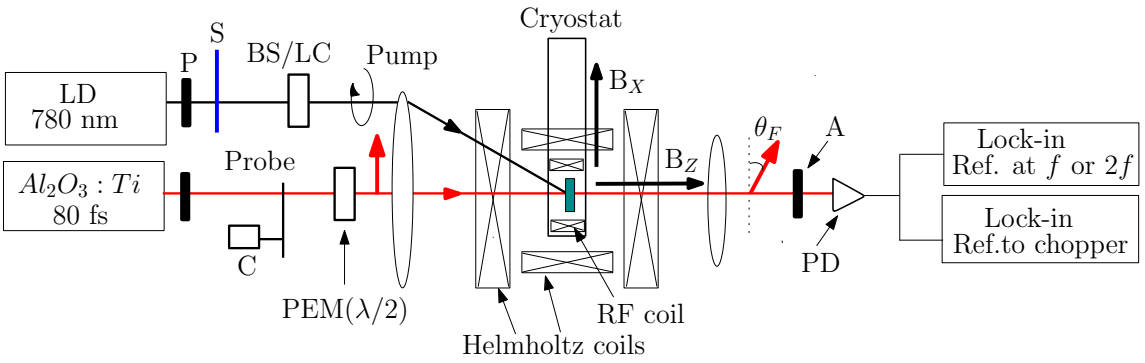


Figure 3.8: The setup for dynamic polarization of nuclei and detection of NMR using Faraday rotation (LD: laser diode, P: polarizer, C: chopper, S: shutter, LC: liquid crystal variable phase retarder, polarization modulator, PEM: photoelastic modulator, BS: Babinet-Soleil compensator, A: analyzer, PD: photodiode).

## 3.4 Summary

In this Chapter, we have discussed in detail about the structure of the GaAs microcavity samples. The quality factor of the samples is very high, Q $\approx$ 18000 for 98P180 (similar Q for the sample C7T76) and the variation of Q with detuning is not significant. We estimated that the effective length the light travels inside the microcavity is about 700 $\mu$m. We have introduced the detection scheme to measure FR. Various experimental techniques were presented to measure the electron and nuclear spin dynamics following optical excitation. We will use cw FR measurements to study the pump power dependence of FR and to check that FR is proportional to the degree of electron spin polarization. From the Hanle effect measurements we will deduce the spin lifetime of the electrons. The evolution of electron spin polarization during pumping and relaxation in the dark will be studied by the time-resolved FR measurements. Nuclear spin cooling experiments will be used to measure the Knight field, Overhauser field and probe the nuclear spin dynamics. Polarized PL measurement will be used to measure the degree of electron spin polarization and compare with the estimation from the Knight field.

# Chapter 4

# Faraday rotation induced by spin polarized electrons

In this Chapter, experimental results on the Faraday rotation (FR) induced by spin polarized electrons created either by optical pumping (Section 4.1) or by magnetic field (Section 4.2) are presented. Optically oriented electrons produce FR of a linearly polarized probe beam. The effects of pump power, pump polarization, and the wavelength of the probe on FR are discussed in Section 4.1.2. Spin lifetime of the electrons is measured using Hanle depolarization of FR in a transverse magnetic field and is presented in Section 4.1.3. The degree of spin polarization of optically oriented electron is measured indirectly from the Knight field measurement [KKF82] and also directly by polarized photoluminescence and presented in Section 4.1.4. A concept of Faraday rotation cross-section is introduced in Section 4.1.5, which provides a measure of the efficiency of a spin density in producing FR. A theory of photoinduced FR is formulated following the theoretical model of Aronov and Ivchenko [AI73]. The photoinduced FR cross-section is calculated theoretically and compared with the one obtained from experimental results (Section 4.1.6).

The FR induced by application of an external magnetic field is studied as a function of detuning and at different temperatures (Section 4.2). The temperature dependent FR is explained by a simple theoretical model and is presented in Section 4.2.1. The field induced FR cross-section is calculated theoretically and compared with the one obtained from experimental results (Section 4.2.2).

In Section 4.3, a comparison of photo induced FR cross-section with that of field induced one is provided. Fast optical switching of photo induced FR in a nanosecond time scale is demonstrated in Section 4.4.

## 4.1 Photoinduced Faraday rotation

As we have seen in Section 2.8.2, spin polarized electrons created by circularly polarized light can produce FR of a linearly polarized probe. The experimental setup used to measure FR induced by optically oriented electrons is described in Section 3.3.3.

### 4.1.1 Dependence on probe wavelength and pump polarization

The preliminary FR measurements were done as a function of detuning of the cavity mode with respect to the energy gap of GaAs, and pump polarization. We measured FR at different positions in the sample, in order to obtain the detuning at which FR is optimum. We find that FR is maximum for energy of about 1.498 eV which is $\sim$ 16 meV below the GaAs band gap (see Fig. 4.1).

The photoinduced FR was measured for different polarizations of the pump and it was observed that FR angle is negative with $\sigma^-$ pump and the rotation is positive for $\sigma^+$ pump as shown in Fig. 4.1. This can be explained on the basis of optical selection rules for zincblende semi-conductors as described in Section 2.1 and 2.8.2. For the case of $\sigma^-$ ($\sigma^+$) polarization of the pump, according to the selection rules, spin polarization $S_z = +1/2$ ($S_z = -1/2$) will be created and we will see in Section 4.1.5 that the FR cross-section is negative ($\sigma_F^{sf} < 0$). Then using Eq. 4.23 it can be seen that the FR angle is positive (negative) for $\sigma^+$ ($\sigma^-$) polarization of the pump.

### 4.1.2 Dependence on pump power

We measure the pump power dependence of FR to check that the FR angle, $\Theta_F$ is proportional to the electron spin polarization, $S_z$. The circularly polarized pump (780 nm) was focussed on a 50 $\mu$m spot diameter with pump power varying from 3

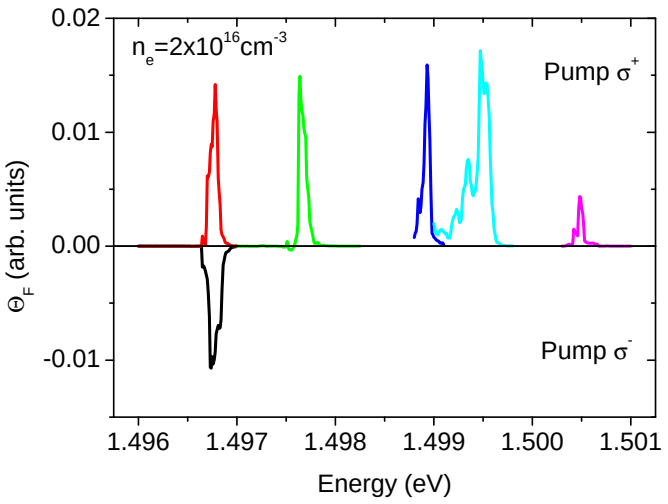


Figure 4.1: The Faraday rotation measured with fixed pump polarizations $\sigma^+(\Theta_F > 0)$ or $\sigma^-(\Theta_F < 0)$ at different detuning.

$\mu$W to 1 mW and the FR is measured at 2 K. The photoinduced FR as a function of pump power density is shown in Fig. 4.2. It can be seen from the figure that the FR increases sublinearly with pump power and saturates at high power at which the rotation exceeds 10°.

Now we try to understand the saturation of FR with pump power. The FR induced by spin polarized electrons has been modeled theoretically by Aronov and Ivchenko [AI73]. It was found that the FR is proportional to electron spin density, $\langle S_z \rangle$ in a spin polarized electron system. The electron spin density is given as:

$$\langle S_z \rangle = (n_{1/2} - n_{-1/2})/2, \tag{4.1}$$

where $n_{1/2}$ ($n_{-1/2}$) is the density of electrons with spin projection in the direction of (opposite to) the light propagation direction. The electron spin polarization degree is given as:

$$\rho_e = (n_{1/2} - n_{-1/2})/(n_{1/2} + n_{-1/2}). \tag{4.2}$$

For the sample 98P180, the density of photo generated electrons is much smaller than resident electron density $n_e$. Hence, electron spin polarization degree can be

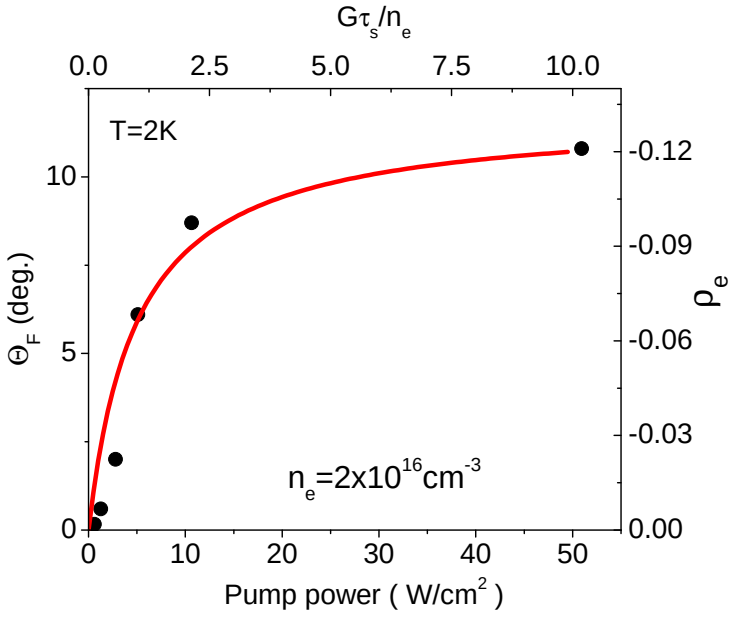


Figure 4.2: Left scale: Faraday rotation as a function of pump power (closed circles). Right scale: electron spin polarization calculated with Eq. 4.5 plotted as a function of $G\tau_s/n_e$ (solid line).

related with electron spin density $\langle S_z \rangle$ as

$$\rho_e = \frac{2\langle S_z \rangle}{n_e}. \tag{4.3}$$

Therefore, the FR is proportional to the spin polarization of the electron gas,

$$\Theta_F = \mu \rho_e. \tag{4.4}$$

where $\mu$ is a proportionality factor, which will be determined experimentally from the measurement of electron spin polarization (Section 4.1.4).

From the rate equations for spin up and spin down electron density in the presence of optical pumping and recombination, and assuming that the excess carrier recombination time is shorter than electron spin relaxation time $\tau_s$ ($\tau_s = 160$ ns for $n_e = 2 \times 10^{16}\text{cm}^{-3}$) (Section 4.1.3), the degree of electron spin polarization is given as ( see Section 2.1),

$$\rho_e = \rho_i G\tau_s/(n_e + G\tau_s), \tag{4.5}$$

where $\rho_i$ is the initial spin polarization of the photoexcited carriers after they have thermalized to the bottom of the conduction band. Since the initial kinetic energy of the carriers is relatively large ($\approx$ 75 meV), they are likely to be partially depolarized before they thermalize [ES71], so that $\rho_i < 0.5$. The holes are assumed to be completely depolarized immediately after photoexcitation, similar to the classical optical orientation experiments in bulk semiconductors [DP71b].

The spin polarization degree calculated using Eq. 4.5 is plotted as a function of generation rate and compared with the pump power dependence of FR [Fig. 4.2]. Here we have used the independently measured value of electron spin polarization $\rho_e = 0.11$ at 50 W/cm$^2$ (Section 4.1.4) and $\tau_s = 160$ ns (Section 4.1.3). For calculation of the generation rate $G$, we assumed absorption coefficient $\alpha = 10^4$ cm$^{-1}$ [Stu62], the reflection coefficient $R = 0.5$ and 50 $\mu$m spot diameter.

It can be seen from Fig. 4.2 that saturation of FR is well reproduced by the saturation of $\rho_e$ and therefore $S_z$.

### 4.1.3 Measurement of electron spin relaxation time

When a transverse magnetic field $B_x$ is applied, the spin polarized electrons created by optical pumping precesses around the field and gets depolarized, known as Hanle effect. The Hanle effect detected by photoluminescence polarization has been used to measure spin relaxation time of electrons in semiconductors [MZ84]. Crooker *et al.* [CCS09] used Hanle effect, detected by FR of a off-resonant probe beam to measure the spin relaxation time of electrons in n-GaAs. We follow the same method here and the setup used for this purpose is shown in Fig. 3.5. The depolarization of FR in transverse field from -30 G to +30 G at temperature 2 K is measured with pump power varying from 3 $\mu$W to 1 mW and are shown in Fig. 4.3(a). The reduction of electron spin polarization and thus $\Theta_F$, in a transverse magnetic field is described by the Lorentz curve,

$$\Theta_F(B) \propto \frac{1}{1 + (g_e \mu_B B_x T_s/\hbar)^2}. \tag{4.6}$$

where $\mu_B$ is the Bohr magneton, $T_s$ is the electron spin lifetime and $g_e$ is the electron g-factor.

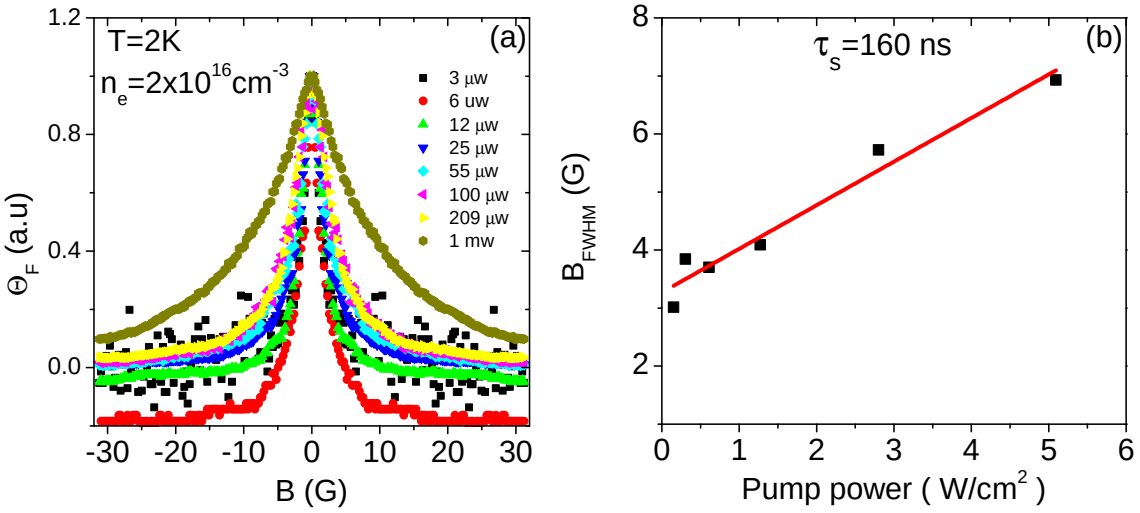


Figure 4.3: (a) Hanle curves acquired at different pump power density. (b) The full width at half maximum of the Hanle curves versus pump power density. Extrapolation to zero pump power density gives $B_{FWHM}$= 3.3 G, corresponding to spin relaxation time of 160 ns.

In case of $n$-doped semiconductor, the effective spin lifetime is given by

$$1/T_s = 1/\tau_s + G/n_e. \tag{4.7}$$

where $\tau_s$ is the electron spin relaxation time, $n_e$ is the concentration of equilibrium electrons and $G$ is the carrier generation rate [DKK+02].

The full width at half maximum (FWHM) of the Lorentz curve is inversely proportional to the spin lifetime:

$$B_{FWHM} = (2\hbar/g_e\mu_B T_s). \tag{4.8}$$

This allows for the measurement of the spin lifetime, and by extrapolation to $G = 0$ the spin relaxation time.

The FWHM of the Hanle curves as a function of pump power density is shown in Fig. 4.3(b) for the sample 98P180. Using Eqs. 4.8 and 4.7, we deduce a spin relaxation time of 160 ns, close to the value reported by Crooker *et al.* [CCS09] for the same doping concentration.

### 4.1.4 Determination of electron spin polarization

For the sample 98P180 there is large negative detuning of the cavity mode with respect to the GaAs energy gap and the interband emission is strongly suppressed. Therefore, direct determination of electron spin polarization from the degree of circular polarization of photoluminescence was not possible. For this reason we started with an indirect method based on the cooling of the nuclear spin system in the electron (Knight) field [KKF82, MZ84]. We have also measured the degree of polarization of electron gas from the polarized photoluminescence (PL) experiments, but in order to enable the detection of interband emission, the upper Bragg mirror was etched from the microcavity sample. Note, however, that this may affect the measured spin polarization for several reasons, such as degradation of the sample quality, and change in the probability of photon recycling.

#### I. Measurement of the Knight field

The nuclear spin temperature ($\Theta_N$) under the condition of steady state optical pumping in an external field $\boldsymbol{B}$ is defined in Eq. 2.23. It can be seen that $\Theta_N$ depends strongly on $(\boldsymbol{B} + \boldsymbol{B}_e)$ and becomes infinite when the external field compensates the Knight field (see Section 2.3.2) i.e, when $(\boldsymbol{B} + \boldsymbol{B}_e \rightarrow 0)$. Measurements of $\Theta_N$ as a function of $\boldsymbol{B}$, allow for determination of the Knight field compensation condition and thus for the electron spin density $\langle S_z \rangle$. Then the average electron spin polarization $\rho_e$ can be obtained using Eq. 4.3.

The setup used for Knight field measurements is shown in Fig. 3.8. The measurements were done in two stages as shown in Fig. 4.4. In the first stage (the cooling stage), the nuclear spin system is cooled down by strong optical pumping (pump power = 500 $\mu$W) in a longitudinal field $B_z$ along the pump direction during few minutes. In the second stage (the detection stage), the longitudinal field $B_z$ is switched off and a small transverse field $B_x$ = 1.5 G - 2.5 G is applied. The pump power during measurement is set to a lower value ( 85 $\mu$W) to minimize repolarization of the nuclei during this stage.

Now according to Eq. 2.23, if the nuclei are cooled down sufficiently during cooling stage, then depending on the sign and value of $B_z$ and $B_e$, the nuclei will repolarize either parallel ($\Theta_N < 0$) or antiparallel ($\Theta_N > 0$) to the transverse field

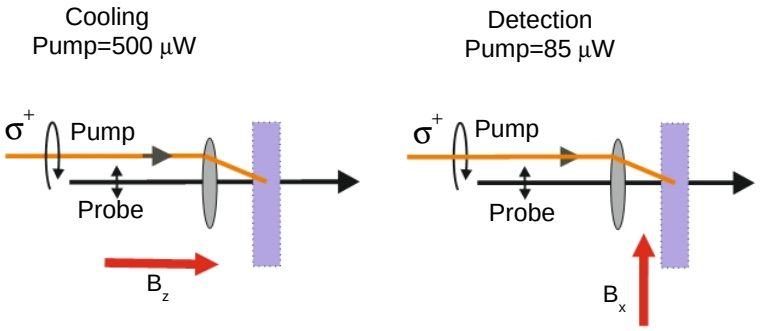


Figure 4.4: Scheme for optical cooling of nuclear spins at relatively large pump power in a longitudinal field (left) and detection in a small transverse field at lower pump power (right).

$B_x$, creating an effective nuclear (Overhauser) field $B_N$ acting on the electrons. If during cooling stage, the external field is such that it compensates the Knight field ($\boldsymbol{B} = -\boldsymbol{B}_e$), then nuclear cooling is not possible ($\Theta_N = 0$) and $B_N = 0$.

The total transverse field experienced by the spin polarized electrons is $B_T = B_x + B_N$. This field causes a change of the electron spin polarization created by the weak pump. The nuclear spin system heats up in the absence of strong pump and as a result the nuclear field relaxes slowly and the electron spin polarization varies with time. It follows a part of the Hanle curve from $B_T = B_x + B_N$ to $B_T = B_x$ when $B_N$ is fully relaxed [Fig. 4.5(a)]. The resulting depolarization of electron spin is monitored by the FR of the probe beam.

Different kinds of depolarization curves [Fig. 4.5(b)-4.5(d)] can be observed depending on the initial value of the total field. If $B_N < 0$ and $|B_N| > B_x$, then $B_T < 0$ [Fig. 4.5(b)]. In this case, the electron spin polarization as well as FR angle $\Theta_F$ first increase, goes through a maximum when $B_T = 0$, then decreases as $B_T$ decreases towards $B_x$ due to nuclear spin relaxation processes. If $B_N < 0$ and $|B_N| < B_x$, then $0 < B_T < B_x$. In this case $\Theta_F$ monotonously decreases [Fig. 4.5(c)]. These two cases will eventually occur when $B_N$ and $B_x$ are antiparallel, i.e. for positive nuclear temperatures, $\Theta_N > 0$. Finally, if $B_N > 0$ , then $B_T > B_x$. This takes place for negative nuclear temperatures $\Theta_N < 0$, and the FR angle $\Theta_F$ increases steadily as $B_T$ decreases towards $B_x$ [Fig. 4.5(d)].

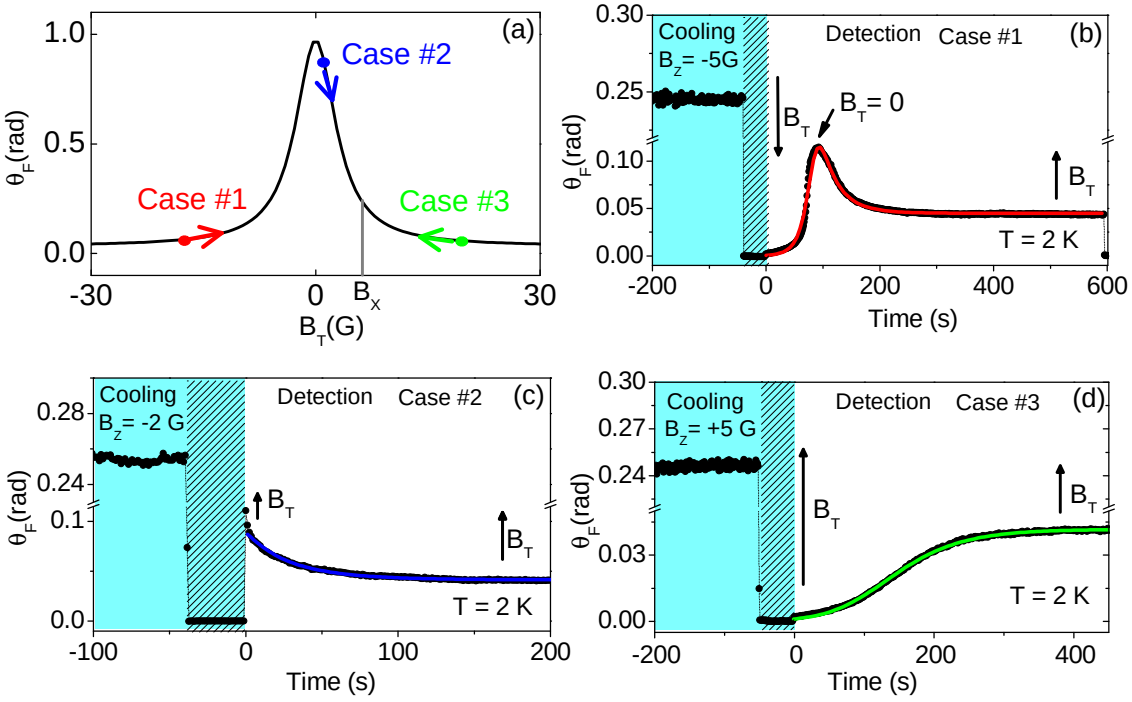


Figure 4.5: (a) Typical Hanle curve versus total field $B_T = B_N + B_x$. Depending on the initial value of $B_T$, Faraday rotation will exhibit different time evolutions as $B_T$ relaxes to $B_x$. (b-d) Time evolution of Faraday rotation during cooling in a longitudinal field (cyan region), and detection in a weak transverse field $B_x$ =1.5 G, for the three cases shown in panel (a). In the shaded area (during cooling) the signal was not recorded to allow for a change in the lock-in sensitivity.

Assuming that the nuclear field decays exponentially, the time evolution of FR can be expressed as

$$\Theta_F(t) = \Theta_F^{max}\left[1 + \left(\frac{B_x + B_{N_0}e^{-t/T_1}}{B_{FWHM}/2}\right)^2\right]^{-1}. \tag{4.9}$$

where $B_{N_0}$ is the initial nuclear field, $T_1$ is the longitudinal nuclear spin relaxation time.

Eq. 4.9 is used also to determine $B_N$ at t=0.

$$B_N(t) = \frac{B_{FWHM}}{2}\left(\frac{\Theta_F^{max}}{\Theta_F(t)} - 1\right)^{1/2} - B_x \tag{4.10}$$

In Chapter 5, we will use this method to measure $B_N$.

Figs. 4.5(b)-4.5(d) show the fits of the depolarization of FR in field $B_T$ using Eq. 4.9, from which we deduce $B_{N_0}$ for each value of $B_z$. This experiment was done at temperatures 2 K, 4 K and 10 K. The resulting values of $B_{N_0}$ for each $B_z$ are shown in Fig. 4.6. One can see in the inset of Fig. 4.6, that the field $B_z$ at which $B_{N_0}$ passes through zero is slightly shifted from zero. This is a direct evidence that the nuclei get polarized in the Knight field created by the electrons, even without external field. From this shift we estimate $B_e = (0.4 \pm 0.1)$ G for the sample 98P180. Note, that the measured Knight field is comparable with the earth field. Therefore precise determination of $B_e$ requires a careful compensation of the earth (laboratory) field.

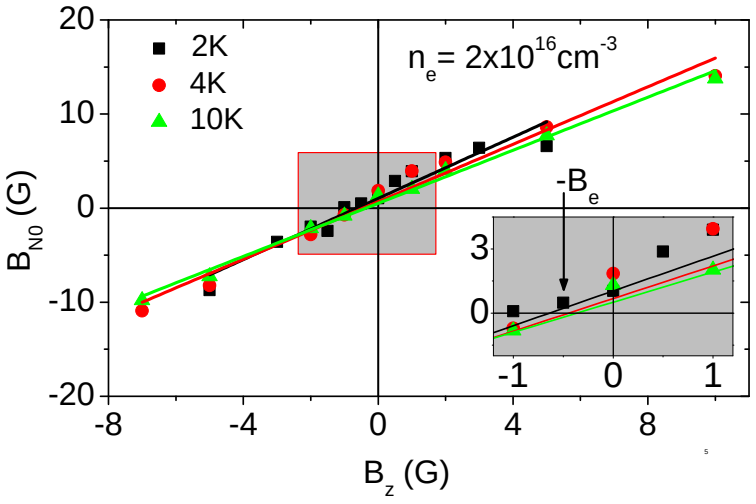


Figure 4.6: The extracted nuclear field as a function of longitudinal field. The observed Knight field of about 0.4 G is independent of sample temperature.

Then the electron spin density, taking $b_e$= 3.7 G ( see Section 2.3.2) and using Eq. 2.7 is,

$$\langle S_z \rangle = \frac{1}{2}\frac{B_e}{b_e} n_e = 1.1 \times 10^{15}\text{cm}^{-3} \tag{4.11}$$

Using Eq. 4.3, we get average electron spin polarization $\rho_e = (11 \pm 3)\%$.

At the same pump power P=500 $\mu$W, corresponding to an intensity of 25 W/cm$^2$, we measured $\Theta_F = 10°$. Therefore, using Eq. (4.4) we get $\mu = \Theta_F/\rho_e = -100° \pm 25°$.

### II. Polarized photoluminescence

Polarized photoluminescence was used to measure the electron spin polarization for both the sample 98P180 and C7T76:

- For the sample 98P180, we took a piece of the sample whose upper Bragg mirror was chemically etched.
- For the sample C7T76, we took a piece of the sample for which the cavity mode was resonant with the energy gap of GaAs.

The excitation energy is 1.59 eV, which is above the energy gap of GaAs and corresponds to the energy of the pump in the FR experiments. The setup used for the PL measurements is shown in Fig. 3.7 and the procedure is described in section 3.3.5.

Fig. 4.7 shows the measured PL intensity and polarization for the sample 98P180. The PL spectrum is broad and there is a characteristic step in the circular polarization on the higher energy tail of the spectrum. These characteristics are typical of degenerate semiconductors [DKK+02] and can be explained in terms of a simple interband emission model in which the k-conservation selection rule is lifted. This model is described as follows:

With $\sigma^+/\sigma^-$ light excitation, electrons are excited from occupied states in the valence band to the empty states above the Fermi level. These spin polarized electrons interacts with each other (e-e interaction) and thermalize to a Fermi-Dirac distribution thereby reducing their average energy. After the thermalization, the electrons can be described with an equilibrium distribution in terms of an electron temperature $T_e$. The Fermi-Dirac distribution functions of the conduction electrons for the two spin subbands are,

$$f_{\pm 1/2}(E) = \frac{1}{1 + e^{\beta_e (E - \mu_\pm)}}, \tag{4.12}$$

where $\beta_e = 1/k_B T_e$ is the inverse electron temperature and $\mu_\pm = \mu \pm \varepsilon$ is the chemical potential of the spin up and spin down electrons respectively.

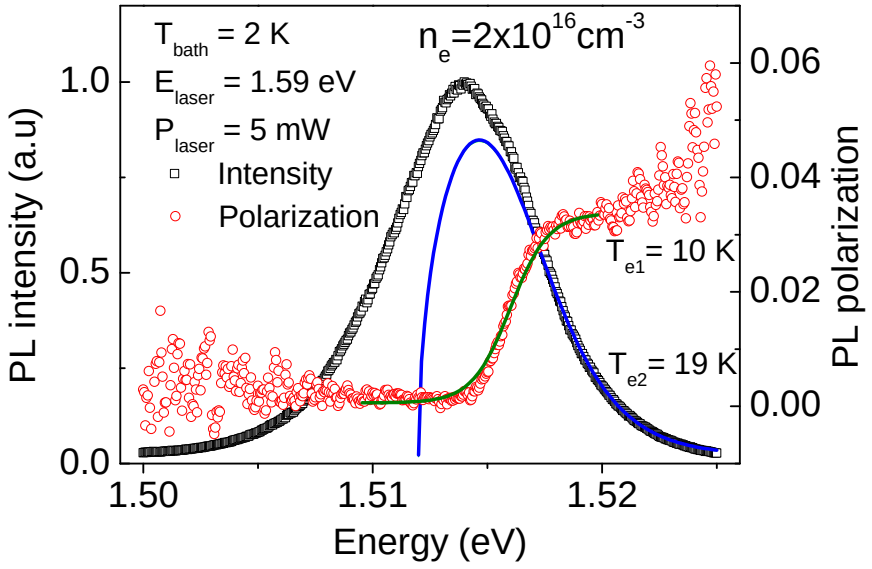


Figure 4.7: The spectrum of PL intensity (open square) and the PL circular polarization from the GaAs microcavity (open circle). The solid lines are fit by the calculated PL intensity and electron spin polarization assuming Fermi distribution of electrons.

As we have seen in Section 2.1, the selection rules, which connect the electron spin and light polarization, are used to selectively couple to a particular spin state which creates non-equilibrium electron spin polarization. The same selection rules connect the polarized electron spins and the polarization of the photoluminescence. The photoluminescence intensity for $\sigma^+$ and $\sigma^-$ polarized components is given as,

$$\begin{aligned} I_+ &= \mathcal{D}(E)[f_{1/2}(E) + 3f_{-1/2}(E)], \\ I_- &= \mathcal{D}(E)[3f_{1/2}(E) + f_{-1/2}(E)], \end{aligned} \tag{4.13}$$

where $\mathcal{D}(E)$ is the density of states in the conduction band. Then the PL intensity is defined as

$$I(E) = I_+ + I_- = \mathcal{D}(E)4[f_{1/2}(E) + f_{-1/2}(E)], \tag{4.14}$$

and the degree of circular polarization of PL is defined as

$$\rho_c(E) = \frac{I_+ - I_-}{I_+ + I_-} = \frac{1}{2}\frac{f_{1/2}(E) - f_{-1/2}(E)}{f_{1/2}(E) + f_{-1/2}(E)}. \tag{4.15}$$

Assuming $\varepsilon$ to be small, the distribution function defined in Eq. 4.12 can be expanded to first order in $\varepsilon$ as follows:

$$f_{\pm 1/2}(E) = \frac{1}{1 + e^{\beta_e(E-\mu) \mp \beta_e \varepsilon}} = \frac{1}{1 + e^{\beta_e(E-\mu)}} \left[ 1 \pm \frac{\beta_e \varepsilon e^{\beta_e(E-\mu)}}{1 + e^{\beta_e(E-\mu)}} \right]. \tag{4.16}$$

$$\begin{aligned} f_{1/2}(E) + f_{-1/2}(E) &= \frac{2}{1 + e^{\beta_e(E-\mu)}}. \\ f_{1/2}(E) - f_{-1/2}(E) &= \frac{2\beta_e \varepsilon e^{\beta_e(E-\mu)}}{[1 + e^{\beta_e(E-\mu)}]^2}. \end{aligned} \tag{4.17}$$

At T=0 K, the chemical potential of the electrons is equal to the Fermi energy [$\mu_{T_{0K}}$=$E_F$] and the non-equilibrium spin polarization is defined by the population above the Fermi level (proportional to $2\varepsilon$). Using Eq. 4.17, the PL intensity defined in Eq. 4.14 reads

$$I(E) \propto \frac{\mathcal{D}(E)}{1 + e^{\beta(E-E_F)}}, \tag{4.18}$$

and the degree of circular polarization of PL defined in Eq. 4.15 reads

$$\rho_c(E) = \frac{1}{2} \frac{\beta_e \varepsilon}{1 + e^{-\beta_e(E-E_F)}}. \tag{4.19}$$

The degree of spin polarization of conduction electrons is,

$$\begin{aligned} \rho_e = \frac{n_{1/2} - n_{-1/2}}{n_e} = \frac{2\varepsilon \mathcal{D}(E_F)}{n_e} = \frac{2\varepsilon}{n_e} \frac{3}{4} \frac{n_e}{E_F} \\ \Rightarrow \varepsilon = \frac{2}{3} E_F \rho_e, \end{aligned} \tag{4.20}$$

where $n_{1/2}$ and $n_{-1/2}$ are density of spin up and spin down electrons respectively and $\mathcal{D}(E_F) = \frac{3}{4}\frac{n_e}{E_F}$ is the density of states at the Fermi energy $E_F$, for a single spin state. Substituting the value of $\varepsilon$ in Eq. 4.19, we get the degree of spin polarization of conduction electrons as:

$$\rho_c(E) = \frac{\frac{1}{3}\beta_e E_F \rho_e}{1 + e^{-\beta_e(E-E_F)}}. \tag{4.21}$$

At low energy the polarization goes to zero, while at high energy the PL polarization degree tends to

$$\rho_c^{\infty} = \frac{1}{3} \beta_e E_F \rho_e. \tag{4.22}$$

Fitting the PL intensity with Eq. 4.18 and PL polarization with Eq. 4.21, we get electron temperature $T_{e1} = 10$ K and $T_{e2} = 19$ K respectively, and $\rho_c^{\infty} = 0.03$ for the sample 98P180. The different electron temperature deduced from PL intensity and polarization indicates that the interband emission model used here is not adequate to describe the observed spectrum, which contains at least two components. However these fits give an estimate of electronic temperature in the range 10-20 K. Taking $E_F$=4 meV and average electron temperature $T_e = 15$ K, we obtain from Eq. 4.22 the electron spin polarization degree $\rho_e = 6 \pm 2$ % for the sample 98P180 in reasonable agreement with the value estimated from the Knight field .

### 4.1.5 Theory of photoinduced Faraday rotation

The efficiency of a nonmagnetic material in producing FR in presence of an external magnetic field along the direction of light is usually characterized by the Verdet constant. It is defined as the FR angle per unit length of the material per unit applied magnetic field. In the case of optically induced FR, there is no magnetic field and the Verdet constant can not characterize the efficiency of the material in producing photoinduced FR accurately. Therefore it is necessary to introduce the concept of ***Faraday rotation cross-section*** ($\sigma_F$) in analogy with other familiar cross sections, to correctly describe the photo induced FR efficiency.

Consider a linearly polarized light propagating along the $z$ direction and interacting with a single particle with spin projection $\hbar$ in this direction. Then $\sigma_F$ is defined as the induced FR per unit surface of the beam cross section. Therefore, for a medium with large number of spins with average spin density $\langle S_z \rangle$ and effective thickness $d_{eff}$, the FR is given by

$$\Theta_F = \sigma_F \langle S_z \rangle d_{eff}. \tag{4.23}$$

We have seen in section 2.8.2 that there are two contributions to FR induced by optically created spin polarized electrons in bulk semiconductors: (1) state filling effects, and (2) exchange splitting of the conduction band/Hartree-Fock effect. We will follow the theoretical model of Aronov and Ivchenko [AI73] to calculate the contribution related with the state filling effect, and following the model of Artemova and Merkulov [AM85] we calculate the contribution related with the exchange interaction.

### I. State filling effect

Let us introduce the frequency dependent dielectric susceptibilities ($\varepsilon_{\pm}(\omega) = \varepsilon'_{\pm}(\omega) + i\varepsilon''_{\pm}(\omega)$) for $\sigma^+$ and $\sigma^-$ polarized light waves propagating in the positive direction of $z$-axis. In the vicinity of the band edge ($\hbar\omega < E_g$) the difference of the real part of the dielectric susceptibilities can be written as [BP72]:

$$\varepsilon'_+ - \varepsilon'_- = \frac{4\pi e^2}{m_0^2 \hbar\omega^2 \mathcal{V}} \sum_{\boldsymbol{k}} \frac{|p_{cv}|^2}{3} \left[ \frac{f_{1/2}(k) - f_{-1/2}(k)}{\omega - E_g/\hbar - \hbar k^2/2\mu_{hh}} + \frac{f_{1/2}(k) - f_{-1/2}(k)}{\omega - E_g/\hbar - \hbar k^2/2\mu_{lh}} \right], \tag{4.24}$$

where $m_0$ is free electron mass, $\mathcal{V}$ is the normalization volume, $p_{cv}$ is the interband momentum matrix element, $\mu_{hh}$ ($\mu_{lh}$) is the reduced electron-heavy hole (electron-light hole) mass, and $f_{\pm 1/2}(k)$ are the distribution functions of electrons with spin projections $\pm 1/2$ onto the $z$-axis.

The spin distribution function of degenerate electrons is given by

$$s_z = \frac{E_{F,1/2} - E_{F,-1/2}}{2} \delta(E - E_F) \propto \frac{n_{+1/2} - n_{-1/2}}{2} \delta(E - E_F), \tag{4.25}$$

where $E$ is the electron energy, $E_F = E_{F,1/2} + E_{F,-1/2}$ is the mean Fermi energy in two spin states.

The electron spin density is given as

$$\langle S_z \rangle = \frac{1}{\mathcal{V}} \sum_{\boldsymbol{k}} s_z(\boldsymbol{k}), \tag{4.26}$$

where

$$s_z(\boldsymbol{k}) = [f_{1/2}(\boldsymbol{k}) - f_{-1/2}(\boldsymbol{k})]/2.$$

Assuming electrons to be strongly degenerate so that summation by $\boldsymbol{k}$ results in taking $k = k_F$, and using Eq. 4.25 the spin density becomes

$$\begin{aligned} \langle S_z \rangle &= \frac{1}{\mathcal{V}} \sum_{\boldsymbol{k}} [f_{1/2}(\boldsymbol{k}) - f_{-1/2}(\boldsymbol{k})]/2 \\ &= (n_{+1,2} - n_{-1/2})/2. \end{aligned} \tag{4.27}$$

Now from Eq. 4.27, we have $\sum_{\boldsymbol{k}} (f_{1/2}(k) - f_{-1/2}(k)) = \mathcal{V}(n_{+1,2} - n_{-1/2})$, which

on substitution in Eq. 4.24, we get

$$\varepsilon'_+ - \varepsilon'_- = \frac{4\pi e^2 |p_{cv}|^2}{3m_0^2\omega^2}(n_{+1/2} - n_{-1/2}) \left( \frac{1}{E_g + \frac{m}{\mu_{hh}}E_F - \hbar\omega} + \frac{1}{E_g + \frac{m}{\mu_{lh}}E_F - \hbar\omega} \right). \tag{4.28}$$

Now from the effective mass sum rule, $|p_{cv}|^2 = m_0^2 E_g/2m$, where $m$ is the electron effective mass. Taking this into account and $S_z = (n_{+1,2} - n_{-1/2})/2$, we get

$$\varepsilon'_+ - \varepsilon'_- = \frac{4\pi e^2 \hbar}{3m\omega} S_z \left( \frac{1}{E_g + \frac{m}{\mu_{hh}}E_F - \hbar\omega} + \frac{1}{E_g + \frac{m}{\mu_{lh}}E_F - \hbar\omega} \right). \tag{4.29}$$

The FR angle is given by

$$\Theta_F = \frac{\omega}{4cn}(\varepsilon'_- - \varepsilon'_+) d_{eff}, \tag{4.30}$$

where $n$ is the background refractive index. Using Eqs. 4.23 and 4.30, we obtain,

$$\sigma_F^{sf} = -\frac{\pi e^2 \hbar}{3mcn} \left( \frac{1}{E_g + \frac{m}{\mu_{hh}}E_F - \hbar\omega} + \frac{1}{E_g + \frac{m}{\mu_{lh}}E_F - \hbar\omega} \right). \tag{4.31}$$

### II. Hartree-Fock effect

The exchange interaction between electrons in the spin polarized electron gas, renormalizes their energy depending on spin orientation. The energy shift is thus different for $s_z = +1/2$ and $s_z = -1/2$ electrons. Therefore the Hartree-Fock effect can be understood as an interaction induced effective magnetic field acting on electron spins [GI04]. This effective field can be written as [Gla12]

$$\Delta_{\mathrm{HF}}(\boldsymbol{k}) = -2 \sum_{\boldsymbol{k}'} V_{\boldsymbol{k}'-\boldsymbol{k}} s_z(\boldsymbol{k}), \tag{4.32}$$

where $V_{\boldsymbol{q}} = 4\pi e^2/[\mathcal{V}\varkappa(q^2 + q_{\mathrm{TF}}^2)]$ is the Fourier transform of electron-electron interaction potential with $q_{\mathrm{TF}} = \sqrt{6\pi N e^2/\varkappa E_F}$ being Thomas-Fermi screening wave vector and $\varkappa$ being background static dielectric constant.

Assuming a strongly degenerate electron gas and low electron spin polarization, the wave vector dependence of $\Delta_{\mathrm{HF}}$ can be neglected and taking its value at $k = k_F$ ,

we get

$$\Delta_{\rm HF}(k_F) = -\frac{2\pi e^2}{\varkappa k_F} \ln\left(1 + \frac{4k_F^2}{q_{\rm TF}^2}\right) S_z. \tag{4.33}$$

The effective field $\Delta_{\rm HF}(k_F)$ causes the splitting of the conduction band and its effect on photoinduced FR can be evaluated similarly to the calculation of the FR induced by nuclei in semiconductors [AM85].

The absorption coefficients for $\sigma^+$ and $\sigma^-$ light polarizations considering the effect of $\Delta_{\rm HF}(k_F)$, and taking into account that $\Delta_{\rm HF}(k_F) < 0$, are given as

$$\alpha_+ = A\left[3\left(\hbar\omega - E_g - \frac{\Delta_{\rm HF}}{2}\right)^{1/2} + \left(\hbar\omega - E_g + \frac{\Delta_{\rm HF}}{2}\right)^{1/2}\right] \tag{4.34}$$

and

$$\alpha_- = A\left[3\left(\hbar\omega - E_g + \frac{\Delta_{\rm HF}}{2}\right)^{1/2} + \left(\hbar\omega - E_g - \frac{\Delta_{\rm HF}}{2}\right)^{1/2}\right], \tag{4.35}$$

where

$$A = \frac{e^2\hbar}{12mcn}\left[\left(\frac{2\mu_{hh}}{\hbar^2}\right)^{3/2} + \left(\frac{2\mu_{lh}}{\hbar^2}\right)^{3/2}\right]. \tag{4.36}$$

Then the difference in absorption coefficients for $\sigma^+$ and $\sigma^-$ polarized light is

$$\alpha_+ - \alpha_- = \frac{A\Delta_{\rm HF}}{\sqrt{\hbar\omega - E_g}}, \tag{4.37}$$

and the difference of imaginary part of the dielectric susceptibilities is

$$\delta\varepsilon''(\omega) = \frac{cn}{\omega}\frac{A\Delta_{\rm HF}}{\sqrt{\hbar\omega - E_g}}. \tag{4.38}$$

At low temperatures in doped semiconductors (and assuming that $m_{hh}, m_{hh} \gg m$), the presence of carriers leads to the shift of the absorption edge from $E_g$ to $E_g + E_F$. Taking this into account and using the Kramers-Kroning relation, we obtain

$$\delta\varepsilon'(\omega) = -\frac{cn}{\omega}\frac{A\Delta_{\rm HF}}{\sqrt{E_g - \hbar\omega}}\left(1 - \frac{2}{\pi}\arctan\sqrt{\frac{E_F}{E_g - \hbar\omega}}\right). \tag{4.39}$$

Then, the FR angle is

$$\Theta_F^{HF} = \frac{\omega}{4cn}\delta\varepsilon'(\omega)d_{eff} = -\frac{A\Delta_{\rm HF}d_{eff}}{\sqrt{E_g-\hbar\omega}}\left(1-\frac{2}{\pi}\arctan\sqrt{\frac{E_F}{E_g-\hbar\omega}}\right). \qquad (4.40)$$

In general case of arbitrary relations between $m_{hh}, m_{hh}$ and $m$, we obtain

$$\sigma_F^{HF} = -\frac{e^2\hbar}{48mcn}\frac{\mathcal{U}_{k_F}}{\sqrt{E_g-\hbar\omega}}\left[\left(\frac{2\mu_{hh}}{\hbar^2}\right)^{3/2}\left(1-\frac{2}{\pi}\arctan\sqrt{\frac{\frac{m}{\mu_{hh}}E_F}{E_g-\hbar\omega}}\right)+\left(\frac{2\mu_{lh}}{\hbar^2}\right)^{3/2}\left(1-\frac{2}{\pi}\arctan\sqrt{\frac{\frac{m}{\mu_{lh}}E_F}{E_g-\hbar\omega}}\right)\right], \qquad (4.41)$$

where $\mathcal{U}_{k_F} = \frac{\Delta_{\rm HF}(k_F)}{S_z}$ is the interaction energy between spin polarized electrons.

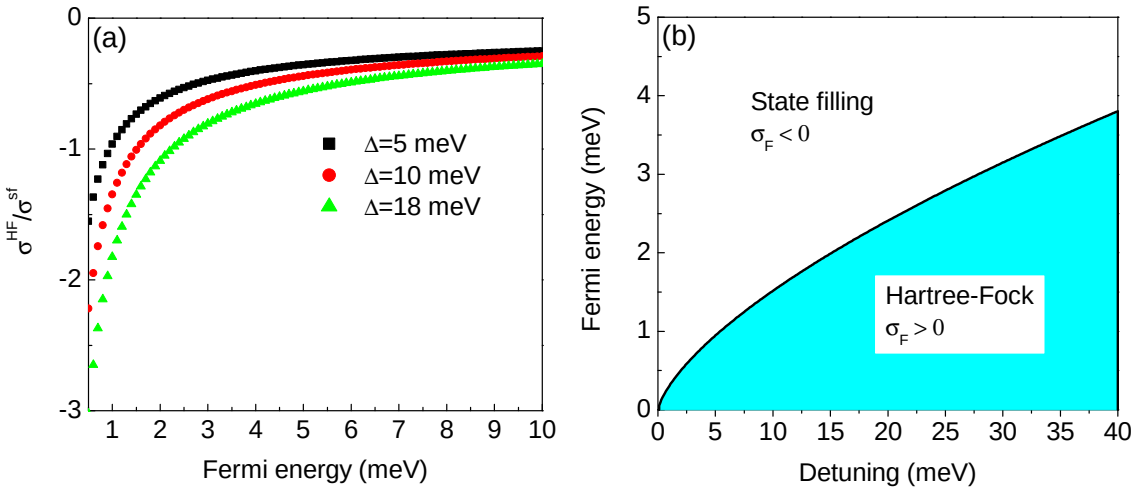


Figure 4.8: (a) Ratio of Hartree–Fock and state–filling contributions to the Faraday rotation cross-section as function of electron Fermi energy, calculated as functions of detuning, $\Delta E$, after Eqs. (4.41), (4.31) respectively. The parameters of GaAs were used. (b) Schematic diagram in the detuning–Fermi energy axes showing dominant contributions to spin Faraday rotation: filled area corresponds to $|\sigma^{HF}| > |\sigma^{sf}|$.

Now from Eqs. (4.31) and (4.41), it can be seen that at relatively high detunings, $\Delta = E_g - \hbar\omega \gg E_F$, the state filling contribution behaves as $\sigma_F^{\rm sf} \propto \Delta^{-1}$, while Hartree-Fock contribution behaves as $\sigma_F^{\rm HF} \propto \Delta^{-1/2}$. In the vicinity of the absorption

edge, the singularity in the state-filling contribution, $\sigma_F^{\rm sf}$, is smeared due to the electron scattering, which results in the broadening of the edge.

From Eqs. (4.31) and (4.41) we see that $\sigma^{HF}$ and $\sigma^{sf}$ have opposite signs. The ratio of the Hartree-Fock and state-filling contributions to the Faraday rotation cross-section is shown in Fig. 4.8(a). This ratio is controlled by (I) the ratio of the Fermi energy and interaction energy $\mathcal{U}_{k_F}$ and (II) the ratio of Fermi energy and detuning. Fig. 4.8(b) schematically shows the areas in the parameter space detuning-Fermi energy where state-filling effect or Hartree-Fock effect dominate: in agreement with Eqs. (4.31) and (4.41) the Hartree-Fock contribution dominates at small Fermi energies and high detunings.

Using the experimental parameters $E_g - \hbar\omega = 18$ meV, $E_F \sim 4$ meV ($m = 0.067m_0$, $n = \sqrt{13}$), we get from Eq. (4.31) $\sigma_F^{sf} \approx -1.9 \times 10^{-15}$ rad×cm$^2$ and from Eq. (4.41) $\sigma_F^{HF} \approx 1.2 \times 10^{-15}$ rad×cm$^2$. The close magnitudes of the state-filling effect and Hartree-Fock effect induced FR results from the relatively low electron density, where the interaction effects become important. As a result, theoretical estimate for the FR cross-section is $\sigma_F^{\rm th} = -0.7 \times 10^{-15}$ rad×cm$^2$.

### 4.1.6 Estimation of photoinduced Faraday rotation cross-section from experiments

The FR cross-section following Eq. 4.23 is

$$\sigma_F = \Theta_F / \langle S_z \rangle d_{eff} \tag{4.42}$$

Now from Eqs. 4.4 and 4.3, we have $\Theta_F = \mu\rho_e$ and $\rho_e = \frac{2\langle S_z \rangle}{n_e}$. Substituting these values in Eq. 4.42, we get

$$\sigma_F = 2\mu / n_e d_{eff} \tag{4.43}$$

From the measurements of photo-induced FR and nuclear spin cooling experiments in the same optical pumping conditions we deduced $\mu = -100° \pm 25°$ for the sample 98P180 (Section 4.1.4) and from interferometric measurements of the quality factor of the sample, we deduced the effective length $d_{eff}$= 0.7 mm (Section 3.1.1). Substituting these values in Eq. 4.43, we get an experimental estimate for the FR cross section

for the sample 98P180 as $\sigma_F = -(2.5 \pm 0.6) \times 10^{-15}$ rad×cm$^2$. This is about three times the theoretical value. But considering the fact that the theoretical value was obtained within a simple model, which neglects electron-hole correlation effects, and uses well-known parameters of GaAs, and thus without any fitting parameters the agreement is reasonable. The main uncertainty in the determination of $\sigma_F$ comes from the uncertainty in the determination of the electron spin density from the Knight shift. The photoinduced FR was found to vary from 19° at the lowest detuning $\Delta = 16$ meV to 14° at the largest detuning $\Delta = 22$ meV. Our results are consistent with the expected inverse detuning dependence of $\sigma_F^{sf}$ , but the available detuning range was too small to identify unambiguously the expected detuning dependence.

## 4.2 Field induced Faraday rotation

The FR in semiconductors induced by an external magnetic field is discussed in Section 2.8.1. The external field makes two contributions to the interband FR. The first contribution is related with the changes of conduction and valence band orbital states induced by the magnetic field (diamagnetic effects). The second contribution is due to the magnetic field induced (equilibrium) spin polarization of charge carriers. The field induced FR in GaAs has been studied as a function of doping concentration, wavelength of light and temperature. It was reported that the Verdet constant in n-GaAs is small [AB68]. The free carrier contribution to FR in n-GaAs was found to be positive and the interband contribution was negative for energy below the direct energy gap and changes sign for energy close to the absorption edge [Pil64, Zvà69].

The FR of the substrate, sample 98P180 and sample C7T76 was measured in magnetic field up to 180 G and is presented in Fig. 4.9(a). It can be seen from the figure that the FR due to the substrate is nearly equal to the FR of the whole structure at the same probe energy. Thus in this small field region and for this wavelength, the FR is entirely dominated by the substrate.

It has been have observed by Zvàra [Zvà69] and Piller [Pil64] that the sign of Verdet constant in GaAs changes in the vicinity of the band edge. The detuning dependence of the Verdet constant for the GaAs substrate is shown in Fig. 4.9(b) along with the data from Zvàra (undoped substrate and compensated n-GaAs) and Piller ($n_e = 2\times10^{16}$ cm$^{-3}$). The n-doped sample of Piller have similar doping

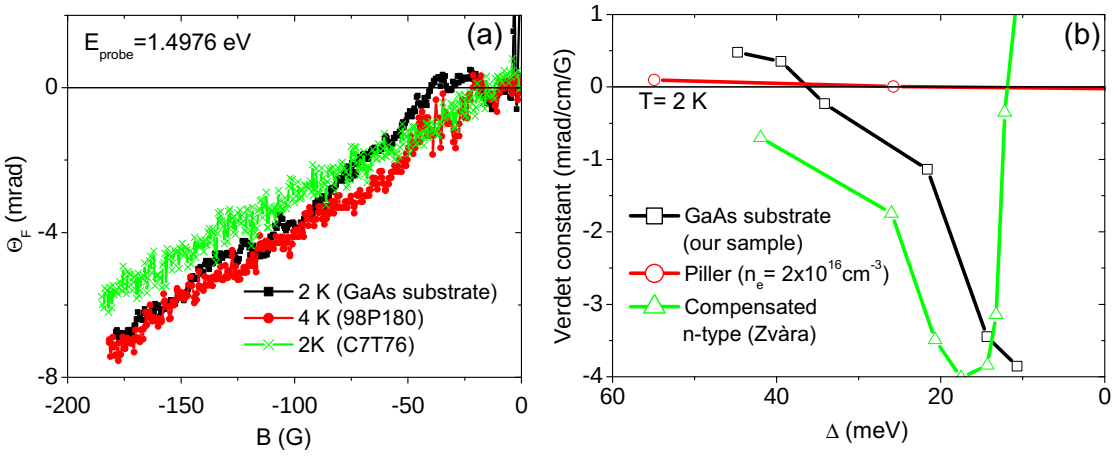


Figure 4.9: (a) Faraday rotation of the GaAs substrate (squares), sample (98P180) (circles) and sample (C7T76) (crosses) as a function of magnetic field. (b) Verdet constant in the GaAs substrate (squares) as a function of detuning of the probe energy with respect to GaAs band gap $E_g$= 1.519 eV and in comparison with data by Piller (circles) [Pil64] and Zvàra (triangles) [Zvà69].

concentration as the sample 98P180 and for the detuning range (determined by the cavity mode in our sample) we have chosen for our experiments (18 meV), the Verdet constant is nearly zero. The Verdet constant of our GaAs substrate and the compensated sample of Zvàra has similar finite value at detuning of 18 meV. This explains the fact that the FR induced by the substrate at the detuning of about 18 meV is exactly same as the FR induced by the whole sample. Therefore the Verdet constant is attributed to the substrate while it could not be measured for the cavity.

We have also measured the field induced FR with field up to 10 T at different temperatures (2 K- 20 K) as shown in Fig. 4.10(a). The FR is independent of temperature for field up to 2 T and thereafter varies with temperature. In this temperature range, the $g$ factor in semiconductors have a small temperature dependence [OR95, OHH+96, ZPB+08]. The energy gap of GaAs, $E_g(T)$ also have a temperature dependence [LGLC87]. This would change the detuning and consequently the FR. If we ignore this temperature dependence of the $g$ factor and the energy gap, the change of FR with temperature can be attributed to that of electron spin polarization. However this contribution is negligible as compared to the diamagnetic contributions. In order to extract the contribution due to spin polarization, we plotted the differences

between FR measured at different temperatures [Fig. 4.10(b)]. We can see that $\Delta\Theta_F^T$ remains close to zero up to B=2 T and starts to increase at higher field. This behaviour is explained in Section 4.2.1 assuming that the temperature dependent contribution comes from spin polarization only.

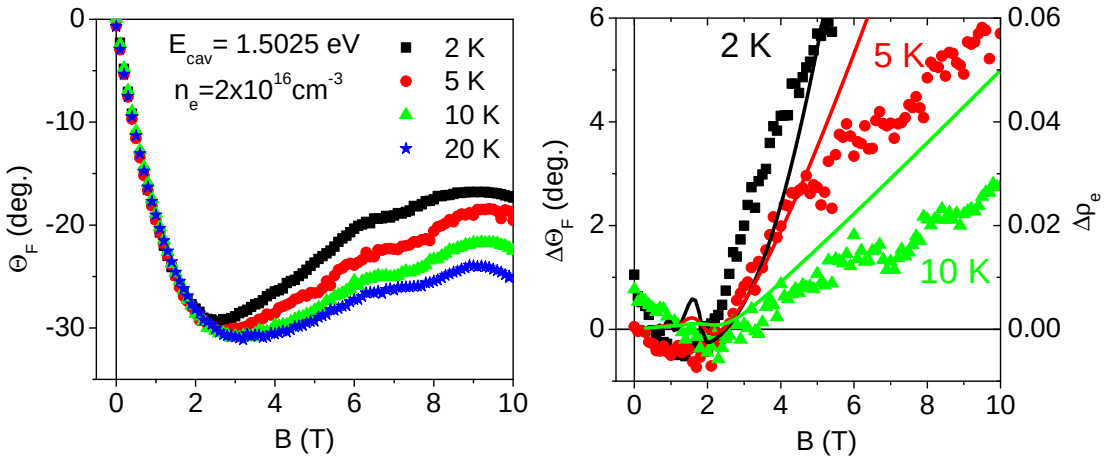


Figure 4.10: (a) Experimentally measured Faraday rotations as a function of magnetic field at different temperatures. (b) Comparison between measured Faraday rotation $\Delta\Theta_F$ (left scale, symbols) and calculated temperature dependent spin polarization $\Delta\rho_e^{2K}$, $\Delta\rho_e^{5K}$, $\Delta\rho_e^{10K}$ (right scale, lines). Here the scale of spin polarization is adjusted to match the FR ( $\Delta\Theta_F(deg.) = 100 \times \Delta\rho_e$).

### 4.2.1 Theory of field induced Faraday rotation

The field and temperature dependence of FR can be explained by a simple model. Here we consider only the paramagnetic contributions of spin polarized electrons to the FR, and not the diamagnetic contributions, which is much more complicated [Rot64]. Thus we will consider the electron spin polarization in the conduction band and assume $\Theta_F \propto \rho_e$.

The energy levels of electrons with spin $z$-component $\pm 1/2$ in a magnetic field are given by

$$E_\pm(k_z, n_L) = \hbar^2 k_z^2/(2m) + \hbar\omega_C(n_L + 1/2) \pm g_e\mu_B B/2,$$

where $k_z$ is the wave vector of electron along the magnetic field, $n_L$ is the Landau level number, $\omega_C = |e|B/(mc)$ is the cyclotron frequency and $g_e\mu_B B/2$ accounts for the Zeeman splitting of the Landau levels. In GaAs, the Landau level energy separation exceeds by far the Zeeman splitting, $\hbar\omega_C/(|g_e|\mu_B B) \approx 60$. The electrons in each spin branch of each Landau level are distributed in accordance with the Fermi-Dirac function

$$f(E) = \{\exp\left[(E - \mu(T,B))/(k_B T)\right] + 1\}^{-1},$$

where $\mu(T,B)$ is the temperature and magnetic field dependent chemical potential. At zero temperature and in the absence of the magnetic field it coincides with the Fermi energy $\mu(0,0) = E_F$.

The electron density in each Landau level is given by

$$n_e = \sum_{n_L,\pm} \int_0^\infty \frac{\mathrm{d}k_z}{2\pi} \mathcal{D}_L f[E_\pm(k_z, n_L)], \tag{4.44}$$

where $\mathcal{D}_L = 1/(2\pi l_B^2)$ is the degeneracy of each Landau level, $l_B = \sqrt{\hbar/(|e|B)}$ is the magnetic length.

The electron spin polarization $\rho_e$ in accordance with Eqs. 4.3 and 4.26 is given by

$$\rho_e = \frac{g_e\mu_B B}{n_e} \sum_{n_L} \int_0^\infty \frac{\mathrm{d}k_z}{2\pi} \mathcal{D}_L f'[\hbar\omega_C(n_L + 1/2) + \hbar^2 k_z^2/(2m)]. \tag{4.45}$$

Here $f'(E) = \mathrm{d}f/\mathrm{d}E$ and we took into account the smallness of Zeeman splitting.

In the weak field limit, where $\hbar\omega_C \ll E_F$, $\mu(T,B) \approx \mu(0,0) \equiv E_F$, the summation over Landau levels can be converted in the integration. Therefore under conditions of low field $\hbar\omega_C \ll E_F$, and low temperature $k_B T \ll E_F$, one can show that the electron spin polarization is given by

$$\rho_e = -\frac{3}{4}\frac{g_e\mu_B B}{E_F}. \tag{4.46}$$

In this limit we recover the well known result for the Pauli susceptibility. The equilibrium spin polarization is determined by the ratio of the Zeeman splitting to the Fermi energy.

The situation becomes qualitatively different if the magnetic field is so strong that $\hbar\omega_C \gg E_F$ and all electrons occupy the lowest Landau level. Due to singularity of electron density of states at low energies, $\mu(T,B) \ll E_F$. Therefore, even at the lowest temperatures, $k_BT \sim \mu(0,B)$ and the electron gas becomes non-degenerate. Its spin polarization is given by

$$\rho_e = -\frac{g_e\mu_B B}{2k_BT}, \tag{4.47}$$

i.e. depends strongly on temperature.

The critical magnetic field for the transition between the two regimes can be estimated analytically from the condition $\hbar\omega_C = \mu(0,B) = \hbar^4 n_e/(8me^2\pi B^2)$, assuming that all electrons occupy the lowest Landau level. This yields $B = 1.9$ T, close to the magnetic field at which the temperature dependence shows up in the experiment. In the general case, the dependence of $\rho_e$ on both temperature and magnetic field is calculated numerically and shown in Fig. 4.10(b).

### 4.2.2 Estimation of field induced Faraday rotation cross-section from experiments

The field induced FR cross-section can be estimated by scaling the numerically calculated $\Delta\rho_e^T = \rho_e^T - \rho_e^{20K}$ with the experimental $\Delta\Theta_F^T$. We introduce the proportionality factor $\mu_{fi}$ such that

$$\Delta\Theta_F^T = \mu_{fi}\Delta\rho_e^T. \tag{4.48}$$

For the calculation of $\rho_e^T$ we assume a degenerate free electron gas, and neglect any eventual field induced metal to insulator transition, as well as disorder and electron-electron interaction effects. One can see in Fig. 4.10(b) that a reasonable agreement between experimental FR data and calculated spin polarization is obtained for $\mu_{fi} = 100° = 1.75$ rad.

From this we deduce $\sigma_F = +2.3 \times 10^{-15}$ rad$\times$cm$^2$, in reasonable agreement with photoinduced FR, excepted for the sign. Indeed, for positive fields the electron spin polarization $\rho_e > 0$ (electron $g$-factor in GaAs is negative), and the corresponding FR $\Delta\Theta_F^T > 0$, in contradiction with photoinduced FR experiments and theoretical

predictions. The origin of this discrepancy is not known. Understanding of the temperature dependence of the FR in GaAs requires further experimental and theoretical study.

## 4.3 Comparison of photo and field induced Faraday rotation

In table 4.1 and 4.2 various estimates of FR cross-sections are summarized. Absolute values of FR cross-sections estimated by photoinduced FR and magnetic field induced FR exceed the theoretical values calculated with Eqs. 4.31 and 4.41.

Table 4.1: Summary of the experimental results of photoinduced and field induced Faraday rotation. The field induced spin polarization is calculated and scaled to match with the experimentally measured FR (see Section 4.2.2).

| Experiment | Electron density ($cm^{-3}$) | Spin polarization $\rho_e$ | FR $\Theta_F(rad)$ |
|---|---|---|---|
| 1. Photoinduced FR | $2 \times 10^{16}$ | $0.11 \pm 0.03$ | 0.17 |
| 2. Field induced FR | $2 \times 10^{16}$ | $\rho_e(B)$ | $1.75 \times \rho_e(B)$ |

Table 4.2: Comparison between measured and calculated Faraday rotation cross-sections using either photoinduced or field induced Faraday rotation.

| Experiment | Detuning $\Delta E$ (meV) | $\sigma_F^{\text{exp}}$ rad×cm$^2$ | $\sigma_F^{\text{th}}$ rad×cm$^2$ |
|---|---|---|---|
| 1. Photoinduced FR | 18 | $-(2.4 \pm 0.6) \times 10^{-15}$ | $-0.7 \times 10^{-15}$ |
| 2. Field induced FR | 12 | $+2.3 \times 10^{-15}$ | $-1.05 \times 10^{-15}$ |

## 4.4 Dynamics of photoinduced Faraday rotation

Time resolved FR on the sample 98P180 was measured using the setup described in Section 3.3.4. The time-resolved FR acquired with a fast acquisition card under pumping by a train of laser pulses with polarization $\sigma^+$ or $\sigma^-$ is shown in Fig. 4.11.

At $T = 2$ K the FR reaches 13° ($\sigma^-$ pump) in about 70 ns, and decays in about 250 ns. For $\sigma^+$ pump, the rotation angle is smaller but rise time and decay time are comparable with that of $\sigma^-$ pump. The asymmetry in the value of FR angle for the two helicities of circular polarizations arises because of birefringence of the Bragg mirrors. The decay time is limited by the electron spin relaxation time. Its value is in reasonable agreement with spin relaxation times deduced from Hanle effect. In contrast, the rise time is determined by the balance between the rate $G/n_e$, at which electron gas gets spin polarized in the presence of the pump, and the spin relaxation rate. In our experiments the condition $n_e/G \ll \tau_s$ is satisfied. In this strong pumping regime the rise time does not depend on the spin relaxation time and can be much shorter than $\tau_s$.

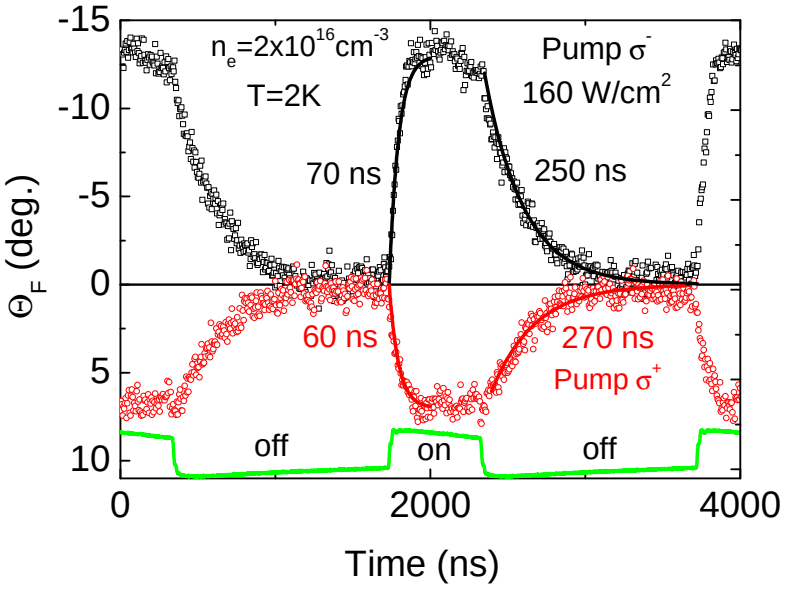


Figure 4.11: Time resolved Faraday rotation for circularly polarized 600 ns pulses (open squares/circles). The solid lines superimposed on experimental data are exponential fits of the rise and decay of the Faraday rotation, and the solid green curve in the figure bottom shows the train of pulses.

The dependence of the decay rate on the temperature is shown in Fig. 4.12. Surprisingly we observe a linear increase with temperature (solid line in Fig. 4.12), which is not expected in this temperature range $k_BT < E_F$ [KA98, DKK+02]. Further

studies are needed to understand this behavior. However, assuming linear growth of the spin relaxation rate with temperature and using Eq. 4.5 one can reasonably well describe the decay of the FR angle when the temperature increases, as shown in Fig. 4.12. This simple interpretation omits the temperature dependence of the absorption edge (5 meV shift at 50 K) and the eventual change of the quality factor with temperature.

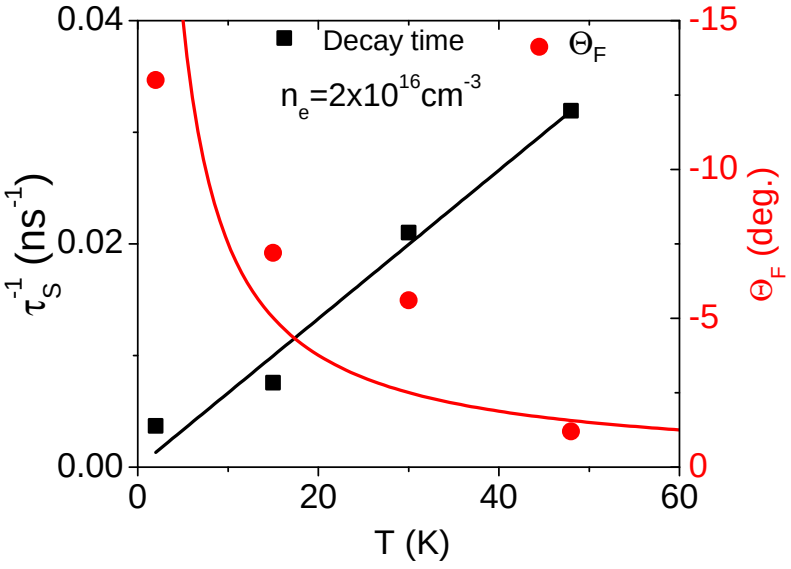


Figure 4.12: Right scale: Faraday rotation angle (closed circles) and its fit (red line) using Eq. 4.5 with measured spin relaxation time. Left scale: Temperature dependence of decay time (closed squares) and its linear fit.

These results show that a high-Q, $n$-doped microcavity can be an efficient fast optically switched Faraday rotator at low temperatures. Large FR can be obtained by reducing the detuning, or optimizing the structure for more efficient spin injection. Much shorter switching times could be reached by using a pair of counter-polarized pump pulses [AAS+98].

## 4.5 Summary

In this Chapter, we have studied the spin dynamics of electrons in $n$-doped GaAs, enclosed in a high-Q planar microcavity. We demonstrated a large FR, up to 19°

induced by optically oriented electrons. The sign of this photoinduced FR depends on the helicity of the pump beam, and it saturates at the highest pump power. This saturation of FR was found to be due to the saturation of the electron spin density. From the Hanle curves, we deduced the electron spin relaxation time $\tau_s$=160 ns. Spin polarization of the electrons were measured using two methods. From the Knight field, we obtained $\rho_e = 11 \pm 3\%$, and from the polarization photoluminescence measurement, we obtained $\rho_e = 6 \pm 2\%$.

We introduced a concept of FR cross-section $\sigma_F$, which describes the efficiency of FR by spin polarized electrons. The FR cross-section $\sigma_F$, relates $\Theta_F$ to the electron spin density, and the thickness of the layer. From independent measurements of $\Theta_F$, $\rho_e$, and $Q$, $\sigma_F$ was determined quantitatively. We found $\sigma_F = -(2.4 \pm 0.6) \times 10^{-15}$ rad$\times$cm$^2$ at 18 meV below the band gap, larger than theoretical prediction. The strong *negative* value of $\sigma_F$ found experimentally confirms that photoinduced FR is dominated by polarization dependent bleaching of absorption, while spin splitting of conduction band induced by electron-electron interactions, which contribute with the opposite sign, is probably less important.

We also found that, the external magnetic field induced FR in the low field regime is entirely dominated by the substrate, and depend strongly on the detuning. In the high field regime, the FR was found to be independent of temperature for field up to 2 T and thereafter shows variation of FR with temperature. From this, the electron spin induced contribution to the FR is extracted. However, in this experiment the spin polarization cannot be measured directly and is calculated under some poorly controlled assumptions. The field induced FR cross-section extracted form these experiments is $\sigma_F = +2.3 \times 10^{-15}$ rad$\times$cm$^2$, which is similar to the one obtained from photoinduced FR. But the sign is *positive*, in contrast to that obtained in theory and by photoinduced FR.

Finally, we demonstrate fast optical switching of FR in sub-microsecond time scale by sampling the FR in a one-shot experiment under pulsed excitation. From the decay time of $\Theta_F$, we deduce the electron spin relaxation time $\tau_s$=250 ns, slightly longer than the value deduced from Hanle curves.

# Chapter 5

# Nuclear Faraday rotation in metallic n-GaAs

In this Chapter, experimental results on the nuclear Faraday rotation (FR) are presented. We consider specifically the results on the sample with electron concentration close to the metal-to-insulator transition (Sample 98P180 with $n_e = 2 \times 10^{16}$ cm$^{-3}$). Various techniques to study nuclear spin dynamics in semiconductors, and in particular the advantages of optical techniques are discussed in Section 5.1. We propose a new technique to study nuclear spin dynamics: Faraday rotation of a non-resonant probe beam in the dark, in the absence of any external perturbation. The FR induced by the dynamically polarized nuclei is studied as a function of time and is presented in Section 5.2. Contrary to expectations, we observed, that the decay of the nuclear FR is non-monotonous, and consists of two components: one which decays very fast and another which decays slowly. In order to verify, that they originates from the nuclei, we did a detailed investigation of the effect of pump helicity and pumping duration (Section 5.2.1), effect of static field during measurement (Section 5.2.3) as well as the effect of rf magnetic field (Section 5.2.4) on the fast and slow components. From these measurements we confirm the nuclear origin of both components. Following the procedure proposed by Kalevich *et al.* [KKF82], we measured the nuclear field created by the nuclei cooled in a longitudinal field by circular polarized pumping (Section 5.3). We introduced a parameter called nuclear Verdet constant, which describes the efficiency of the nuclear field in producing

FR, and we experimentally determined this constant for the slow component, which is presented in Section 5.4. A theory on the origin of the two components of nuclear FR is proposed and is presented in Section 5.5.

## 5.1 Optical detection of nuclear spin polarization

Dynamic polarization of nuclear spins (DNP) was first observed by Lampel in n-Si [Lam68], and revealed by an increase in nuclear magnetic resonance signal upon excitation with circularly polarized light. Ekimov and Safarov [ES72a, ES72b] studied the DNP by optical methods. They were able to optically detect nuclear magnetic resonance in AlGaAs by observing the resonance changes in degree of circular polarization of luminescence. The dynamically polarized nuclei create an effective magnetic field, which act on the electrons due to hyperfine interaction, and thereby on the circular polarization of the luminescence. DNP in p-GaAs, and the effect of a small external magnetic field on the electron-nuclear spin system was studied in detail by Paget *et al.*, using luminescence depolarization due to Hanle effect [PLSS77]. Paget studied the the nuclear spin relaxation process in GaAs using optically detected NMR [Pag82]. Direct measurement of nuclear field induced spin splitting has been achieved by high resolution photoluminescence. The NMR was detected from the shift of the PL spectrum induced by the effective nuclear field [GSS+96, GBS+97, MKI09]. Kikkawa and Awschalom observed magnetic resonance behaviour in n-type GaAs, induced as well as detected optically. The NMR was detected form the measurement of electron Larmor precession frequency, which was probed by time resolved Kerr/Faraday rotation [KA00]. Nuclear spin dynamics in semiconductors has also been studied by magnetic and electrical techniques as well, such as NMR, transport measurements [LHK+06, KZF+12].

The optical techniques are the most sensitive and commonly used to study spin dynamics in semiconductors. The optical techniques rely on the dynamic polarization of nuclei by optical pumping, which allows cooling of the nuclei below the lattice temperature. In these mechanisms, angular momentum is transferred from the electronic to the nuclear spins through mutual spin flips, or flip-flop interactions. Even a small number of spin polarized nuclei can provide a large optical response through nuclear field acting on the electron spins. However, in all the optical methods,

the presence of spin polarized carriers in the sample is necessary in order to observe either circular polarization of luminescence, or the Larmor resonance frequency shift (Overhauser shift) due to nuclear magnetization. The spin polarized electrons used for the measurement, can also provide a strong feedback, which may greatly complicate and modify the behaviour of nuclear spin system [MZ84]. This also leads to nonlinear phenomena such as spontaneous oscillation and bistability [Dya08, UMA+13]. In addition, because the time needed for nuclear polarization build up or relaxation is much longer than recombination and even spin relaxation time in semiconductors, no single-shot measurements is possible by these techniques. This means that the measured nuclear field is averaged over many realizations

Artemova and Merkulov proposed, that all these problems can be avoided if the experiment could be carried out in two stages [AM85]. First, nuclear spins are polarized by optical pumping with circularly polarized light in the presence of a longitudinal magnetic field. Then, the pump beam is switched off and the time evolution of the nuclear field is detected via Faraday rotation of the weak linearly polarized non-resonant probe beam.

In a bulk material, there is a strong absorption of the pump light. The nuclei can be polarized only in a small area, and the nuclear FR is expected to be very weak. To increase the sensitivity, we use the same microcavity structure as used for study of electron spin dynamics in the previous chapter.

This novel detection scheme along with the microcavity structure is used here to study nuclear spin dynamics in bulk n-GaAs. Bulk n-GaAs is particularly interesting in order to study nuclear spin dynamics because of long nuclear spin-lattice relaxation time. The system is similar to QDs in the low doping regime. However, in this chapter, we will study the sample 98P180 with electron concentration close to the metal-to-insulator transition ($n_e = 2 \times 10^{16}$ cm$^{-3}$). In this doping regime, the nuclear spin relaxation is expected to be dominated by Korringa mechanism [Abr61, LHK+06].

## 5.2 Nuclear Faraday rotation

The nuclear spins were cooled down during 3 minutes pumping with $\sigma^-$ polarized light in a longitudinal field $B_z$=150 G at T=2 K. Then, the pump is switched off at $t = 0$. The FR of the probe beam is recorded during cooling, as well as during

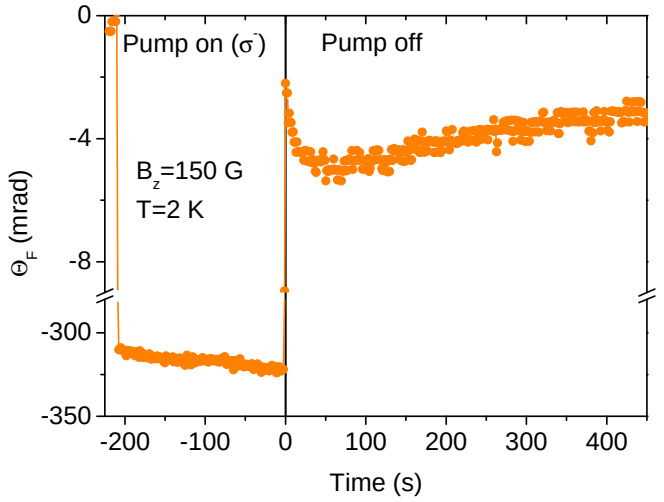


Figure 5.1: Faraday rotation spectra during cooling with $\sigma^-$ polarized light at $B_z$=150 G (t<0) as well as during measurement in the dark (t>0) at the same field.

measurement stage as shown in Fig. 5.1. During the cooling stage, optically created electron spin polarization produces a strong FR (about 19 deg). One can see, that the FR builds up during pumping, which indicates the build up of nuclear polarization. When the pump is switched off, the photoinduced spin polarization of electrons disappears immediately (spin relaxation time = 160 ns) and the FR is very small (t > 0). This comes from the nuclei, and we expect this FR to decay monotonously [AM85]. However, a non-monotonous behavior is observed. There are two contributions to the FR signal in the dark with different signs and large difference in their relaxation time. The fast relaxing component has a characteristic time of about few seconds, and the slow relaxing component has a characteristic time of about few minutes. These time scales are much larger than the spin relaxation time of the electrons. Therefore, we attribute the two components to the polarization of nuclear spins.

In order to get a clear understanding of the origin of these two components, we study the effect of pump helicity, pumping time, as well as static and radio frequency magnetic fields, on the observed FR signal. We will discuss about these in the following sections.

### 5.2.1 Effect of pump helicity and pump duration

Here we want to study the effect of pump helicity and pumping duration on the FR signal in the dark. Nuclear spins were cooled down either by $\sigma^+$ or $\sigma^-$ pumping at $B_z = 50$ G. Then, the pump was switched off and the FR due to nuclei in the dark was detected at the same field as shown in Fig. 5.2. One can see the non-monotonous evolution of nuclear FR, and the sign of both the components are reversed when the helicity of the pump is reversed.

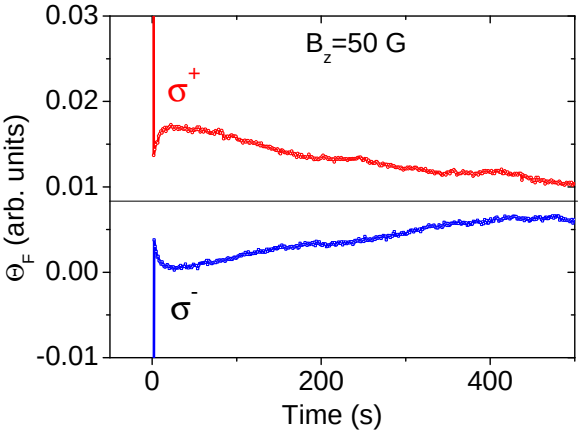


Figure 5.2: Faraday rotation induced by nuclear polarization at $B_z$=50 G after prepared by $\sigma^+$ (upper curve) and $\sigma^-$ (lower curve) pumping in the same field at $T = 2$ K.

In the next set of experiments, nuclear spins were cooled down at $B_z = 200$ G by $\sigma^-$ pumping during 1 to 30 minutes and the FR due to the nuclei in the dark was detected in the same field (see Fig. 5.3(a)). One can see the non-monotonous evolution of nuclear FR irrespective of the pumping duration. The corresponding amplitudes and decay times are deduced from the fits of the bi-exponential decay of the nuclear FR and are shown in Fig. 5.3(b, c). The amplitudes of the two components have different signs, and the amplitude of the slow component increases with pumping time. This effect is so strong that the sign of the FR at $t = 0$ depends on the pumping duration. The decay times of the two components differ by a factor of 50 and do not depend on pumping time.

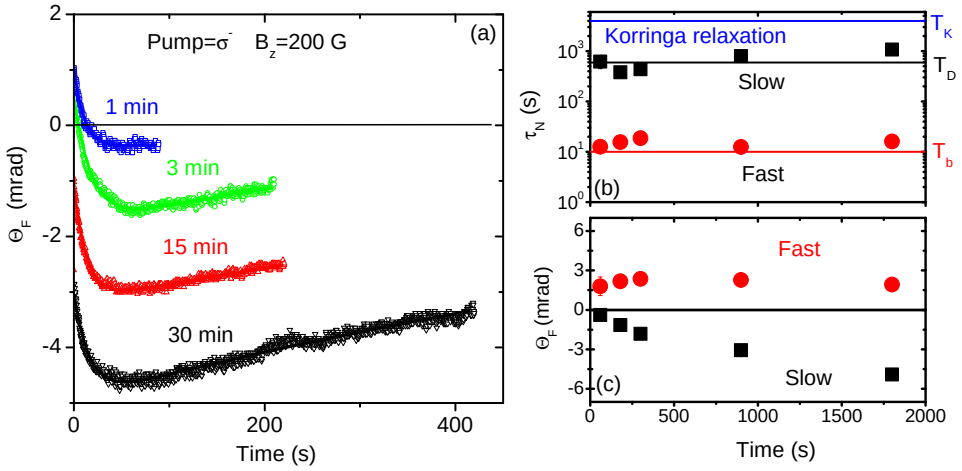


Figure 5.3: (a) Faraday rotation induced by nuclear polarization at $B_z$=200 G after prepared by $\sigma^-$ pumping (pumping during 1 to 30 minutes) in the same field at $T = 2$ K. The solid lines are fit of the bi-exponential decay. The decay times (b) as well as amplitudes (c) of the two FR components extracted from the fits of bi-exponential decay of time dependence as shown in (a). Solid lines are theoretical estimation for nuclear spin relaxation times under the orbit of localized electrons $T_b$, diffusion limited relaxation $T_d$, and Korringa relaxation $T_K$.

### 5.2.2 Hypothesis on the origin of fast and slow components of nuclear FR

In the previous sections, we have observed that there are two contributions to the nuclear FR. An important clue to understand the origin of these two components is provided by their vastly different relaxation times.

In the sample under study (98P180), the doping density is close to the metal-insulator transition. At this concentration (Fermi energy $E_F$= 4 meV) it is possible to have both free as well as localized electrons. These electrons interact with the nuclei. Under the condition of optical pumping, the nuclei are polarized both via free as well as localized electrons and the direction of nuclear polarization is the same. When the pump is switched off, the nuclear field induced FR is realized both via free as well as localized electrons. We will estimate quantitatively the nuclear spin relaxation time due to interaction with these two groups of electrons.

### I. Nuclear spin relaxation by donor bound electrons

Since, in our sample, the doping density is close to the metal-insulator transition (MIT), single donors can not bind electrons because of screening by the electron gas. Therefore, the density of shallow bound states is determined by the number of closely spaced donor pairs [SE84]. If the distance between the donors is less than the screening length, then they form a localized state. Assuming Poisson distribution of the localized states and Fermi wavelength $\approx$ 10 nm, the concentration of localized states can be estimated to be $N_b$=2$\times$ $10^{15}$ cm$^{-3}$ [SE84]. The relaxation of nuclei by localized electrons is given as [DP74]:

$$\frac{1}{T_b} = \omega_N^2 \tau_c, \tag{5.1}$$

where $\omega_N = g_n \mu_N B_e$ is the precession frequency of nuclear spin in the Knight field ($B_e$) created by the localized electrons, $\tau_c$ is the correlation time of the localized electron spin ($\approx 10^{-11}$ s), determined by exchange scattering with free electrons [Pag81, Kav08].

The amplitude of the Knight field created by the localized electrons at the center of the donor site is $B_e \approx 100$ G [PLSS77] . Then, using Eq. 5.1, we obtain $T_b \approx 10$ s, close to the values measured for the relaxation of the fast component. Therefore, the fast component can be associated with the nuclei under the orbit of localized electrons.

### II. Nuclear spin relaxation by free electrons and spin diffusion

In addition to the nuclei under the orbit of localized electrons, there are nuclei situated away from the localizing centers. Under optical pumping condition, these remote nuclei can be dynamically polarized by free electrons [HCL$^+$12], also by spin diffusion from localizing centers [Pag81]. However, these processes are much slower than dynamic nuclear polarization by localized electrons. Therefore, the pumping time required for the build up of the slow component is much longer, consistent with experimental results presented in Section 5.2 and 5.2.1.

The spin relaxation of the remote nuclei is expected to be induced by flip-flops with the electrons from the thermally broadened Fermi edge, a process known as

Korringa mechanism [Abr61, LHK+06]. The Korringa relaxation time at $T$= 2 K for $n_e$=2×10$^{16}$ cm$^{-3}$ is estimated to be $T_K \approx 10^4$ s. This time is much longer than the observed relaxation time of the slow component.

We suggest that, the nuclear relaxation is due to the nuclear spin diffusion to the donor centers. The time of this diffusion-limited relaxation can be estimated as [Gen58]:

$$\frac{1}{T_D} = 4\pi D N_b a, \tag{5.2}$$

where $D \approx 10^{-13}$ cm$^2$/s is the nuclear spin diffusion coefficient [Pag82], and $a$ is the localization radius of the electron on the center.

Assuming $a$= 10 nm, we obtain $T_D \approx 10^3$ s, close to the values measured for the relaxation of the slow component. Therefore, nuclear spin relaxation is limited by spin diffusion to the donor centers, where efficient relaxation involving localized electrons takes place.

### 5.2.3 Effect of static magnetic field

Here we studied the effect of longitudinal field on the amplitude as well as decay time of the fast and slow components. Nuclei were cooled down at 2 K under $\sigma^-$ polarized pumping at $B_z$=150 G. Then the pump is switched off at $t = 0$ and the Faraday rotation of the probe is recorded at different longitudinal magnetic fields as shown in Fig. 5.4(a). One can see, that for the lowest field $B_z = 3$ G, the fast component relaxes very fast and the decaying component mainly comes from the slow component. But for higher fields, both components could be observed clearly.

The relaxation times of these two FR components is extracted from the fits of the data at different fields, and are shown in Fig. 5.4(b). The relaxation time of the fast component varies between 1-15 s and the relaxation time of the slow component varies between 100-500 s as field increases. The amplitudes of the two components are also extracted from the fits and are shown in Fig. 5.4(c) (black and red symbols). Amplitudes of both the components decreases, when magnetic field decreases.

We have also measured the FR directly, after the pump is switched off and the cooled nuclei are repolarized in field from 180 to 0 G. This field dependence is plotted together with the amplitudes of fast and slow components and is shown in Fig. 5.4(c)

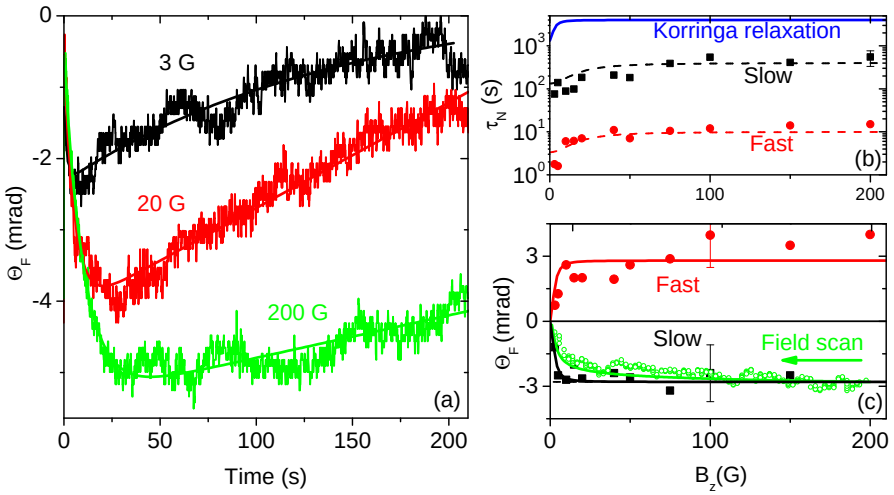


Figure 5.4: (a) FR in the darkness due to nuclear polarization prepared by 4 minutes of pumping in $\sigma^-$ polarization under $B_z = 150$ G, as a function of time at different fixed values of magnetic fields. Solid lines are fits to the bi-exponential decay. Relaxation times (b), and the amplitudes (c), of the two FR components extracted from the data in (a). The green symbols in (c) are the FR measured with the field sweep from 180 G to 0 (sweep time, t=40 s).

(green symbols). The field dependence is similar in both cases at higher fields, but at lower fields the field dependence is different. This can be explained as follows:

The initial inverse spin temperature is given by (see Eq. 2.23)

$$\beta_{N0} \propto \frac{\boldsymbol{B}_0.\boldsymbol{S}}{\boldsymbol{B}_0^2 + \xi \boldsymbol{B}_L^2}, \tag{5.3}$$

where $\boldsymbol{B}_0$ is the initial field in which the nuclei have been cooled, and here we neglect the small Knight field. Then, assuming that the experiment is carried out in a short time compared to $T_1$, the nuclear demagnetization is an isentropic process in which the inverse spin temperature $\beta_N$ changes according to [AP58]

$$\frac{\beta_{N0}}{\beta_N} = \left( \frac{\boldsymbol{B}^2 + \boldsymbol{B}_L^2}{\boldsymbol{B}_0^2 + \boldsymbol{B}_L^2} \right)^{1/2}. \tag{5.4}$$

A more detailed calculation by Paget *et al.* [PLSS77] shows that $\boldsymbol{B}_L^2$ should be

replaced by $\xi \boldsymbol{B}_L^2$ in Eq. 5.4. Hence, we get

$$\beta_N \propto \frac{\boldsymbol{B}_0.\boldsymbol{S}}{(\boldsymbol{B}_0^2 + \xi \boldsymbol{B}_L^2)^{1/2}(\boldsymbol{B}^2 + \xi \boldsymbol{B}_L^2)^{1/2}}. \tag{5.5}$$

Finally, the average nuclear spin polarization during demagnetization is given by

$$\langle \boldsymbol{I} \rangle \propto \beta_N \boldsymbol{B} \propto \frac{(\boldsymbol{S}.\boldsymbol{B}_0)\boldsymbol{B}}{(\boldsymbol{B}_0^2 + \xi \boldsymbol{B}_L^2)^{1/2}(\boldsymbol{B}^2 + \xi \boldsymbol{B}_L^2)^{1/2}}. \tag{5.6}$$

As in our experiment, $\boldsymbol{B}_0 \gg \boldsymbol{B}_L$, Eq. 5.6 simplifies to

$$\langle \boldsymbol{I} \rangle \propto \frac{(\boldsymbol{S}.\boldsymbol{n})\boldsymbol{B}}{(\boldsymbol{B}^2 + \xi \boldsymbol{B}_L^2)^{1/2}}, \tag{5.7}$$

where $\boldsymbol{n} = \boldsymbol{B}_0/B_0$.

When $\boldsymbol{B} \sim \boldsymbol{B}_L$, $\langle \boldsymbol{I} \rangle$ becomes larger than the polarization obtained by direct cooling in the field $\boldsymbol{B}$. This is because dynamic nuclear polarization becomes inefficient in the field less than $\boldsymbol{B}_L$.

$$\langle \boldsymbol{I} \rangle \propto \frac{(\boldsymbol{S}.\boldsymbol{n})\boldsymbol{B}^2}{(\boldsymbol{B}^2 + \xi \boldsymbol{B}_L^2)}. \tag{5.8}$$

We see, that where as Eq. 5.8 fits the experimental data obtained by cooling in different fields (black and red lines in Fig. 5.4(c) ), Eq. 5.7 does not fit the data obtained by cooling in $B_0 = 180$ G, and sweeping the field to zero. We attribute this to relaxation during demagnetization. Taking into account the relaxation and assuming that nuclear spin-lattice relaxation does not depend on the external field, the average nuclear spin polarization during demagnetization is given by

$$\langle \boldsymbol{I} \rangle \propto \frac{(\boldsymbol{S}.\boldsymbol{B}_0)\boldsymbol{B}}{(\boldsymbol{B}_0^2 + \xi \boldsymbol{B}_L^2)^{1/2}(\boldsymbol{B}^2 + \xi \boldsymbol{B}_L^2)^{1/2}} \exp(-t/\tau_N). \tag{5.9}$$

Eq. 5.9 fits the experimental data obtained by cooling in $B_0 = 180$ G, and sweeping the field to zero (green curve in Fig. 5.4(c)). We get the green curve with $\tau_N$= 470 s.

### 5.2.4 Effect of rf magnetic field (NMR experiments)

We did nuclear magnetic resonance experiment (NMR) to obtain information about the contribution from different species of nuclei to the two components of Faraday rotation. We used the setup described in section 3.3.6 for this purpose. A small Helmholtz coil surrounding the sample is used to apply radio frequency field. We measure the NMR signal associated with the fast and slow components separately.

Since the fast component decays in about 10 s and coexist with the long component, it is difficult to apply rf field during the measurement stage to extract the NMR signal associated with the fast component. Therefore the idea was to apply the rf field during cooling stage itself. When the rf field is in resonance with any of the isotopes, they will depolarize, which will result in decrease of the amplitude of the fast component.

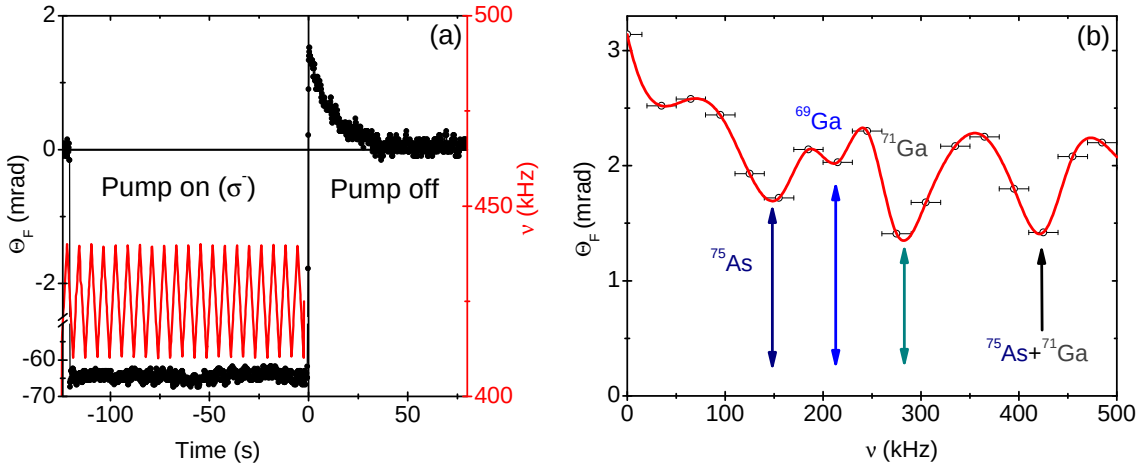


Figure 5.5: NMR detected by fast component of the FR. (a) FR measured after preparation under $\sigma^-$ pumping during 2 minutes at $B_z$=150 G with transverse magnetic field $B_{rf}$= 2.5 G oscillating at radio frequency. (b) Amplitude of FR as a function of radio frequency range applied during pumping.

Nuclei were cooled down at 2 K under $\sigma^-$ polarized pumping during 2 minutes at $B_z$=150 G with transverse magnetic field $B_{rf}$= 2.5 G oscillating at radio frequency, $\nu$ with frequency span $\Delta\nu$ = 30 kHz. Then the pump is switched off and the amplitude of the fast component of FR is measured [Fig. 5.5(a)]. The amplitude of the fast component of FR is measured at different radio frequencies and is shown in Fig.

5.5(b). It can be seen from the figure that the amplitude of FR dips at certain frequencies. We identify the dips to known resonant frequencies of different GaAs isotopes. We can also observe multispin resonances such as ($^{75}$As+$^{71}$Ga) in the signal. Thus all the isotopes of GaAs contributes to the fast component of FR.

We use another scheme to extract the NMR signal associated with slow component. Nuclei were cooled down at 2 K under $\sigma^-$ polarized pumping during 5 minutes at $B_z$=150 G. Then the pump is switched off and we wait for about 1 minute to allow the fast component to decay completely. Then a transverse magnetic field $B_{rf}$= 2.5 G oscillating at radio frequency sweeping from 100 to 300 kHz is applied for about 1 minute. The FR in the dark is recorded as a function of time. The amplitude of FR measured as a function of time during the rf frequency sweep is shown in Fig. 5.6(a). When the frequency passes through the NMR resonance of a nuclear species, depolarization of that particular isotope results in the signal dips. One can observe clearly the resonances of both the Ga isotopes but the $^{75}$As is less visible. Thus all the isotopes contribute to the slow component also.

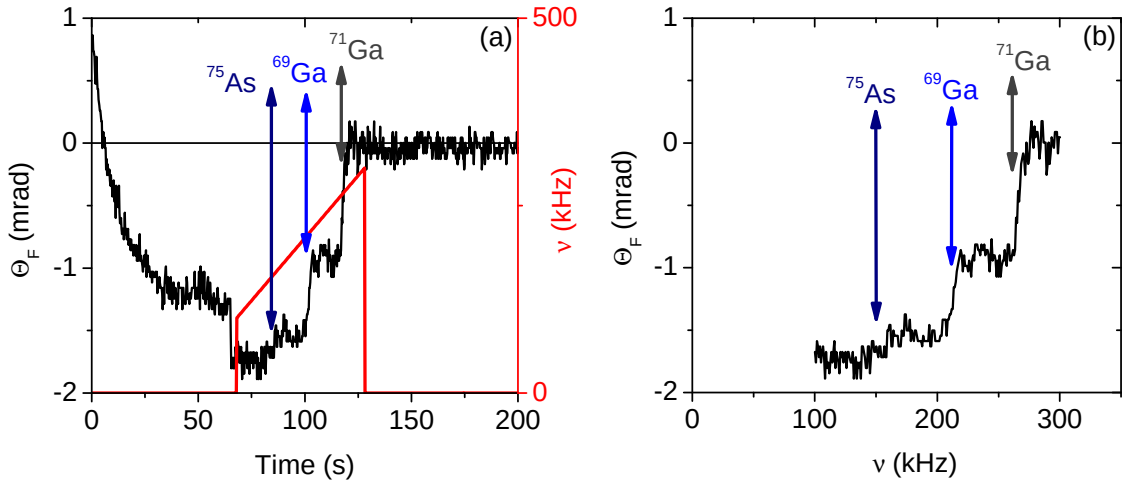


Figure 5.6: NMR detected by slow component of the FR. (a) FR measured after preparation under $\sigma^-$ pumping during 5 minutes at $B_z$=150 G. A transverse magnetic field $B_{rf}$= 2.5 G oscillating at radio frequency is applied 1 minute after the pump is switched off, when the fast component is completely relaxed. (b) The signal shown in (a), presented as a function of radio frequency.

Therefore, we conclude from the NMR experiments that all the isotopes of GaAs contributes to both the fast as well as slow component of the nuclear FR and the

difference in nuclear spin dynamics is not related with any particular species of nuclei.

We did also measurements for different spans of the sawtooth sweeps $\Delta\nu$, in the NMR of the fast component. The largest dips were obtained for $\Delta\nu$= 30 kHz, which gives us estimates of the broadening of the NMR resonance. This is much broader than resonances detected in the slow components. Since broadening is due to disorder in the system, different broadening of the NMR resonance for the two components suggest that they comes from different localization in the sample.

### 5.2.5 Repolarization of nuclei in an external magnetic field

Here we want to demonstrate the repolarization of the cooled nuclei in an external magnetic field. The nuclear spins were cooled down during 4 minutes pumping with $\sigma^-$ polarized light in longitudinal field $B_z$=150 G at T=2 K. Then the pump is switched off at $t = 0$ and simultaneously we set $B_z$=+7 G, or $B_z$=-7 G, or alternating field $B_z$=±7 G is applied. The Faraday rotation of the probe beam is recorded during cooling as well as during measurement stage as shown in Fig. 5.7.

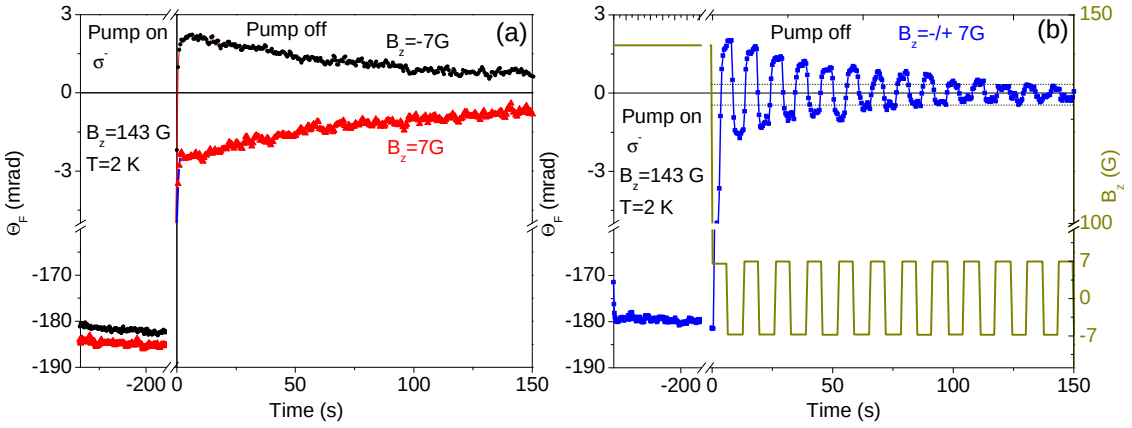


Figure 5.7: Faraday rotation during cooling of the nuclei at $B_z$=143 G in $\sigma^-$ pumping at $T = 2$ K as well as in the dark when the pump is switched off and field $B_z = 7$ G (red triangles) or $B_z = -7$ G (black circles) is applied (a), as well as when alternating field $B_z = \pm 7$ G (blue squares) is applied (b).

When the pump is switched off, since the applied field has a small value, the fast component is negligibly small and decays on the time scale of 1 s. The FR signal in the dark consists of two parts: the decaying part originates from the nuclear

magnetization while the constant part comes from the external field (dashed lines). We can see clearly from the figure that the sign of rotation can be changed by changing the direction of the external field. One can also see in Fig. 5.7(a) that, when the external field is reversed, both the nuclear field induced and external field induced FR keeps the same sign. This can be explained considering the fact that the nuclear spin orientation is fully destroyed by dipole-dipole interaction when the external field passes through zero and the nuclear field always rebuilds in the direction opposite to the external field. This also illustrates the concept of nuclear spin temperature in n-GaAs. The average spin of nuclei cooled down to temperature $\Theta_N$ is given by the Curie law:

$$\langle \boldsymbol{I} \rangle = \frac{I(I+1)\mu_N \boldsymbol{B}}{3k_B \Theta_N}, \tag{5.10}$$

where $k_B$ is the Boltzman constant, I=3/2 is nuclear spin [Dya08].

Using Eq. 2.6, we get

$$\boldsymbol{B}_N = \frac{AI(I+1)\mu_N \boldsymbol{B}}{3k_B \Theta_N \mu_B g_e}. \tag{5.11}$$

From the value of $B_N$ we deduce $\Theta_N = 10^{-4}$ K. Therefore, at a given spin temperature, the nuclear spin polarization and the Overhauser field are controlled by the external field, and the resulting spin dynamics can be studied by FR at any external field, on time scales much longer than electron spin relaxation time.

## 5.3 Measurement of the nuclear field

We have measured the nuclear field created by circular polarized pump in a longitudinal magnetic field, using the setup described in Section 3.3.6. Cooling of the nuclear spin system in a longitudinal magnetic field under circularly polarized pump and the behaviour of cooled nuclear spin system in a transverse magnetic field in the weak pumping regime is discussed in Appendix C. The nuclear field is measured using the method proposed and applied by Kalevich *et al.* [KKF82]. In their experiment, the time evolution of the electron spin polarization was detected by photoluminescence. Here we use FR of a linearly polarized probe to observe the time evolution of the electron spin polarization.

Nuclear spin were cooled down by strong optical pumping (2 mW for about 3 min) in a longitudinal magnetic field $B_z$=100 G at T= 4 K. Then the longitudinal magnetic field was set to zero, transverse magnetic field $B_x$= 7 G was applied and the pump power was reduced to 80 $\mu$W in order to reduce repolarization of the nuclear spins as much as possible. Fig. 5.8 shows the time evolution of the FR signal with the laboratory time $t$ in the presence of transverse magnetic field. The nuclear field is much stronger than the applied magnetic field and has opposite direction. This correspond to $t = t_1$ in the Hanle curve. With time the nuclear field decreases and so also the total transverse field. This results in increasing electron spin polarization and the FR signal follows. At $t = t_2$, the nuclear field exactly compensates the external field and FR signal reaches its maximum. The nuclear field continues to decrease and goes to zero and the FR signal then decreases. At $t = t_3$, the FR signal is due to the spin polarization corresponding to external field only.

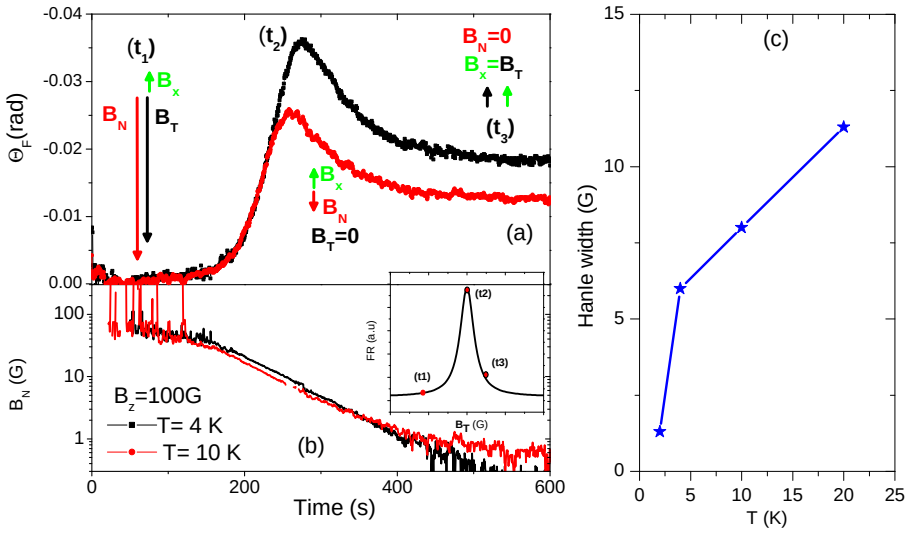


Figure 5.8: Measurement of nuclear field prepared by the pumping in $\sigma^-$ polarization under magnetic field $B_z = 100$ G. (a) Time evolution of the Faraday rotation in a transverse field, and (b) the corresponding nuclear field obtained using Eq. 4.10. (c) Hanle width extracted from the fits at different temperatures.

Since the pump induced FR is proportional to the electron spin polarization degree, the time dependence of the FR signal can be described by the time dependent

Hanle formula [MZ84]:

$$\Theta_F^{pump}(t) \propto S_e(t) = \frac{1}{1 + (B_x + B_N(t))^2/B_H^2} \tag{5.12}$$

where $B_H$ the full width at half maximum of the Hanle curve, that is the magnetic field such that $\Omega\tau_s = 1/2$. Here $\Omega$ and $\tau_s$ are electron spin precession frequency and relaxation time, respectively.

Fitting the time evolution of FR shown in Fig. 5.8(a) with Eq. 5.12, we obtain the value of Hanle width $B_H = 7$ G at 4 K. Because electron spin relaxation accelerates with temperature, $B_H$ also increases with temperature as shown in Fig. 5.8(c).

The variation of nuclear field with time at T= 4 K is shown in Fig. 5.8(b). It can be seen that in the time interval where the signal is strong enough, nuclear field decreases exponentially. Assuming exponential relaxation yields $B_N(t = 0) = 350$ G in the external field $B_v = 7$ G, and nuclear spin relaxation time $T_1 = 60$ s.

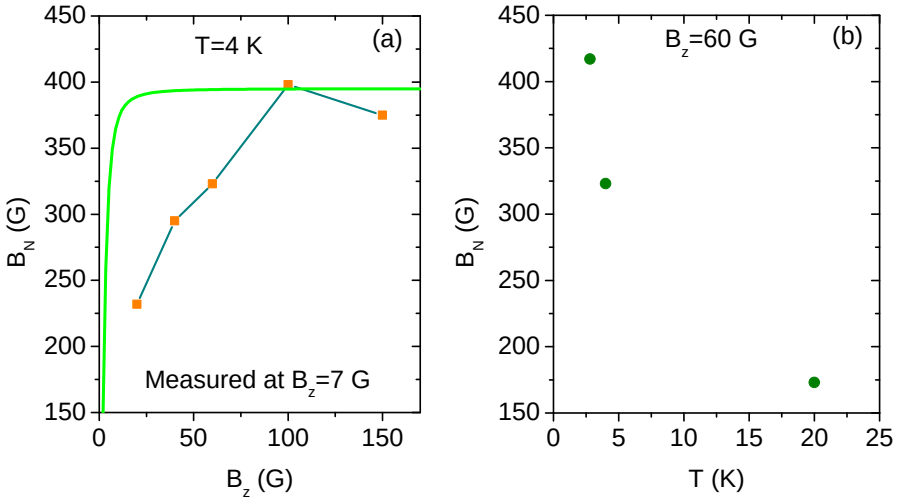


Figure 5.9: (a) Dependence of nuclear field on the longitudinal field applied during pumping at T=4 K. The green curve is the calculated field dependence of nuclear field using Eq. 5.15. (b) Dependence of nuclear field on temperature for the system cooled in longitudinal field $B_z$=60 G.

We repeated this experiment for different $B_z$ (Fig. 5.9(a)), and at different temperatures (Fig. 5.9(b)). It can be seen, that the nuclear field increases with $B_z$ at T=4 K.

We recall that the nuclear spin temperature under steady state optical pumping conditions in an external field $\boldsymbol{B}_z$ can be expressed as [DP75, FDZ76]:

$$\beta_{Nz} = (k_B \Theta_N)^{-1} = \frac{4I}{\mu_N} \frac{\boldsymbol{B}_z.\boldsymbol{S}}{\boldsymbol{B}_z^2 + \xi B_L^2}. \tag{5.13}$$

The field is then reduced from $\boldsymbol{B}_z$ to $\boldsymbol{B}_x$. Then the final temperature of the nuclei will be ($\boldsymbol{B}_x^2 \gg \xi B_L^2$)

$$\beta_{Nx} \simeq \frac{|\boldsymbol{B}_z|}{|\boldsymbol{B}_x|} \beta_{Nz}. \tag{5.14}$$

After adiabatic demagnetization, the nuclear field is given by

$$\boldsymbol{B}_N \propto \frac{\langle I \rangle}{I} = \frac{\mu_N I(I+1)\boldsymbol{B}_x}{3I} \beta_{Nx} = \frac{4}{3} I(I+1) \frac{(\boldsymbol{B}_z.\boldsymbol{S})|\boldsymbol{B}_z|}{\boldsymbol{B}_z^2 + \xi B_L^2}. \tag{5.15}$$

One can see that the nuclear field $\boldsymbol{B}_N$ does not depend on $|\boldsymbol{B}_x|$, the field at which it was measured. Eq. 5.15 is plotted in Fig. 5.9(a), together with the experimental data. One can see that the variation of nuclear field is completely different from the experimental data.

For $\boldsymbol{B}_z \gg \boldsymbol{B}_L$, $\boldsymbol{B}_N \propto \boldsymbol{S}$. Let us assume that $\boldsymbol{S}$ is not constant. Then from Eq. 5.16

$$\boldsymbol{S} = \boldsymbol{S}_0 \frac{G\tau_s}{G\tau_s + n_e}. \tag{5.16}$$

For localized electrons, the relaxation time is given by [Abr61]

$$\tau_s = \tau_s(0)[1 + \Omega^2 \tau_c^2], \tag{5.17}$$

where $\tau_c$ is the correlation time, which is a measure of interaction between donors due exchange interaction between electrons or electrons hoping form donors to donors.

Thus $\boldsymbol{S}$ could increase with $\boldsymbol{B}_z$, resulting in an increase of $\boldsymbol{B}_N$ with $\boldsymbol{B}_z$, if $\Omega\tau_c \gg 1$. However the correlation time in this doping regime ($n_e = 2 \times 10^{16}$ cm$^{-3}$) is short $\tau_c \approx 10^{-11}$ s [DKK+02]. Therefore the field dependence of nuclear field is not clearly understood.

## 5.4 Determination of the nuclear Verdet constant

The efficiency of FR in a magnetic field is usually characterized by the Verdet constant, $V$ and the FR is proportional to $V$ (see Section 2.7).

In analogy with this definition, we define the nuclear Verdet constant $V_N$ which determines the efficiency of FR induced by the nuclear field. Then the nuclear FR is given as,

$$\Theta_F = V_N B_N L \tag{5.18}$$

The sign of this rotation is defined to be positive if the rotation is clockwise for the observer looking in the direction of the field.

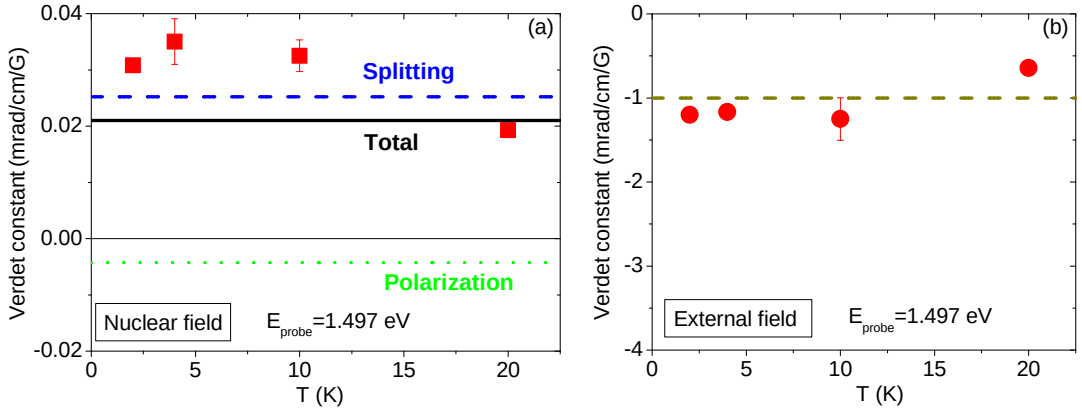


Figure 5.10: (a) Efficiency of the FR due to nuclear field (Nuclear Verdet constant) measured at different temperatures (squares). Solid lines are calculated from Eq. 5.27 as described in Section 5.5. (b) Efficiency of the FR due to external field (Verdet constant), measured at different temperatures (circles). Solid line is obtained from the independent measurement of FR as a function of magnetic field in the absence of nuclear polarization as shown in Fig. 4.9(a).

The Overhauser field is measured experimentally as a function of external field as well as temperature as described in Section 5.3. Using the values of $B_N$ we deduced the Verdet constant at different temperatures. Fig. 5.10 shows the temperature dependence of nuclear Verdet constant as well as that of conventional Verdet constant characterizing FR in an external field. The nuclear Verdet constant is about $V_N$=0.03 rad/cm/G and does not show any significant temperature dependence. This

corresponds to the slow component of the FR while it was not possible to determine the Verdet constant associated with the fast component. The conventional Verdet constant has a negative sign. Also we note that $V_N \approx -V/30$. Since $V$ depends strongly on detuning of the probe energy with respect to the gap, $\Delta = E_g - \hbar\omega$ (see section 4.2), $V_N$ will also be very sensitive to $\Delta$.

## 5.5 Theory of nuclear Faraday rotation

In the sample under study (98P180), the doping density is close to the metal insulator transition. At this concentration (Fermi energy $E_F$= 4 meV) it is possible to have both free as well as localized electrons. These electrons interact with the nuclei. Under the conditions of the optical pumping, the nuclei are polarized both via delocalized and localized states and the direction of nuclear polarization is the same. But the localized electrons are much more efficient in polarizing the nuclei. When the pump is switched off, the nuclear field induced FR is realized both via free as well as localized electrons. In the following sections, we will discuss the nuclear field induced FR and calculate the nuclear Verdet constant.

### 5.5.1 Contribution of interband transitions to Nuclear FR

In this section we discuss the sign of the nuclear field induced FR via delocalized electrons and will calculate the efficiency of FR associated with it.

The nuclear field $B_N$ causes the splitting of the conduction electron spin state, $\Delta_N = |g_e \mu_B B_N|$. If one choose as quantization axis for the spin, the direction of the field, then for $g_e < 0$, the lowest spin branch corresponds to $+1/2$ (and conversely) ( see Appendix B). Following the calculation by Artemova and Merkulov [AM85], the absorption coefficients for $\sigma^+$ and $\sigma^-$ light polarizations are given as

$$\alpha_+ = A\left[3\left(\hbar\omega - E_g + \frac{\Delta_N}{2}\right)^{1/2} + \left(\hbar\omega - E_g - \frac{\Delta_N}{2}\right)^{1/2}\right] \tag{5.19}$$

and

$$\alpha_- = A\left[3\left(\hbar\omega - E_g - \frac{\Delta_N}{2}\right)^{1/2} + \left(\hbar\omega - E_g + \frac{\Delta_N}{2}\right)^{1/2}\right], \tag{5.20}$$

where

$$A = \frac{e^2\hbar}{12mcn}\left[\left(\frac{2\mu_{hh}}{\hbar^2}\right)^{3/2} + \left(\frac{2\mu_{lh}}{\hbar^2}\right)^{3/2}\right]. \tag{5.21}$$

Then

$$\alpha_+ - \alpha_- \cong \frac{A\Delta_N}{\sqrt{\hbar\omega - E_g}} = \frac{A\Delta_N}{\sqrt{\Delta}}, \tag{5.22}$$

where $\Delta = \hbar\omega - E_g$ is the detuning between the cavity mode and energy gap of GaAs.

Then the the difference of imaginary part of the dielectric susceptibilities is

$$\delta\varepsilon''(\omega) = \frac{cn}{\omega}\frac{A\Delta_N}{\sqrt{\Delta}}. \tag{5.23}$$

At low temperatures in doped semiconductors (and assuming that $m_{hh}, m_{hh} \gg m$), the presence of carriers leads to the shift of the absorption edge from $E_g$ to $E_g + E_F$. Taking this into account and using the Kramers-Kroning relation, we obtain

$$\delta\varepsilon'(\omega) = -\frac{cn}{\omega}\frac{A\Delta_N}{\sqrt{\Delta}}\left(1 - \frac{2}{\pi}\arctan\sqrt{\frac{E_F}{\Delta}}\right). \tag{5.24}$$

Then the Faraday rotation angle is

$$\Theta_F = \frac{\omega}{4cn}\delta\varepsilon'(\omega)d_{eff} = -\frac{A\Delta_N d_{eff}}{\sqrt{\Delta}}\left(1 - \frac{2}{\pi}\arctan\sqrt{\frac{E_F}{\Delta}}\right). \tag{5.25}$$

In general case of arbitrary relations between $m_{hh}, m_{hh}$ and $m$, we obtain

$$\Theta_F = V_N^f d_{eff} B_N, \tag{5.26}$$

where $V_N^f$ is the nuclear Verdet constant associated with the free electrons and is given as

$$V_N^f = -\frac{e^2\hbar}{48mcn}\frac{g_e\mu_B}{\sqrt{\Delta}}\left[\left(\frac{2\mu_{hh}}{\hbar^2}\right)^{3/2}\left(1-\frac{2}{\pi}\arctan\sqrt{\frac{\frac{m}{\mu_{hh}}E_F}{\Delta}}\right)+\left(\frac{2\mu_{lh}}{\hbar^2}\right)^{3/2}\left(1-\frac{2}{\pi}\arctan\sqrt{\frac{\frac{m}{\mu_{lh}}E_F}{\Delta}}\right)\right]. \quad (5.27)$$

Now, taking $E_F$= 4 meV, $\Delta$= 18 meV and standard GaAs parameters, we obtain $V_N^f$= 0.2 mrad/cm-G. This is close to the experimentally determined Verdet constant ($V_N$= 0.1 mrad/cm-G) for the slow component of the nuclear FR.

### 5.5.2 Contribution of transition from valence band to localized states to Nuclear FR

In this section we discuss the sign of the nuclear field induced FR via localized electrons and will calculate the efficiency of FR associated with it.

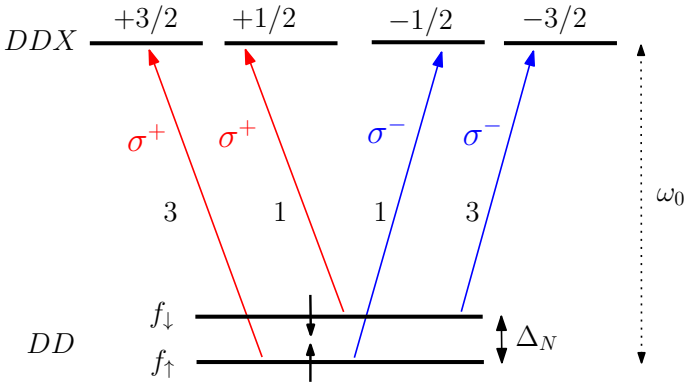


Figure 5.11: Energy levels of the DD-DDX system in GaAs and the optical selection rules for $\sigma^+$ and $\sigma^-$ polarized light excitations.

We have seen in Section 5.2.2, that closely spaced donor pairs can form a localized state. Each of these donor pairs (double donors, DD) can bind a single electron. This is the initial state. The DD bound electron, under the influence of the nuclear field, splits into two levels denoted by magnetic quantum numbers $m_s = \pm 1/2$. In the excited state DDX, the two electrons in the complex form a spin singlet. The energy

of the DDX state is thus determined by the spin of the bound hole $m_h = \pm 1/2; \pm 3/2$, as well as holes's effective mass and angular momentum. Possible transitions are shown in Fig. 5.11.

The dielectric susceptibility for $\sigma^+$ and $\sigma^-$ polarized light excitations in the spectral vicinity of the neutral donor bound exciton resonance is given as:

$$\varepsilon_+ \propto \varepsilon_b + \frac{3\lambda f_\uparrow}{\omega - (\omega_0 + \Delta_N/2) + i\Gamma} + \frac{\lambda f_\downarrow}{\omega - (\omega_0 - \Delta_N/2) + i\Gamma} \tag{5.28}$$

$$\varepsilon_- \propto \varepsilon_b + \frac{\lambda f_\uparrow}{\omega - (\omega_0 + \Delta_N/2) + i\Gamma} + \frac{3\lambda f_\downarrow}{\omega - (\omega_0 - \Delta_N/2) + i\Gamma}, \tag{5.29}$$

where $\lambda$ is the oscillator strength of the transition, $f_\uparrow$ and $f_\downarrow$ are the occupation factors, $\omega_0$ is the resonance frequency and $\Delta_N$ is the nuclei induced splitting of the neutral donor electron.

Then the difference in dielectric susceptibility for $\sigma^+$ and $\sigma^-$ polarized light is given as,

$$\varepsilon_+ - \varepsilon_- = \frac{2\lambda}{(\omega - \omega_0 + i\Gamma)^2 + (\Delta_N/2)^2}[(f_\uparrow - f_\downarrow)(\omega - \omega_0 + i\Gamma) + \Delta_N/2]. \tag{5.30}$$

Now let us assume that $(f_\uparrow - f_\downarrow) = \tanh(\beta\Delta_N/2)$, where $\beta = 1/k_BT$. Then

$$\delta\varepsilon'(\omega) = (\varepsilon'_- - \varepsilon'_+) = -\frac{2\lambda \tanh(\beta\Delta_N/2)(\omega - \omega_0) + \Delta_N/2}{(\omega - \omega_0)^2 - (\Delta_N/2)^2}. \tag{5.31}$$

The FR angle is

$$\Theta_F = \frac{\omega}{4cn}\delta\varepsilon'(\omega)d_{eff}. \tag{5.32}$$

Now, $\Theta_F$ changes sign when $\delta\varepsilon'(\omega) = (\varepsilon'_- - \varepsilon'_+) = 0$. This implies

$$\begin{aligned} \tanh(\beta\Delta_N/2)(\omega - \omega_0) + (\Delta_N/2) = 0 \\ \Rightarrow \omega = \omega_0 - (\Delta_N/2)\coth(\beta\Delta_N/2). \end{aligned} \tag{5.33}$$

Now $\beta\Delta_N \ll 1$, which implies $\omega = \omega_0 - 1/\beta = \omega_0 - k_BT$. When $\omega < \omega_0 - k_BT$, phase space filling effect dominates over spin splitting due to nuclei and $\delta\varepsilon'(\omega) = (\varepsilon'_+ - \varepsilon'_-) < 0$. Thus the Faraday rotation due to localized electrons have a sign

different to that of free electrons.

The contribution to nuclear FR due to localized electrons is given as:

$$\Theta_F = V_N^b d_{eff} B_N, \tag{5.34}$$

where $V_N^b$ is the nuclear Verdet constant associated with the bound electrons and is given by [Gla12, SG12, FYY+10]

$$V_N^b = \frac{\pi\hbar^3 c^2}{E_0^2 \tau_r n} \frac{N_b g_e \mu_B}{4k_B T(\Delta - E_b)}, \tag{5.35}$$

where $N_b$ is the density of donors, $E_b$ is the binding energy of the localized electrons, $n$ is the background refractive index and $\tau_r$ is the radiative lifetime associated with the dipole transition at the resonance energy $E_0 = \hbar\omega_0$.

Taking $\tau_r = 250$ ps, $E_b = 3$ meV, $\Delta = 18$ meV and standard GaAs parameters, we obtain $V_N^b$= -0.05 mrad/cm-G. This value is about three times smaller than the Verdet constant due to free electrons and has a opposite sign, consistent with the experimental results.

## 5.6 Summary

In this Chapter, we have studied the nuclear spin dynamics in an n-GaAs layer with doping density close to the metal-insulator transition ($n_e = 2 \times 10^{16}$ cm$^{-3}$). We have developed a non-perturbative method of optical detection of nuclear spin polarization in semiconductor structures based on Faraday rotation amplified by a microcavity. It does not require the presence of non-equilibrium electrons in contrast with other methods, and gives a possibility to measure the spin dynamics of preliminary initialized nuclei in a single-shot experiment.

The nuclear FR is found to be non-monotonous and consists of two components with vastly different time constants, comparable amplitudes and opposite signs. The nuclear origin of these two components is verified from the study of the effects of pump helicity, pump time, and static as well as rf-magnetic field. From the optically detected NMR, it is confirmed that, all the nuclear spin species contributes to the two components. We found that the complex pattern of nuclear spin relaxation is

due to contributions from two groups of spatially separated nuclei: nuclei close to the donors, and all other nuclei away from the donors. The nuclei situated close to the donor pairs exhibit fast relaxation due to interaction with bound electrons. Relaxation of all other nuclei is much slower. It is dominated by the spin diffusion towards the donor pairs, which provide an efficient relaxation.

We measured the nuclear field as a function of external magnetic field at different temperatures. The nuclear field increases with field and this dependence is not clearly understood. The nuclear Verdet constant associated with the slow component of the nuclear FR was determined experimentally, $V_N$= 0.1 mrad/cm-G, while it was not possible to determine it for the fast component.

The contribution to nuclear FR from free as well as bound electrons is calculated theoretically. The corresponding Verdet constants are $V_N^f$= 0.2 mrad/cm-G and $V_N^b$= -0.05 mrad/cm-G. The value of $V_N^f$ is close to the experimentally determined Verdet constant for the slow component of the nuclear FR. The sign of the fast component is correctly reproduced. Its smaller absolute value is also consistent with our experimental findings.

# Chapter 6

# Nuclear Faraday rotation in insulating n-GaAs

In this Chapter, nuclear Faraday rotation (FR) on the sample with doping concentration in the insulating regime (Sample C7T76 with $n_e = 2 \times 10^{15}$ cm$^{-3}$) is studied. The mechanisms of nuclear polarization in the insulating regime in n-GaAs is discussed in Section 6.1. In Section 6.2, FR in the presence of optical pumping is presented. Strong enhancement of FR is observed when nuclear field builds up. It could be explained in terms of field dependent electron spin relaxation. In order to verify this, we studied the effect of strong longitudinal field during pumping on the FR. In Section 6.3, we report the results on the FR in the dark, induced by the spin polarized nuclei. The results are compared with the results obtained on the metallic sample. Contrary to the results on metallic sample, we observed that the decay of the nuclear FR is monotonous but still consists of two components. The role of band (free) and bound (localized) states are discussed, and the effect of nuclear spin diffusion on the FR signal is demonstrated. The last Section is devoted to the measurements of FR in the presence of strong field.

The experimental results presented in this chapter, were measured in two different pieces of the sample C7T76 (namely C7T76R and C7T76M1), in order to be able to vary the detuning of the cavity mode energy with respect to the GaAs energy gap. The data presented in Fig. 6.1, Fig. 6.3, and Fig. 6.5 are obtained from C7T76R, where the detuning of the cavity mode was $\Delta = 14$ meV. The data presented in Fig.

6.2, Fig. 6.6, Fig. 6.7, and Fig. 6.8 are obtained from C7T76M1, where cavity mode was at lower energy, $\Delta = 17$ meV.

## 6.1 Nuclear polarization in the insulating regime

In Chap. 5, we have studied the dynamic nuclear polarization (DNP) due to delocalized electrons. It has been observed that the dynamic nuclear polarization due to localized electrons in n-GaAs differ significantly from the dynamic nuclear polarization due to free electrons [HCL+12]. In this chapter we will study the DNP in the sample with doping concentration in the insulating regime (Sample C7T76 with $n_e = 2 \times 10^{15}$ cm$^{-3}$), which is an order of magnitude below the concentration corresponding to the metal-insulator transition (MIT) and electron density in 98P180. This means that in the absence of pumping all the carriers are localized on the Si donors. A compensation of up to 10 - 50 % could be possible which would eventually further reduce the density of the donor sites occupied by electrons. Thus, in contrast with the metallic sample, the Fermi level lies below the conduction band minimum. Since the nuclear polarization by localized electrons is much more effective than by free electrons [PLSS77], so we expect stronger polarization of nuclei. On the other hand, localized electrons are also an efficient source of nuclear spin relaxation, because of fluctuations of the electrons spin. The direct nuclear spin relaxation time is given by [DP74]

$$T_{1e}(0) = \frac{1}{\omega_N^2 \tau_c}, \tag{6.1}$$

where $\omega_N$ is the nuclear spin precession frequency in the Knight field created by electrons.

The direct nuclear spin relaxation time is expected to be shorter in the insulating sample, because the correlation time in this doping regime is $\tau_c \approx 10^{-10}$ s [DKK+02], much longer than in the metallic sample. This gives the nuclear spin relaxation time of the order of 1 s, instead of 10 s for the metallic sample. However, we know from the previous studies of insulating samples by PL and NMR that in spite of this fast relaxation under the orbit of the donor, it is possible to polarize the nuclei situated far away from the donors by spin diffusion [Pag82]. Therefore, as in the

metallic sample, nuclear spin polarization created by optical pumping is expected to be quite inhomogeneous, revealing the relaxation via diffusion towards the donor sites occupied by electrons. To test these ideas, we performed FR experiments similar to that done for the metallic sample, except that the probe beam is now spectrally filtered to improve the stability of the signal.

## 6.2 Faraday rotation during optical pumping

Here we study the FR due to electrons under pumping with $\sigma^+/\sigma^-$ polarized light as well as when the pump polarization is modulated, in the presence of a longitudinal field. The longitudinal field is either parallel or anti-parallel to the direction of light.

Fig. 6.1 shows the FR under $\sigma^+$ polarized pumping as well as when the pump polarization is modulated between $\sigma^+/\sigma^-$, in a longitudinal field $B_z$=150 G at T=2 K. One can see, that in contrast with the metallic sample, the FR builds up during pumping with $\sigma^+$ polarized light, which indicates the build up of nuclear polarization (for comparison with the metallic sample one can refer to Fig. 6.3).

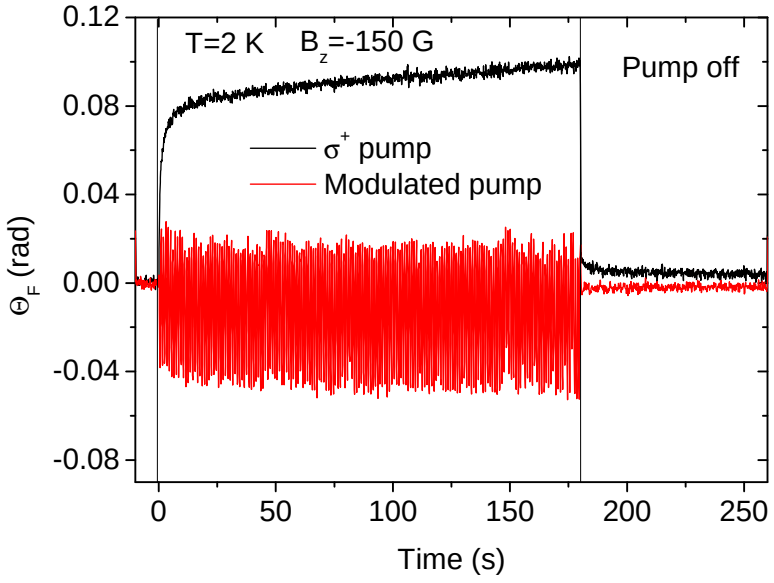


Figure 6.1: Faraday rotation spectra during pumping with $\sigma^+$ polarized light (black line) as well as when the pump polarization is modulated between $\sigma^+/\sigma^-$ (red line), at $B_z$=150 G.

In order to isolate FR induced by spin polarized electrons from the nuclear effects we did an identical experiment, but instead of $\sigma^+$ polarized pump, we used a liquid crystal (LC) variable phase retarder which modulates the pump polarization with period of 1 s (see Section 3.3.6 for the experimental set up). This technique is often used to suppress the formation of nuclear polarization which needs more than $10^{-4}$ s to build up. On the other hand, electron spin polarization is immediate on this scale, so that FR oscillate at the retarder frequency. One can see, that the FR induced by electrons in the absence of nuclear field is much smaller, and does not depend on the pumping duration. Note, that the slight asymmetry in the FR signal in $\sigma^+$ and $\sigma^-$ polarizations arises because of birefringence of the Bragg mirrors. Thus, we can conclude, that the strong increase of the FR with the pumping time is induced by the nuclear field. However this enhancement is much larger than the nuclear FR in the absence of optical pumping (In Fig. 6.1, pump is switched off at t=180 s). This surprising finding can be explained as follows:

If electron spin relaxation time depends on nuclear field, then this may produce the enhancement of the FR, since $\Theta_F \propto \tau_s$ in the case of weak pumping. The increase of electron spin relaxation time in the presence of longitudinal magnetic field has already been reported [CKBG04] and interpreted in terms of motional narrowing. Indeed, in the insulating regime, the main source of electron spin relaxation is hyperfine coupling. The nuclear field seen by an electron is averaged with the characteristic time $\tau_c$. As already mentioned, in this sample $\tau_c$=$10^{-10}$ s. The inverse $1/\tau_c$ is a measure of the rate of change in the local magnetic field that an individual electron sees. Therefore, in the motional narrowing regime [MZ84, DP74]

$$\tau_s = \tau_s(0)[1 + \Omega^2\tau_c^2], \tag{6.2}$$

where $\Omega$ is the Larmor precession frequency, in the total magnetic field given by both external and effective magnetic field created by nuclei. Thus $\tau_s$ increases when magnetic field is increased.

To check the validity of this hypothesis for our sample, we perform optical pumping experiments in strong external magnetic fields, comparable with the effective magnetic field created by the nuclei. To avoid the DNP, we use a PEM for the pump beam (same configuration as for red curve in Fig. 6.1). Fig. 6.2(a) shows the FR induced

by optically oriented electrons in the presence of the longitudinal magnetic field for different excitation powers. One can see, indeed, that FR increases with magnetic field.

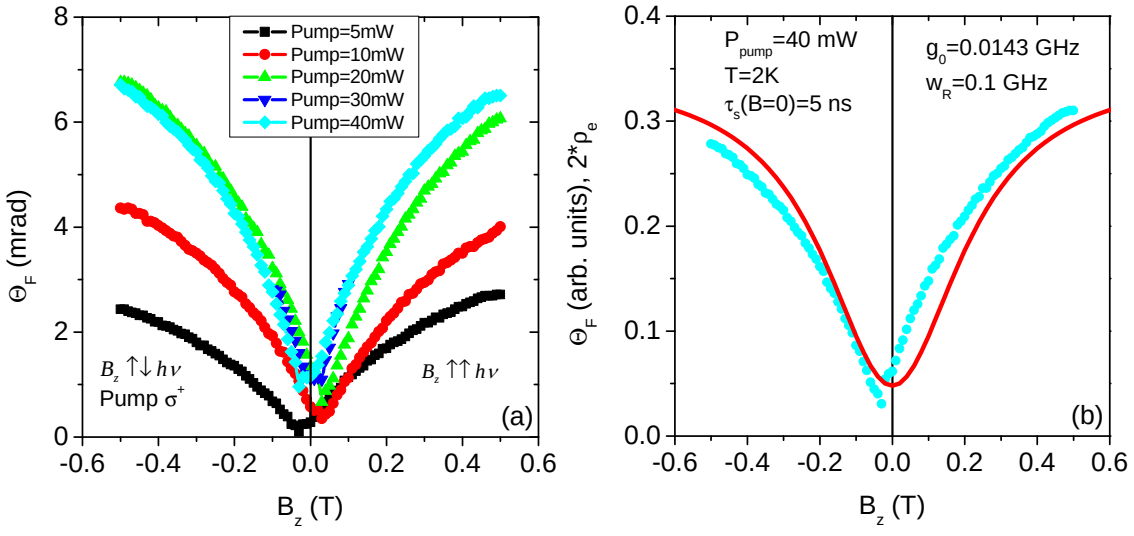


Figure 6.2: (a) Faraday rotation spectra as a function of external longitudinal magnetic field $B_z$ under $\sigma^+$ pumping at 2 K, measured at different pump intensity. (b) Fitting one of the curves (P=40 mW) shown in (a) with Eq. D.12.

In order to describe properly the steady state polarization under $\sigma^+$ optical pumping, we develop a model accounting for donor bound exciton states $D^0X$ and donor bound electrons. The solution of the corresponding system of three rate equations (see Appendix D) for the $D^0X$, $n_{+1/2}$ and $n_{-1/2}$ gives the following expression for the electron spin polarization:

$$\rho_e = \frac{\tanh\left(\frac{\Delta E}{2k_BT}\right) - \frac{g_0}{W_0}}{1 + \frac{2g_0}{W_0} + \frac{g_0}{W_R}\left[\frac{1+3\exp\left(\frac{\Delta E}{k_BT}\right)}{1+\exp\left(\frac{\Delta E}{k_BT}\right)} + 3\frac{g_0}{W_0}\left(1+\exp\left(\frac{\Delta E}{2k_BT}\right)\right)\right]} \tag{6.3}$$

Here $\Delta E = g\mu_B B$ is the Zeeman splitting of the electron spin states; $g_0$ and $W_R$ are the generation and recombination rates, respectively; $W_0$ is the spin flip rate, which we suppose to be field dependent:

$$W_0 = \frac{\gamma}{[1 + \Omega^2 \tau_c^2]}, \tag{6.4}$$

where $\tau_c$ is the correlation time, and $\gamma = 1/\tau_s(0)$ is the spin relaxation rate at zero magnetic field.

We note that Eq. D.12 has only three parameters: $g_0$, $W_R$ and $\tau_c$. The zero field spin relaxation time $\tau_s(0) = 5$ ns, was determined independently from Hanle experiments. The numerical application of this expression assuming $\tau_c$=3×10$^{-10}$ s, $g_0$=0.23×10$^8$ s$^{-1}$, and $W_R$=2×10$^8$ s$^{-1}$ is shown in Fig. 6.2(b).

The correlation time $\tau_c$ is in excellent agreement with the results of Dzhioev *et al.* [DKK+02]. Thus, we conclude that the observed increase of the FR during pumping on the several minutes scale can be, in principle, understood in terms of nuclear field induced increase of the spin relaxation time. However, to go further in the understanding of the underlying dynamics of nuclear spin polarization, it is instructive to consider first the FR in the dark, where optically polarized electrons do not obscure nuclear spin polarization.

## 6.3 Faraday rotation in the dark

Fig. 6.3 shows the FR measured after 5 min pumping in $\sigma^-$ polarization at $B_z$=200 G at T=2K. The FR for the insulating sample (red line) is compared here to that of the metallic sample. One can see that for the insulating sample, the nuclear FR decays monotonously. However, the fast and slow component shows up as well, but have the same sign. The slow component of nuclear spin relaxation signal looks quite similar in both samples. The interpretation can thus be the same: nuclear spins situated far from the neutral donors loose their spin polarization by diffusion towards these donor sites, where efficient relaxation by spin flip with localized electrons is possible. Remarkably, the decay time is similar for these two samples, in agreement with the above argument. Indeed, in the insulating sample, neutral donor density $n_e = 2 \times 10^{15}$ cm$^{-3}$, that is similar to the density of donor pairs in the metallic sample. The fast decay could be then due to fast relaxation under the donor orbit. The sign of the signal indicates that FR is determined by the hyperfine splitting of the band states, and not the occupation of the bound states. It remains unclear at

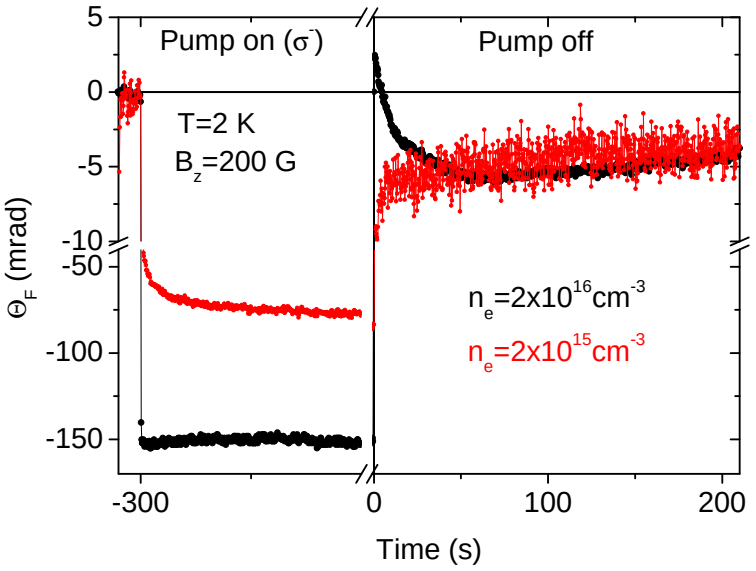


Figure 6.3: Faraday rotation spectra during cooling with $\sigma^-$ polarized light at $B_z$=200 G (t<0), as well as during measurement in the dark (t>0) at the same field, of the insulating sample (red line) plotted together with that of the metallic sample (black line).

this stage, why the contribution to the FR from the occupation of the bound states is not observed in the insulating sample. One of the reasons could reside in much longer electron spin correlation time. Indeed, in the metallic sample, $\tau_c \sim 10^{-11}$ s, while in the insulating sample, even under optical pumping $\tau_c$=3$\times$ $10^{-10}$ s. It can be expected to increase further in the absence of optical excitation. Thus, from Eq. 6.1, the upper limit for the direct nuclear spin relaxation induced by fluctuating electron spin is $T_{1e}$=0.3 s, which is close to our temporal resolution $\sim$ 0.1 s.

## 6.4 Modelling spatial distribution of nuclear spin and resulting FR

To get deeper insight into the nuclear spin distribution in the sample, both under pumping and in the dark, we use the diffusion equation taking into account optical pumping, direct relaxation and spin diffusion [Blo49, Pag82].

As explained in the previous section, FR in this sample is given by the electron

spin splitting (band states) induced by nuclear field. On the other hand, nuclear spin polarization takes place under the orbit of the electrons localized on the shallow donors. Therefore, it is convenient to write diffusion equation on the sphere centered at the donor site and use the radial symmetry of the problem. The size of the sphere should be given by the half distance between donors, $R_{12}$ and periodic boundary condition should be assumed (Fig. 6.4).

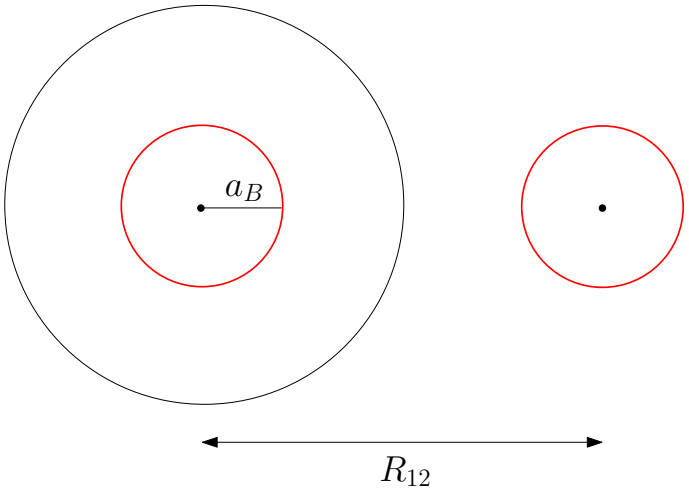


Figure 6.4: Schematic representation of the nuclear spin relaxation model used for the insulating n-GaAs. The nuclei situated within the orbit of an electron bound to shallow donors (red spheres) undergo direct relaxation by interaction with electrons. For nuclei situated outside, spin relaxation is dominated by diffusion towards the donor site. The black sphere shows the size of the simulation cell, chosen to be half of average distance between donors.

Following Paget [Pag82], we write the diffusion equation as:

$$\frac{dI(r)}{dt} = D\Delta I(r) - \frac{1}{T_1(r)}[I(r) - I_0], \tag{6.5}$$

where $D$ is the nuclear spin diffusion coefficient, $T_1(r)$ is the coordinate-dependent nuclear spin relaxation time. Because electron density decreases exponentially as a function of the distance from the donor, it should have the form

$$T_1(r) = T_1(0)\exp(4r/a_B), \tag{6.6}$$

where $a_B$ is the Bohr radius of the donor. The steady state nuclear spin polarization $I_0$ is proportional to the mean electron spin under pumping, and $I_0$=0 in the dark.

In contrast with NMR signal detected by PL [Pag82], where the intensity of the signal was given by hyperfine field experienced by electrons trapped on donors ($B_N = b_n \int_0^{R/2} I(r)\mathrm{e}^{-2r/a_B}\, r^2\mathrm{d}r$), here FR signal is determined by the hyperfine field experienced by electron band states:

$$B_N = b_n \int_0^{R/2} I(r) r^2 \mathrm{d}r. \tag{6.7}$$

Thus, we can model the dynamics of nuclear field $B_N(t)$ starting from I(r)=0 at t=0, both under pumping during $t_{pump}$, and consequent relaxation in the dark.

The dynamics of nuclear field calculated within the above model in the dark can be directly compared with the measured FR. Under optical pumping, the FR signal is dominated by spin polarized electrons, but the signal strongly increases as nuclear field builds up. It was proposed in the previous section to describe this enhancement of the electron spin polarization as being due to the increasing electron spin relaxation time $\tau_s = \tau_s(0)[1 + \Omega^2\tau_c^2]$, where $\tau_c$ was determined in independent experiment under external magnetic field. The Larmor frequency of the electron spin precession is given by the total magnetic field: applied field and effective field created by nuclei. This effective field is given by Eq. 6.7, since we suppose that under moderate pumping, total electron density is of the order of donor density, and all electrons remain bound to shallow donors. The resulting polarization of electron gas can then be calculated using Eq. D.12.

## 6.5 Comparison with experiment

### 6.5.1 FR during pumping and in the dark

Fig. 6.5 shows how the modelling compares with the FR scan both under pumping and in the dark. The parameters of the electron gas $\tau_c = 3 \times 10^{-10}$ s, $\tau_s = 5 \times 10^{-9}$ s, as well as the parameters defining pumping conditions $g_0 = 0.23 \times 10^8$ $\mathrm{s}^{-1}$, $W_R = 2 \times 10^8$ $\mathrm{s}^{-1}$ were fixed as determined from the independent experiments. Direct nuclear spin relaxation time $T_{1e}(0)$ at the donor position is estimated from

$\tau_c$ as $T_{1e}(0) = (\omega_N^2 \tau_c)^{-1} \sim 0.3$ s. This value however, was used only to model the signal under optical pumping. In the dark, much shorter time $T_{1e}(0)$=5 ms was taken to reproduce nuclear spin relaxation in the dark, namely, the presence of the fast component of nuclear spin relaxation. The value of nuclear magnetization at saturation of electron spin polarization was fixed at $I_0$=0.2 . This corresponds to the nuclear field $B_N$=1 T. This choice was dictated by the experiments on nuclear polarization at strong magnetic field, discussed in Section 6.6. The donor Bohr radius $a_B$=10 nm, is a standard well known value for GaAs, and $R_{12}$= 80 nm is an average distance between donors for $n_e \sim 2 \times 10^{15}$ cm$^{-3}$. The value of nuclear spin diffusion as well as $T_{1e}(0)$ appeared to be critical to reproduce the experimental data. We had to set $D = 10^{-14}$ cm$^2$/s, that is 10 times smaller than in Ref. [Pag82] in order to reproduce the fast initial decay of nuclear spin polarization in the dark, followed by much smaller relaxation. The reason for this difference must be elucidated in the future work. Note, however that the assumption of such slow nuclear spin diffusion is mandatory only in the dark. The FR measured under pumping can still be correctly described using $D = 10^{-13}$ cm$^2$/s.

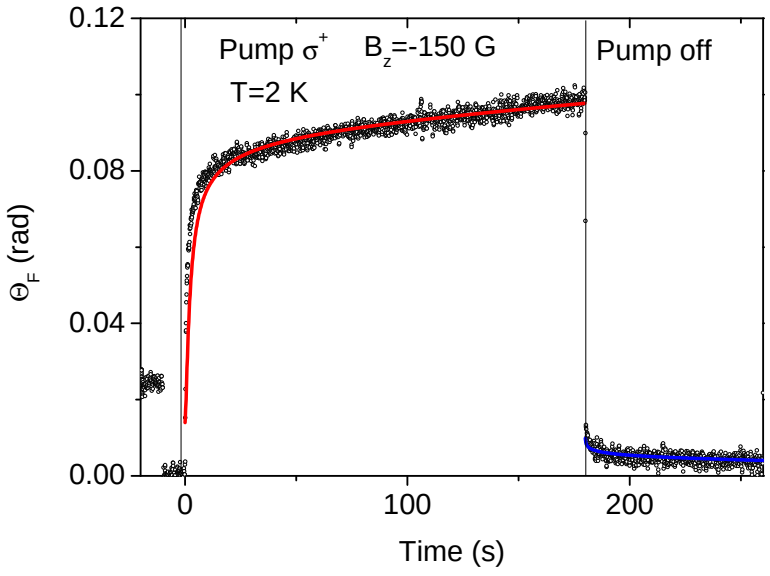


Figure 6.5: Faraday rotation during pumping, and in the dark (same data as shown in Fig. 6.1), plotted together with the theoretical curve obtained using the model described in Section 6.4.

### 6.5.2 Repolarization of nuclei under optical pumping of different helicities

To further test our understanding of the FR induced by spin polarized electrons in the presence of nuclear field, we performed the following experiments. The sample was placed in the longitudinal field $B_z$=150 G and optically pumped in $\sigma^+$ polarization during 10 minutes. Changing the helicity of the pump immediately reverses the polarization of the electron gas, and thus the sign of the FR (see Fig. 6.6). However, nuclear spin polarization needs seconds to be reversed. Because FR strongly depends on the total field value, and total field must change sign under pumping with opposite helicity, we see a minima in the FR signal several seconds after the change of the pump helicity. This minimum corresponds to the compensation of the external field by the nuclear field.

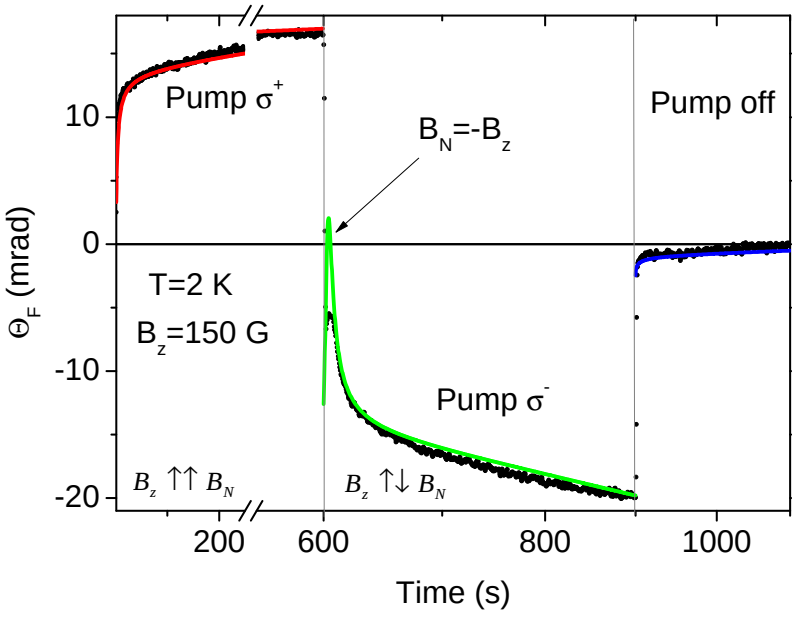


Figure 6.6: Faraday rotation during pumping with $\sigma^+$ (t < 600 s) and $\sigma^-$ (600 s < t < 900 s) polarized light at $B_z$=150 G, as well as in the dark (t > 900 s), plotted together with the theoretical curve obtained using the model described in Section 6.4.

This behaviour is reasonably reproduced by the model. We have assumed stronger pumping power in $\sigma^-$ polarization ($I_0$=0.45, $g_0$=0.05×$10^8$ $s^{-1}$). This is probably due to linear dichroism of the microcavity sample. The minimum of the FR is,

however much more pronounced in the calculated curve. We attribute this to the inhomogeneity of the nuclear field in the sample. These results allows us to elaborate the idea that FR induced by spin polarized electron gas is determined by nuclear field building up at several minutes scale. Note, that the data presented in Fig. 6.6 are obtained at different point of the sample, where cavity mode was at lower energy, $\Delta = 17$ meV.

## 6.6 FR and DNP at strong magnetic field

In order to model nuclear spin dynamics and the resulting FR signal presented so far, we assumed that nuclear field was of the order of 1 T. We use the strong dependence of the FR induced by electron spin polarization on the magnetic field to measure nuclear field. To do so, we realize a set of experiments, where applied field rises from -1 T to +1 T. Each time FR is measured during pumping (5 minutes, $\sigma^+$ polarization), and subsequently in the dark. The results are shown in Fig. 6.7. One can see, that at low field, $B_z$=± 0.1 T, the direction of external field does not play any role. This means, that nuclear field is much stronger than the external field, and

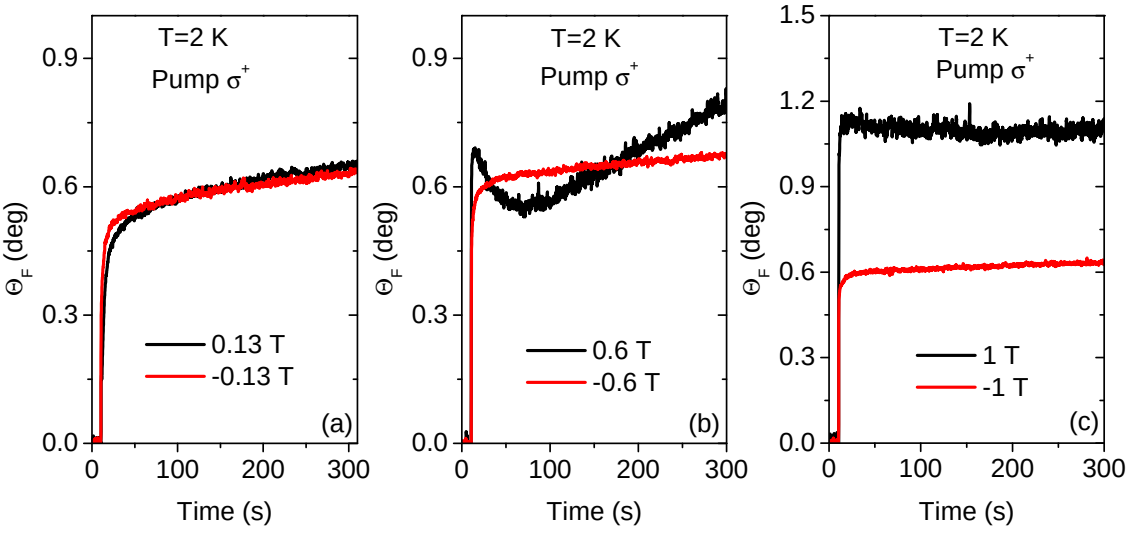


Figure 6.7: Faraday rotation during pumping with $\sigma^+$ polarized light at $B_z$=± 0.13 T (a), $B_z$=± 0.6 T (b), and $B_z$=± 1.0 T (c). The direction of the external field plays an important role for field greater than 0.6 T, where the external field is comparable to the nuclear field.

nuclear spin relaxation rate does not depend on the nuclear spin temperature.

The situation changes drastically at $B_z$=± 0.6 T. The two direction of the field are not equivalent any more. Indeed at $B_z < 0$ ($B_z$ parallel to $B_N$), monotonous increase of FR under pumping is observed similar to lower field measurements. In contrast, for $B_z > 0$ ($B_z$ antiparallel to $B_N$), FR under optical pumping has a minimum after about 1 min pumping, and then starts to increase. This means, that total field ($B_N + B_z$) first decreases, then reaches zero at $B_N = -B_z$, and then increases when $|B_N| > B_z$. From this we conclude that $|B_N| > 0.6$ T, at saturation of nuclear field under these pumping conditions. Thus, to obtain the estimation of the maximum nuclear field that can be obtained under given pumping conditions, we further increase the external field, until the value where no variation of the FR is observed, when nuclear field builds up. This happens at $B_z$=1 T in these experiments, which corresponds to 20% of nuclear spin polarization.

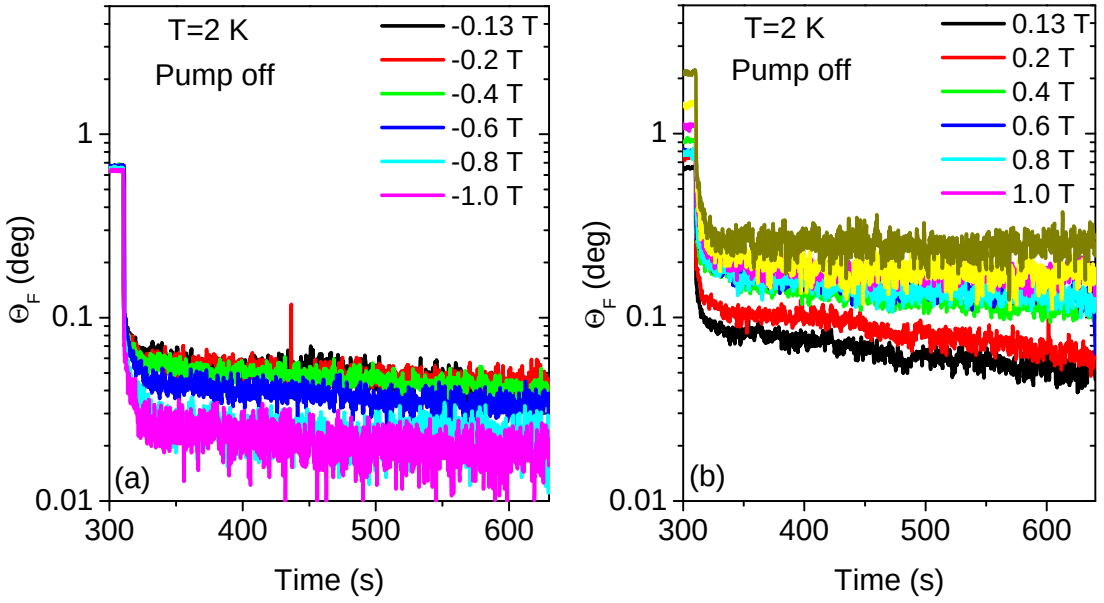


Figure 6.8: Faraday rotation in the dark, after preparation under pumping with $\sigma^+$ polarized light at different $B_z$, either antiparallel (a), or parallel (b) to the direction of light. Nuclear FR strongly depend on mutual orientation of nuclear and external field.

Another interesting observation concerns FR in the dark, measured at two opposite directions of the applied field. Systematic measurements of nuclear FR in the dark

are shown in Fig. 6.8. At $|B_N| > 0.1$ T, nuclear FR is much stronger in the antiparallel configuration ($B_z$ antiparallel to $B_N$) (Fig. 6.8(b)). It also contains the more important fast relaxation component.

We are planning to analyze in details these data, but for the moment we only give qualitative discussion of these results. Indeed, at strong magnetic fields, the difference between electron spin splitting and nuclear spin splitting grows up. This makes DNP less efficient, and thus reduces nuclear FR. However, electron spin splitting is determined by the total field $B_N + B_z$. Therefore, in the configuration where $B_N.B_z < 0$, formation of the nuclear field will favor DNP, while for $B_N.B_z > 0$, the situation is inversed. Therefore, nuclear polarization and resulting FR in the dark is much smaller. The same argument is valid for the relaxation: the stronger is the mismatch between electron and nuclear spin splitting, the slower is the relaxation of nuclei.

## 6.7 Summary

In this Chapter, we have studied the nuclear spin dynamics in a non-degenerate n-GaAs layer with doping density $n_e = 2 \times 10^{15}$ cm$^{-3}$. We have used the same experimental protocol as was used for the metallic sample to study the nuclear spin dynamics. The observed FR is found to be quite different from the metallic sample.

Under optical pumping, FR is always due to optically created spin polarization. In contrast with the metallic sample, here electron spin polarization strongly increases when nuclear field builds up. This results in huge increase of the FR.

The nuclear FR is found to be monotonous and consists of two components with same sign. Microscopic mechanism of the FR in the dark is identified as conduction band splitting induced by the nuclear field. The two components of nuclear spin relaxation are interpreted in terms of direct relaxation under the orbit of donor bound electrons (fast component), and nuclear spin diffusion towards remote donor sites (slow component).

Measurements of nuclear field by compensation in the external magnetic field provides the estimation for nuclear field $B_N \sim 1$ T. Strong effect of the nuclear field direction with respect to the external magnetic field, on the FR, for $B_z \sim B_N$, is demonstrated.

# Chapter 7

# Conclusions

In conclusion, we have studied in this thesis, the spin dynamics of electrons and nuclei in $n$-doped GaAs layers with different doping concentrations, enclosed in a high-Q planar microcavity.

Using the most metallic sample, we demonstrated a large Faraday rotation (FR) induced by a spin polarized electron gas. FR angles up to 19° were obtained by optical pumping, and for electron spin polarization $\rho_e$ of only few percents. Independent measurements of $\Theta_F$, $\rho_e$, and $Q$ provide a quantitative determination of the Faraday rotation cross-section $\sigma_F$, which relates $\Theta_F$ to the electron spin density, and the thickness of the layer. We found $\sigma_F = -(2.4 \pm 0.6) \times 10^{-15}$ rad$\times$cm$^2$ at 18 meV below the band gap, larger than theoretical prediction. The strong *negative* value of $\sigma_F$ found experimentally confirms that photoinduced Faraday rotation is dominated by polarization dependent bleaching of absorption, while spin splitting of conduction band induced by electron-electron interactions, which contribute with the opposite sign, is probably less important.

We also demonstrated fast optical switching of FR in sub-microsecond time scale by sampling the FR in a one-shot experiment under pulsed excitation. From the decay time of $\Theta_F$ we deduce the electron spin relaxation time $\tau_s$=250 ns, slightly longer than the value deduced from Hanle curves $\tau_s$=160 ns.

We have developed a non-perturbative method of optical detection of nuclear spin polarization in semiconductor structures based on FR amplified by a microcavity. It gives a possibility to measure the spin dynamics of preliminary initialized nuclei in a single-shot experiment. We used this method to study nuclear spin dynamics in

n-GaAs with different doping concentrations.

The nuclear FR of the metallic $n$-GaAs layer was found to be non-monotonous and consists of two components with vastly different time constants, comparable amplitudes and opposite signs. The nuclear origin of these two components was verified from the study of the effects of pump helicity, pump time, and static as well as rf-magnetic field. From the optically detected NMR, it was confirmed that, all the nuclear spin species contributes to the two components. It was found that the complex pattern of nuclear spin relaxation is due to contributions from two groups of spatially separated nuclei: nuclei close to the donors, and all other nuclei away from the donors. The nuclei situated close to the donor pairs exhibit fast relaxation due to interaction with bound electrons. Relaxation of all other nuclei is much slower. It is dominated by the spin diffusion towards the donor pairs, which provide an efficient relaxation.

Nuclear FR of the insulating $n$-GaAs layer, in contrast with the metallic sample, was found to vary monotonously, but again consists of two components. The fast component was even faster than that of the metallic sample, and the slow component decays in the same time scale as that of the metallic sample. We interpret the slow relaxation similar to the metallic sample: nuclear spins situated far from the neutral donors loose their spin polarization by diffusion towards these donor sites, where efficient relaxation by spin flip with localized electrons is possible. The fast decay is due to fast relaxation under the orbit of donor bound electrons. The sign of the signal indicates, that FR is determined by the hyperfine splitting of the band states, and not the occupation of the bound states.

# Appendix A

# Variation of cavity mode energy with position

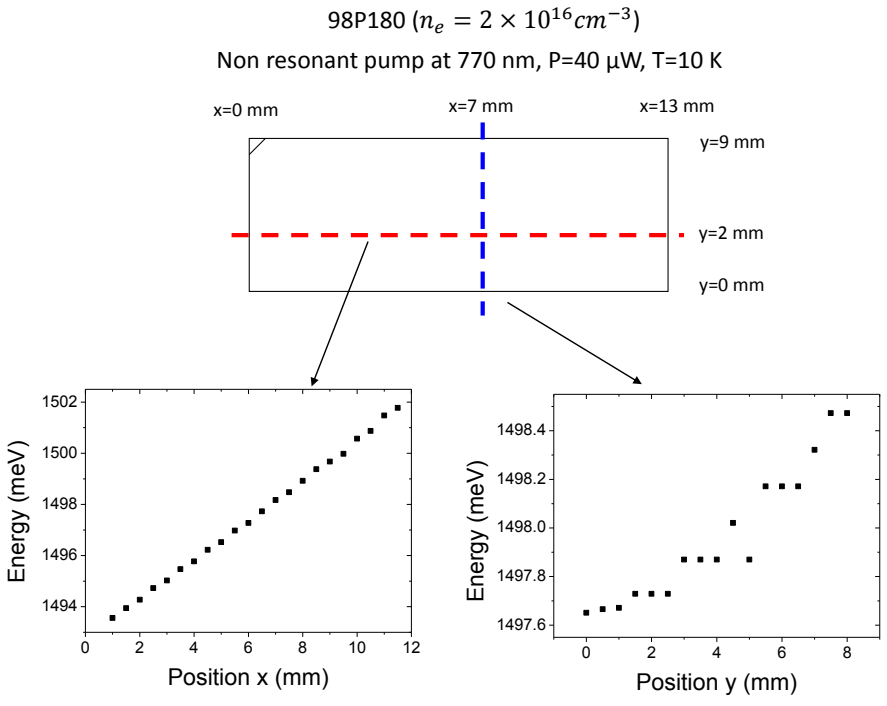


Figure A.1: Variation of cavity mode energy along the x and y axis of the sample 98P180.

# Appendix B

# Zeeman splitting of spin levels

The Zeeman energy of an electron spin $\boldsymbol{S}$ in a static magnetic field $\boldsymbol{B}$ is

$$E_Z^e = -\boldsymbol{M}.\boldsymbol{B} = g_e \mu_B \boldsymbol{S}.\boldsymbol{B} \tag{B.1}$$

Where $\boldsymbol{M} = -g_e \mu_B \boldsymbol{S}$, is the magnetic moment of the electron, $\mu_B$ is the Bohr magneton, $g_e$ is the electron spin g-factor. Since $g_{GaAs} = -0.44 < 0$, the spin and magnetic moment for an electron are aligned. The lower energy state is the one with the magnetization parallel to the magnetic field.

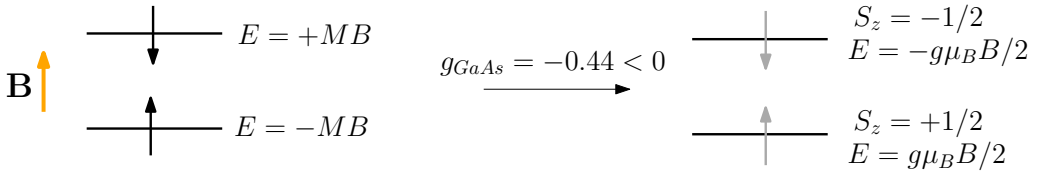


Figure B.1: Energy levels for an electron spin $S = 1/2$ in a magnetic field

The Zeeman energy of a nuclear spin $\boldsymbol{I}$ is

$$E_Z^N = -g_n \mu_N \boldsymbol{I}.\boldsymbol{B} \tag{B.2}$$

Where $\mu_N$ is the nuclear magneton, $g_n$ is the g-factor of the nucleus.

As $\mu_B \approx 2000 \mu_N$, splitting of electron and nuclear spin level differ by three orders of magnitude.

# Appendix C

# Spin temperature

## C.1 Negative spin temperature

The direction of electron and nuclear spin polarization under left circularly polarized excitation is shown in Fig. C.1(a) with the external field in the direction opposite to the light excitation. The energy levels of the nuclear spins in the field $B_z$, are shown in Fig. C.1(b). Since the field is antiparallel to the nuclear spin, the upper level is populated more which means the nuclear spin temperature $\Theta_N$ is negative. Now if the longitudinal field is switched off, the electron spin polarization vanishes quickly owing to short relaxation time of electrons in n-GaAs ($\sim ns$) and there by the nuclear spin polarization/field ($T_2$=$10^{-4}$s), but the nuclear spin heats up slowly because of the long spin-lattice relaxation time. By application of a small transverse magnetic field $B_x$, the nuclear spins orients either parallel or antiparallel to the field, depending on the spin temperature. For negative spin temperature, the nuclear spins orients antiparallel to the vertical field. Since the nuclear field is antiparallel to nuclear spin polarization, we have $B_x \uparrow\uparrow B_N$ [Fig. C.1(c, d)]. The polarization of the electron spin created by the pump will be affected by the total transverse field $B_T = B_x + B_N$ which can be detected by Hanle depolarization of photoluminescence or Faraday rotation of a probe. Since the nuclear field relaxes with time, the electron spin polarization will follow a part of the Hanle curve as shown in Fig. C.1(e).

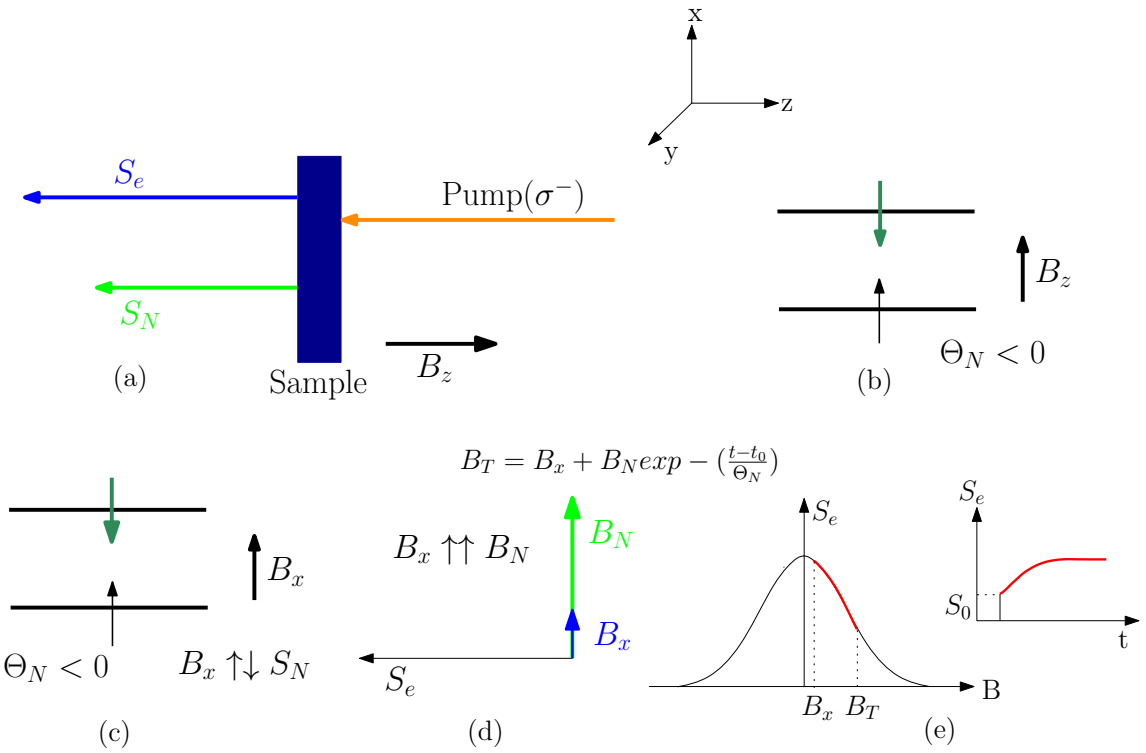


Figure C.1: Schematic view of the optical cooling of nuclear spins with strong $\sigma^-$ pumping with external field $B_z$ in the opposite direction to light and the orientation of electron and nuclear spin polarization (a, b); the alignment of nuclear spins in a weak transverse field (c, d) and the effect of total transverse field (nuclear+external) on the time evolution of the electron spin polarization in weak pumping regime (e).

## C.2 Positive spin temperature

If the external magnetic field is in the same direction as the light excitation, then the nuclear spin is parallel to the external field $B_z$ [Fig. C.2(b)] and in this case the the lower level is populated more and the corresponding spin temperature is positive. By application of a small transverse field as in the case described above, the nuclear spins orients parallel to the vertical field. Since the nuclear field is parallel to nuclear spin polarization, we have $B_x \uparrow\downarrow B_N$ [Fig. C.2(c, d)]. The part of the Hanle curve followed in this case by electron spin polarization is shown in Fig. C.2(e).

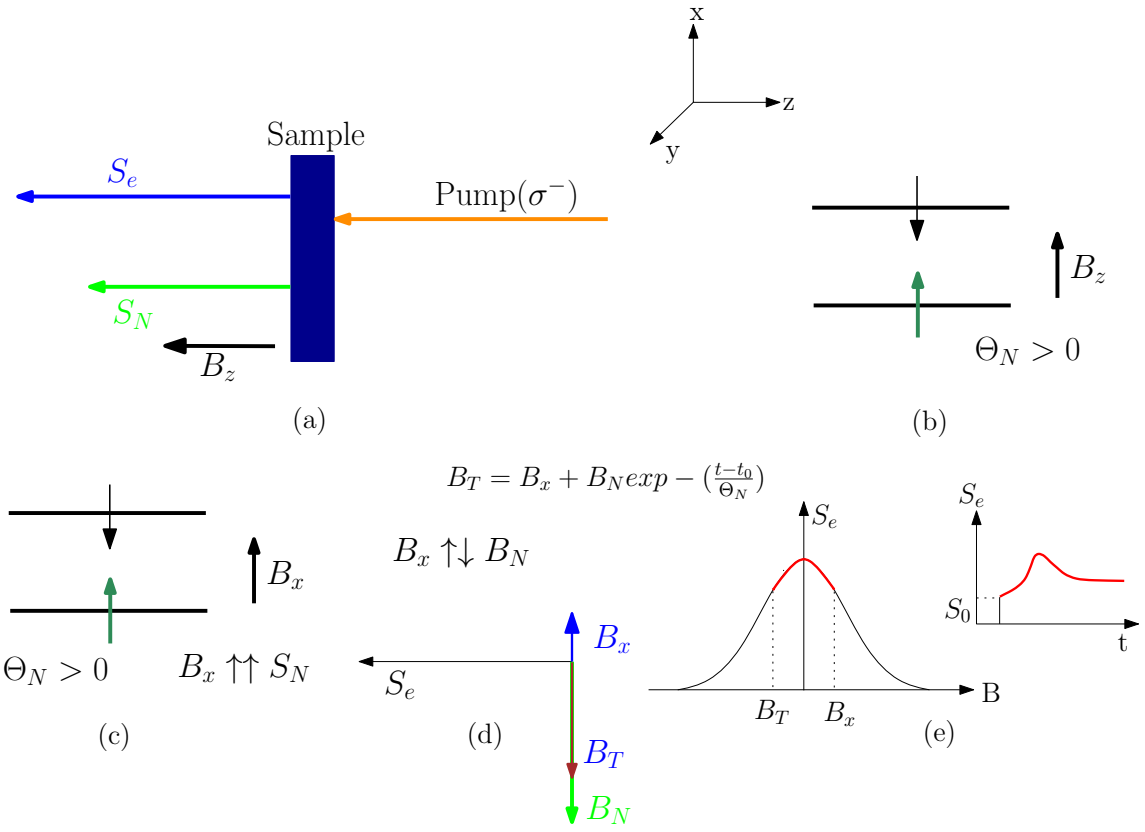


Figure C.2: Schematic view of the optical cooling of nuclear spins with strong $\sigma^-$ pumping with external field $B_z$ along the light and the orientation of electron and nuclear spin polarization (a, b); the alignment of nuclear spins in a weak transverse field (c, d); and the effect of total transverse field (nuclear+external) on the time evolution of the electron spin polarization in weak pumping regime (e).

# Appendix D

# Modelling field dependence of electron spin polarization

The steady state spin polarization of a non-degenerate electron gas under $\sigma^+$ optical pumping can be described, taking into account the (i) optical generation of excitons and their capture at donor sites at rate $4g_0$ ($1g_0$ for $J$=+1, $3g_0$ for $J$=-1), (ii) exciton recombination at spin independent rate $W_R$, and (iii) electron spin flip rates $W_+$ and $W_-$, as illustrated in Fig. D.1.

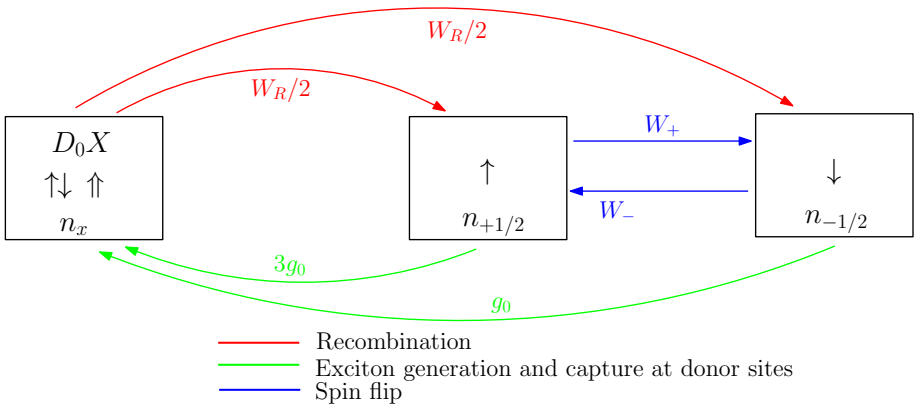


Figure D.1: Schematic representation of the generation and recombination dynamics of donor bound exciton states $D^0X$, and donor bound electrons under $\sigma^+$ optical pumping.

Here $n_x$ is the density of neutral donors, $n_{\pm 1/2}$ are the density of spin up and spin down electrons. The rate equations for the $D^0X$, $n_{+1/2}$ and $n_{-1/2}$ under $\sigma^+$ optical

pumping are given by

$$\dot{n}_x = 3g_0 n_{+1/2} - W_R n_x + g_0 n_{-1/2} \tag{D.1}$$

$$\dot{n}_{+1/2} = \frac{W_R}{2} n_x - W_+ n_{+1/2} + W_- n_{-1/2} - 3g_0 n_{+1/2} \tag{D.2}$$

$$\dot{n}_{-1/2} = \frac{W_R}{2} n_x + W_+ n_{+1/2} - W_- n_{-1/2} - g_0 n_{-1/2} \tag{D.3}$$

Solving these rate equations in the steady state, we obtain

$$n_{-1/2} = \frac{2W_+ + 3g_0}{g_0 + 2W_-} n_{+1/2} \tag{D.4}$$

$$n_x = \frac{g_0}{W_R} \left( 3 + \frac{2W_+ + 3g_0}{g_0 + 2W_-} \right) n_{+1/2} \tag{D.5}$$

From Eq. D.4 and Eq. D.5, we obtain

$$\begin{aligned} n &= n_x + n_{+1/2} + n_{-1/2} \\ &= \left[ \frac{g_0}{W_R} \left( 3 + \frac{2W_+ + 3g_0}{g_0 + 2W_-} \right) + \frac{2W_+ + 3g_0}{g_0 + 2W_-} + 1 \right] n_{+1/2} \end{aligned} \tag{D.6}$$

$$n_{-1/2} = \frac{2W_+ + 3g_0}{g_0 + 2W_-} \frac{n}{\left[ \frac{g_0}{W_R} \left( 3 + \frac{2W_+ + 3g_0}{g_0 + 2W_-} \right) + \frac{2W_+ + 3g_0}{g_0 + 2W_-} + 1 \right]} \tag{D.7}$$

$$\rho_e = \frac{n_{+1/2} - n_{-1/2}}{n} = \frac{1 - \frac{2W_+ + 3g_0}{g_0 + 2W_-}}{\left[ \frac{g_0}{W_R} \left( 3 + \frac{2W_+ + 3g_0}{g_0 + 2W_-} \right) + \frac{2W_+ + 3g_0}{g_0 + 2W_-} + 1 \right]} \tag{D.8}$$

$$\rho_e = \frac{(W_- - W_+) - g_0}{(W_- + W_+) + 2g_0 + \frac{g_0}{W_R}(3W_- + W_+ + 3g_0)} \tag{D.9}$$

The electron spin flip rates are given by

$$W_+ = \frac{W_0}{1 + \exp(\beta \Delta E)} \tag{D.10}$$

$$W_- = \frac{W_0 \exp(\beta \Delta E)}{1 + \exp(\beta \Delta E)} \tag{D.11}$$

Here $\Delta E = g\mu_B B$ is the Zeeman splitting of the electron spin states. Then the degree of spin polarization is given by

$$\rho_e = \frac{\tanh\left(\frac{\Delta E}{2k_B T}\right) - \frac{g_0}{W_0}}{1 + \frac{2g_0}{W_0} + \frac{g_0}{W_R}\left[\frac{1+3\exp\left(\frac{\Delta E}{k_B T}\right)}{1+\exp\left(\frac{\Delta E}{k_B T}\right)} + 3\frac{g_0}{W_0}\left(1 + \exp\left(\frac{\Delta E}{2k_B T}\right)\right)\right]}. \tag{D.12}$$

The spin flip rate $W_0 = 2(W_+ + W_-)$, which we suppose to be field dependent, is given by

$$W_0 = \frac{\gamma}{[1 + \Omega^2 \tau_c^2]}, \tag{D.13}$$

where $\tau_c$ is the correlation time, and $\gamma = 1/\tau_s(0)$ is the spin relaxation rate at zero magnetic field.

# Bibliography


[AAS+98] R. Akimoto, K. Ando, F. Sasaki, S. Kobayashi, and T. Tani. Optical control of Larmor precession of $Mn^{2+}$ moments in CdTe/$Cd_{1-x}Mn_xTe$ quantum wells. *Journal of Applied Physics*, 84:6318, 1998. [4.4]

[AB68] R. R. Alfano and D. H. Baird. Use of the Faraday effect to determine electron concentrations and concentration profiles in n-GaAs. *Journal of Applied Physics*, 39:2931, 1968. [2.8.1, 2.8.1, 4.2]

[Abr61] A. Abragam. *Principles of Nuclear Magnetism*. Clarendon Press, 1961. [2.4, 5.1, 5.2.2, 5.3]

[AI73] A. G. Aronov and E. L. Ivchenko. Dichroism and optical anisotropy of media with oriented spins of free electrons. *Soviet physics- Solid state*, 15:160, 1973. [1.1, 2.8.2, 4, 4.1.2, 4.1.5]

[AM85] A. G. Artemova and I. A. Merkulov. Nuclear field and Faraday effect in semiconductors. *Sov. phys. Solid state*, 27:941, 1985. [1.1, 4.1.5, 4.1.5, 5.1, 5.2, 5.5.1]

[AP58] A. Abragam and W. G. Proctor. Spin Temperature. *Physical Review*, 109:1441, 1958. [2.2, 2.2, 2.6, 5.2.3]

[BHL62] I. M. Boswarva, R. E. Howard, and A. B. Lidiard. Faraday effect in semiconductors. *Proc. R. Soc. London Ser.*, (A 269):125, 1962. [2.7, 2.7, 2.8.1]

[BL63] I. M. Boswarva and A. B. Lidiard. Faraday effect in semiconductors II. *Proc. R. Soc. London Ser.*, page 588, 1963. [2.8.1]

[Blo49] N. Bloembergen. On the interaction of nuclear spins in a crystalline lattice. *Physica*, 15:386, 1949. [6.4]

[Bos64] I. M. Boswarva. Analysis of the Faraday rotation spectrum of Indium antimonide in the absorption edge region. *Proc. Phys. soc., 1964,*, 84:389, 1964. [2.7, 2.8.1]

[BP72] G. L. Bir and G. E. Pikus. *Symmetry and Deformation Effects in Semiconductors*. Moscow, Nauka, 1972. [4.1.5]

[BW02] M. Born and W. Wolf. *Principles of Optics*. Cambridge U. Press, 7th edition, 2002. [3.2]

[Car61] M. Cardona. Electron effective masses of InAs and GaAs as a function of temperature and doping. *Physical Review*, 121:752, 1961. [2.7, 2.8.1]

[CCS09] S. Crooker, L. Cheng, and D. Smith. Spin noise of conduction electrons in n-type bulk GaAs. *Physical Review B*, 79:035208, 2009. [1.1, 2.8.2, 4.1.3, 4.1.3]

[CHL+11] Y. S. Chen, J. Huang, A. Ludwig, D. Reuter, A. D. Wieck, and G. Bacher. Manipulation of nuclear spin dynamics in n-GaAs using an on-chip microcoil. *Journal of Applied Physics*, 109:016106, 2011. [1.1]

[CHR+11] Y. S. Chen, J. Huang, D. Reuter, A. Ludwig, A. D. Wieck, and G. Bacher. Optically detected nuclear magnetic resonance in n-GaAs using an on-chip microcoil. *Applied Physics Letters*, 98:081911, 2011. [1.1]

[CKBG04] J. S. Colton, T. A. Kennedy, A. S. Bracker, and D. Gammon. Microsecond spin-flip times in n-GaAs measured by time-resolved polarization of photoluminescence. *Physical Review B*, 69:121307, 2004. [6.2]

[CRWB11] Y. S. Chen, D. Reuter, A. Wieck, and G. Bacher. Dynamic nuclear spin resonance in n-GaAs. *Physical Review Letters*, 107:167601, 2011. [1.1]

[DKK+02] R. I. Dzhioev, K. V. Kavokin, V. L. Korenev, M. V. Lazarev, B. Ya Meltser, M. N. Stepanova, B. P. Zakharchenya, D. Gammon, and D. S.

Katzer. Low-temperature spin relaxation in n-type GaAs. *Physical Review B*, 66:245204, 2002. [1.1, 2.9, 2.9, 4.1.3, 4.1.4, 4.4, 5.3, 6.1, 6.2]

[DP71a] M. I. Dyakonov and V. I. Perel. Feasibility of optical orientation of electrons in semiconductors. *JETP Lett.*, 13:144, 1971. [1.1]

[DP71b] M. I. Dyakonov and V. I. Perel. Spin orientation of electrons associated with the interband absorption of light in semiconductors. *Soviet Physics JETP*, 33:1053, 1971. [4.1.2]

[DP74] M. I. Dyakonov and V. I. Perel. Optical orientation in a system of electrons and lattice nuclei in semiconductors. Theory. *Soviet Physics JETP*, 38:177, 1974. [5.2.2, 6.1, 6.2]

[DP75] M. I. Dyakonov and V. I. Perel. Coling of a system of nuclear spins following optical orientation of electrons in semiconductors. *Soviet Physics JETP*, 41:759, 1975. [1.1, 2.6, 2.6, 5.3]

[Dya08] M. I. Dyakonov, editor. *Basics of Semiconductor and Spin Physics*. Spin Physics in Semiconductors. Springer, 2008. [5.1, 5.2.5]

[DZKS97] R. I. Dzhioev, B. P. Zakharchenya, V. L. Korenev, and M. N. Stepanova. Spin diffusion of optically oriented electrons and photon entrainment in n-GaAs. *Phys. Solid State*, 39:1765, 1997. [1.1]

[ES70] A. I. Ekimov and V. I. Safarov. Optical orientation of carriers in interband transitions in semiconductors. *JETP Lett.*, 12:198, 1970. [1.1, 2.1]

[ES71] A. I. Ekimov and V. I. Safarov. Observation of optical orientation of equilibrium electrons in n-type semiconductors. *JETP Lett.*, 13:177, 1971. [1.1, 4.1.2]

[ES72a] A. I. Ekimov and V. I. Safarov. Optical detection of dynamic polarization of nuclei in semiconductors. *JETP Lett.*, 15:179, 1972. [1.1, 5.1]

[ES72b] A. I. Ekimov and V. I. Safarov. Optical electron-nuclear resonance in semiconductors. *JETP Lett.*, 15:319, 1972. [1.1, 5.1]

[FDZ76] V. G. Fleisher, R. I. Dzhioev, and B. P. Zakharchenya. Optical cooling of a nuclear spin system of a conductor in a weak oscillating magnetic field. *JETP Lett.*, 23:18, 1976. [1.1, 2.6, 5.3]

[Fow89] G. Fowles. *Introduction to Modern Optics*. Dover, 2nd edition, 1989. [3.2]

[FYY+10] L. V. Fokina, I. A. Yugova, D. R. Yakovlev, M. M. Glazov, I. A. Akimov, A. Greilich, D. Reuter, A. D. Wieck, and M. Bayer. Spin dynamics of electrons and holes in InGaAs/GaAs quantum wells at millikelvin temperatures. *Physical Review B*, 81:195304, 2010. [5.5.2]

[GBS+97] D. Gammon, S. W. Brown, E. S. Snow, T. A. Kennedy, D. S. Katzer, and D. Park. Nuclear spectroscopy in single quantum dots: Nanoscopic raman scattering and nuclear magnetic resonance. *Science*, 277:85, 1997. [1.1, 5.1]

[Gen58] P. G. de Gennes. Nuclear relaxation in ionic crystals. *J. Phys. Chem. Solids*, 7:345, 1958. [5.2.2]

[GES71] D. Z. Garbuzov, A. I. Ekimov, and V. I. Safarov. Measurement of the lifetime and of the spin-relaxation time of electrons in semiconductors by the optical-orientation method. *JETP Lett.*, 13:24, 1971. [1.1]

[GI04] M. M. Glazov and E. L. Ivchenko. Effect of electron-electron interaction on spin relaxation of charge carriers in semiconductors. *Journal of Experimental and Theoretical Physics*, 99:1279, 2004. [4.1.5]

[Gla12] M. M. Glazov. Coherent spin dynamics of electrons and excitons in nanostructures (A Review). *Physics of the Solid State*, 54:1, 2012. [4.1.5, 5.5.2]

[GLJ+02] C. Gourdon, G. Lazard, V. Jeudy, C. Testelin, E. L. Ivchenko, and G. Karczewski. Enhanced Faraday rotation in CdMnTe quantum wells embedded in an optical cavity. *Solid State Communications*, 123:299, 2002. [1.1]

[GSS+96] D. Gammon, E. S. Snow, B. V. Shanabrook, D. S. Katzer, and D. Park. Fine structure splitting in the optical spectra of single GaAs quantum dots. *Physical Review Letters*, 76:3005, 1996. [5.1]

[Han24] W. Hanle. The magnetic influence on the polarization of resonance fluorescence. *Z. Phys.*, 30:93, 1924. [2.9]

[HCL+12] J. Huang, Y. S. Chen, A. Ludwig, D. Reuter, A. D. Wieck, and G. Bacher. Electron-nuclei spin coupling in GaAs-Free versus localized electrons. *Applied Physics Letters*, 100:132103, 2012. [1.1, 5.2.2, 6.1]

[JGAF94] H. J. Jiménez-González, R. L. Aggarwal, and G. Favrot. Infrared Faraday rotation of n-type InSb. *Physical Review B*, 49:4571, 1994. [2.8.1, 2.8.1]

[KA98] J. M. Kikkawa and D. D. Awschalom. Resonant spin amplification in n-type GaAs. *Physical Review Letters*, 80:4313, 1998. [1.1, 4.4]

[KA99] J. M. Kikkawa and D. D. Awschalom. Lateral drag of spin coherence in gallium arsenide. *Nature*, 397:139, 1999. [1.1]

[KA00] J. M. Kikkawa and D. D. Awschalom. All-Optical magnetic resonance in semiconductors. *Science*, 287:473, 2000. [1.1, 5.1]

[Kav08] K. V. Kavokin. Spin relaxation of localized electrons in n-type semiconductors. *Semiconductor Science and Technology*, 23(11):114009, 2008. [1.1, 5.2.2]

[KKF82] V. K. Kalevich, V. D. Kulkov, and V. G. Fleisher. Onset of a nuclear polarization front due to optical spin orientation in a semiconductor. *JETP Lett.*, 35:20, 1982. [2.4, 2.5, 2.6, 4, 4.1.4, 5, 5.3]

[KVK97] A. V. Kavokin, M. Vladimirova, and M. A. Kaliteevski. Resonant Faraday rotation in a semiconductor microcavity. *Physical Review B*, 56:1087, 1997. [1.1, 2.10]

[KZF+12] D. Kölbl, D. Zumbühl, A. Fuhrer, G. Salis, and S. Alvarado. Breakdown of the Korringa law of nuclear spin relaxation in metallic GaAs. *Physical Review Letters*, 109:086601, 2012. [1.1, 5.1]

[Lam68] G. Lampel. Nuclear dynamic polarization by optical electronic saturation and optical pumping in semiconductors. *Physical Review Letters*, 20:491, 1968. [1.1, 5.1]

[LGLC87] P. Lautenschlager, M. Garriga, S. Logothetidis, and M. Cardona. Interband critical points of GaAs and their temperature dependence. *Physical Review B*, 35:9174, 1987. [4.2]

[LHK+06] J. Lu, M. Hoch, P. Kuhns, W. Moulton, Z. Gan, and A. Reyes. Nuclear spin-lattice relaxation in n-type insulating and metallic GaAs single crystals. *Physical Review B*, 74:125208, 2006. [1.1, 2.4, 5.1, 5.2.2]

[Lut56] J. M. Luttinger. Quantum theory of cyclotron resonance in semiconductors: General theory. *Physical Review*, 102:1030, 1956. [2.3]

[MKI09] P. Maletinsky, M. Kroner, and A. Imamoglu. Breakdown of the nuclear-spin-temperature approach in quantum-dot demagnetization experiments. *Nature Physics*, 5:407, 2009. [1.1, 5.1]

[MZ84] F. Meier and B. P. Zakharchenya, editors. *Optical Orientation*, volume 8 of *Modern proplems in condensed matter sciences*. North-Holland, 1984. [1.1, 2, 2.8.2, 4.1.3, 4.1.4, 5.1, 5.3, 6.2]

[OHH+96] M. Oestreich, S. Hallestein, A. P. Heberle, K. Eberl, E. Bauser, and W. W. Ruhle. Temperature and density dependence of the electron Landé g-factor in semiconductors. *Physical Review B*, 53:7911, 1996. [4.2]

[OR95] M. Oestreich and W. Rühle. Temperature dependence of the electron Landé g-factor in GaAs. *Physical Review Letters*, 74:2315, 1995. [4.2]

[Pag81] D. Paget. Optical detection of NMR in high-purity GaAs under optical pumping: Efficient spin-exchange averaging between electronic states. *Physical Review B*, 24:3776, 1981. [5.2.2]

[Pag82] D. Paget. Optical detection of NMR in high-purity GaAs: Direct study of the relaxation of nuclei close to shallow donors. *Physical Review B*, 25:4444, 1982. [1.1, 2.5, 5.1, 5.2.2, 6.1, 6.4, 6.4, 6.4, 6.5.1]

[Par69] R. R. Parsons. Band-to-band optical pumping in solids and polarized photoluminescence. *Physical Review Letters*, 23:1152, 1969. [1.1, 2.9]

[Pil63] H. Piller. Electron effective mass in Gallium antimonide determined by Faraday rotation measurements. *Journal of Physics and Chemistry of Solids*, 24:425, 1963. [2.8.1]

[Pil64] H. Piller. Free-carrier and interband Faraday rotation in Gallium antimonide an Gallium arsenide. In M. Hulin, editor, *Physics of Semiconductors-proceedings of the 7th international conference*, page 297. Academic Press, New York, 1964. [2.8.1, 4.2, 4.2, 4.9]

[PLSS77] D. Paget, G. Lampel, B. Sapoval, and V. I. Safarov. Low field electron-nuclear spin coupling in gallium arsenide under optical pumping conditions. *Physical Review B*, 15:5780, 1977. [1.1, 2.3, 2.3.1, 2.3.2, 5.1, 5.2.2, 5.2.3, 6.1]

[PP63] H. Piller and V. A. Patton. Interband Faraday effect in Aluminium antimonide, Germanium, and Gallium antimonide. *Physical Review*, 129:1169, 1963. [2.8.1]

[RBM+10] M. Römer, H. Bernien, G. Müller, D. Schuh, J. Hübner, and M. Oestreich. Electron-spin relaxation in bulk GaAs for doping densities close to the metal-to-insulator transition. *Physical Review B*, 81:075216, 2010. [1.1]

[Rot64] Laura M. Roth. Theory of the Faraday effects in solids. *Physical Review*, 133:A542, 1964. [2.8.1, 4.2.1]

[SE84] B. I. Shklovskii and A. L. Efros. *Electronic Properties of Doped Semiconductors*. Springer Series in Solid-State Sciences. Springer, 1984. [5.2.2]

[SG12] D. S. Smirnov and M. M. Glazov. Spin coherence generation and detection in spherical nanocrystals. *Journal of Physics: Condensed Matter*, 24:345302, 2012. [5.5.2]

[SM05] G. Salis and M. Moser. Faraday-rotation spectrum of electron spins in microcavity-embedded GaAs quantum wells. *Physical Review B*, 72:115325, 2005. [1.1, 2.10]

[Stu62] M. Sturge. Optical absorption of Gallium arsenide between 0.6 and 2.75 ev. *Physical Review*, 127:768, 1962. [4.1.2]

[UMA+13] B. Urbaszek, X. Marie, T. Amand, O. Krebs, P. Voisin, P. Maletinsky, A. Högele, and A. Imamoglu. Nuclear spin physics in quantum dots: An optical investigation. *Reviews of Modern Physics*, 85:79–133, 2013. [1.1, 5.1]

[ZFD+71] B. I. Zakharchenya, V. G. Fleisher, R. I. Dzhioev, Yu. P. Veshchunov, and I. B. Rusanov. Effect of optical orientation of electron spins in a GaAs crystal. *JETP Lett.*, 13:137, 1971. [1.1]

[ZPB+08] W. Zawadzki, P. Pfeffer, R. Bratschitsch, Z. Chen, S. Cundiff, B. Murdin, and C. Pidgeon. Temperature dependence of the electron spin g-factor in GaAs. *Physical Review B*, 78:245203, 2008. [4.2]

[Zvà69] M. Zvàra. Faraday rotation and Faraday ellipticity in the exciton absorption region of GaAs. *Physica Status solidi*, 36:785, 1969. [4.2, 4.2, 4.9]

**Titre de la thèse en français:**

Dynamique de spin des électrons et des noyaux dans les microcavités GaAs

**Résumé de la thèse en français:**

Nous avons obtenu des angles de rotation Faraday (RF) allant jusqu'à 19° par orientation optique d'un gaz d'électrons dans GaAs de type n inclus dans une microcavité (Q=19000), sans champ magnétique. Cette forte rotation est obtenue en raison des multiples allers-retours de la lumière dans la cavité. Nous avons également démontré la commutation optique rapide de la RF à l'échelle sub-microseconde enéchantillonnant le signal de RF sous excitation impulsionnelle mono-coup. De la dépolarisation de la RF en champ magnétique transverse, nous avons déduit un temps de relaxation de spin de 160 ns. Le concept de section efficace de RF, coefficient de proportionnalité entre l'angle RF, la densité de spin électronique, et le chemin parcouru, a été introduit. La section efficace de RF, qui définit léfficacité du gaz d'électrons à produire une RF, a été estimée quantitativement, et comparée avec la théorie. Nous avons également démontré la possibilité de mesurer de manière non destructive láimantation nucléaire dans GaAs-n, via la RF amplifiée par la cavité. Contrairement aux méthodes existantes, cette détection ne nécessite pas la présence d'électrons hors équilibre. Par cette technique nous avons étudié la dynamique de spin nucléaire dans GaAs-n avec différents dopages. Contrairement à ce qu'on pourrait attendre, le déclin de la RF nucléaire est complexe et consiste en deux composantes ayant des temps de relaxation très différents. Deux effets à lórigine de la RF nucléaire sont identifiés: le splitting de spin de la bande de conduction, et la polarisation en spin des électrons localisés, tous deux induits par le champ Overhauser. Le premier effet domine la RF nucléaire dans les deux échantillons étudiés, tandis que la RF induite par les électrons localisés n'a été observée que dans l'échantillon métallique.

**Mots clés en français:**

Rotation Faraday, Microcavité, Dynamique de spin, Relaxation de spin, Diffusion de spin, GaAs isolant et metallique

**Titre de la thèse en anglais:**

Electron and nuclear spin dynamics in GaAs microcavities

**Résumé de la thèse en anglais:**

We obtained Faraday rotation (FR) up to 19° by using optical orientation of electron gas in n-doped bulk GaAs confined in a microcavity (Q=19000), in the absence of magnetic field. This strong rotation is achieved because the light makes multiple round trips in the microcavity. We also demonstrated fast optical switching of FR in sub-microsecond time scale by sampling the FR in a one-shot experiment under pulsed excitation. From the depolarization of FR by a transverse magnetic field, we deduce electron spin relaxation time of about 160 ns. A concept of FR cross-section as a proportionality coefficient between FR angle, electron spin density and optical path is introduced. This FR cross-section which defines the efficiency of spin polarized electrons in producing FR was estimated quantitatively and compared with theory. We also demonstrated non-destructive measurement of nuclear magnetization in n-GaAs via cavity enhanced FR. In contrast with the existing optical methods, this detection scheme does not require the presence of detrimental out-of-equilibrium electrons. Using this technique, we studied nuclear spin dynamics in n-GaAs with different doping concentrations. Contrary to simple expectation, the nuclear FR is found to be complex, and consists of two components with vastly different time constants. Two effects at the origin of FR have been identified: the conduction band spin splitting and the localized electron spin polairzation both induced by the Overhauser field. The first effect dominates the FR in both studied samples, while the FR induced by the localized electrons has been observed only in the metallic sample.

**Mots clés en anglais:**

Faraday rotation, Microcavity, Spin dynamics, Spin relaxation, Spin diffusion, Metallic and insulating GaAs